Vertebral bending mechanics and xenarthrous morphology in the nine-banded armadillo (Dasypus novemcinctus)

Jillian Oliver, Katrina Jones, Lionel Hautier, W. Loughry, Stephanie Pierce

© 2016. Published by The Company of Biologists Ltd | Journal of Experimental Biology (2016) 219, 2991-3002 doi:10.1242/jeb.142331

RESEARCH ARTICLE

Vertebral bending mechanics and xenarthrous morphology in the nine-banded armadillo (*Dasypus novemcinctus*)

Jillian D. Oliver[1,*], Katrina E. Jones[1], Lionel Hautier[2], W. J. Loughry[3] and Stephanie E. Pierce[1,*]

ABSTRACT

The vertebral column has evolved to accommodate the broad range of locomotor pressures found across vertebrate lineages. Xenarthran (armadillos, sloths and anteaters) vertebral columns are characterized by xenarthrous articulations, novel intervertebral articulations located in the posterior trunk that are hypothesized to stiffen the vertebral column to facilitate digging. To determine the degree to which xenarthrous articulations impact vertebral movement, we passively measured compliance and range of motion during ventroflexion, dorsiflexion and lateral bending across the thoracolumbar region of the nine-banded armadillo, *Dasypus novemcinctus*. Patterns of bending were compared with changes in vertebral morphology along the column to determine which morphological features best predict intervertebral joint mechanics. We found that compliance was lower in post-diaphragmatic, xenarthrous vertebrae relative to pre-xenarthrous vertebrae in both sagittal and lateral planes of bending. However, we also found that range of motion was higher in this region. These changes in mechanics are correlated with the transition from pre-xenarthrous to xenarthrous vertebrae, as well as with the transition from thoracic to lumbar vertebrae. Our results thus substantiate the hypothesis that xenarthrous articulations stiffen the vertebral column. Additionally, our data suggest that xenarthrous articulations, and their associated enlarged metapophyses, also act to increase the range of motion of the post-diaphragmatic region. We propose that xenarthrous articulations perform the dual role of stiffening the vertebral column and increasing mobility, resulting in passively stable vertebrae that are capable of substantial bending under appropriate loads.

KEY WORDS: Xenarthra, Dasypodidae, Vertebral column, Morphology, Biomechanics, Locomotion

INTRODUCTION

Throughout evolutionary history, the vertebral column has adapted to support the disparate modes of locomotion found in vertebrates, ranging from axial swimming in fish, to high-speed running in several land animals, to powered flight in birds and bats (e.g. Boszczyk et al., 2001; Buchholtz, 2001; Cullinane and Bertram, 2000; Filler, 2007; Gál, 1993a,b; Gaudin and Biewener, 1992; Hebrank et al., 1990; Hildebrand, 1959; Jones and German, 2014; Jones and Pierce, 2016; Molnar et al., 2014; Pierce et al., 2011; Rockwell et al., 1938; Schilling, 2011; Shapiro, 1995; Slijper, 1946; Ward and Mehta, 2014). Vertebral evolution is facilitated by regionalization, the *Hox*-mediated division of the column into morphological and functional units (Head and Polly, 2015; Schilling, 2011; Wellik, 2007). In mammals, the thoracic and lumbar regions are foremost implicated in locomotion, prompting investigations into the functional link between thoracolumbar morphology and mechanical properties of intervertebral joints (e.g. Boszczyk et al., 2001; Gál, 1993a,b; Gaudin and Biewener, 1992; Granatosky et al., 2014; Jones, 2016; Long et al., 1997; Nyakatura and Fischer, 2010; Pierce et al., 2011; Russo, 2010; Shapiro, 1995, 2007; Slijper, 1946). These studies illustrate the morphological and mechanical diversity of thoracolumbar vertebrae within and between mammals, and demonstrate that morphological predictors of mechanics can vary according to size, taxon and mode of locomotion. Thus emphasized is the need for mechanical investigations into animals with varied morphologies and modes of locomotion, as well as the different roles that the thoracic and lumbar vertebrae play during movement.

Xenarthrans (armadillos, anteaters and sloths) are a fascinating group of animals in which to study vertebral mechanics, yet they have received limited attention. Xenarthrans are hypothesized to have evolved as ancestrally fossorial mammals (Simpson, 1931). Several traits characterizing this major mammalian lineage are used as evidence for this hypothesis, including the limb morphology of modern and fossil xenarthrans, the lack of color vision in living xenarthrans, and the xenarthrous articulation (Emerling and Springer, 2015; Frechkop, 1949; Jenkins, 1970; Nyakatura and Fischer, 2011; Olson et al., 2016; Vizcaíno and Milne, 2002). Xenarthrous articulations, or xenarthrae, are ancillary intervertebral articulations found across the posterior thoracic and lumbar vertebrae, spanning the post-diaphragmatic region of xenarthrans (e.g. Gaudin, 1999). These articulations are formed between the enlarged anapophysis of the cranial vertebra, and the enlarged metapophysis of the caudal vertebra in an articulating pair of vertebrae (Fig. 1A). Although enlarged metapophyses and anapophyses are not uncommon across modern mammals (Filler, 2007), the two only articulate this way in xenarthrans. In the fossil record, however, xenarthrous articulations are not limited to xenarthrans, and have evolved convergently in unrelated Mesozoic mammals (Luo and Wible, 2005; Martin et al., 2015). The condition of xenarthry is found in all known modern and fossil xenarthrans with two exceptions: modern sloths and extinct glyptodonts. Modern sloths have secondarily lost the articulation, and the corresponding vertebrae in glyptodonts are instead fused to each other and to the massive carapace (Gaudin, 1999).

Xenarthrous articulations are thought to stiffen the vertebral column (Frechkop, 1949; Gaudin, 1999; Gaudin and Biewener, 1992; Jenkins, 1970). By stabilizing the trunk, xenarthrae are hypothesized to help brace the body, thereby freeing and providing leverage to the forelimbs when digging (Frechkop, 1949; Jenkins,

[1]Museum of Comparative Zoology and Department of Organismic and Evolutionary Biology, Harvard University, Cambridge, MA 02138, USA. [2]Institut des Sciences de l'Evolution, UMR 5554, CNRS, IRD, EPHE, Université de Montpellier, 34090 Montpellier, France. [3]Department of Biology, Valdosta State University, Valdosta, GA 31698-0015, USA.

*Authors for correspondence (spierce@oeb.harvard.edu; jillian_oliver@brown.edu)

S.E.P., 0000-0003-0717-1841

Received 3 May 2016; Accepted 14 July 2016

Journal of Experimental Biology (2016) 219, 2991-3002 doi:10.1242/jeb.142331

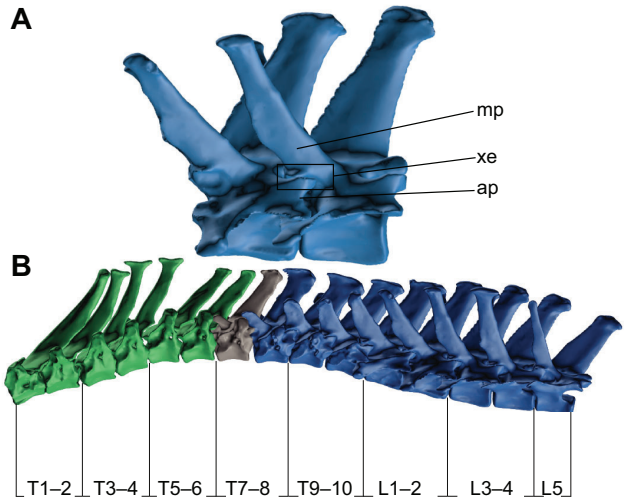

Fig. 1. The xenarthrous articulation and motion segments of *Dasypus novemcinctus* used in experimentation. (A) The second and third lumbar vertebrae are shown in articulation, with the metapophysis (mp), anapophysis (ap) and xenarthrous articulation (xe) labeled. (B) The 10 thoracic vertebrae (T1–10) are subdivided into five, and the first four lumbar vertebrae (L1–4) are subdivided into two motion segments. The first six thoracic vertebrae (T1–6, green), divided into three motion segments, are pre-xenarthrous and pre-diaphragmatic. T7 (grey) is the diaphragmatic vertebra, and all vertebrae caudad (T8–L5, blue) are xenarthrous and post-diaphragmatic. The four motion segments caudal to T6 articulate via xenarthrous and post-diaphragmatic articulations (T7–L4).

1970). Additionally, xenarthrae have been suggested to increase the vertebral surface area available to resist compression, resulting in the safer transmission of axial forces generated by digging (Gaudin and Biewener, 1992). Gaudin and Biewener (1992) investigated the involvement of xenarthry in axial stability with a biomechanical study of the armadillo vertebral column. They found an increase in lateral and dorsal stiffness, as well as shear, in the xenarthrous region of the nine-banded armadillo (*Dasypus novemcinctus*) relative to the corresponding region in the opossum, their choice of ancestral mammal, thus corroborating Frechkop and Jenkins' hypotheses (Frechkop, 1949; Jenkins, 1970). They were, however, unable to directly link this increased stiffness to the xenarthrous morphology itself.

Here we further explore the mechanical implications of xenarthrous articulations by conducting a detailed examination of the functional association between xenarthrous morphology and vertebral bending mechanics in the nine-banded armadillo, *D. novemcinctus* Linnaeus 1758. To do this, we quantify multi-axis bending mechanics of excised thoracolumbar joints spanning the pre-xenarthrous and xenarthrous regions, and correlate this with the bony morphology of individual vertebrae. By examining both pre- and xenarthrous regions, we are able to add context to the findings of Gaudin and Biewener (1992), who focused on the mechanics of xenarthrous vertebrae alone. In addition to allowing a direct comparison with the mechanical work of Gaudin and Biewener (1992), we chose to study *D. novemcinctus* because it displays a generalized plesiomorphic xenarthrous morphology, is considered a good model for the evolution of xenarthry, and is readily accessible because of its wide ecological range and large population sizes (Gaudin, 1999; Loughry and McDonough, 2013). Our approach provides the opportunity to link xenarthrous vertebrae to the mechanical and morphological regionalization of the *D. novemcinctus* vertebral column, thereby affording more insight into the role of these articulations during movement.

MATERIALS AND METHODS

Specimens and vertebra preparation

We examined eight wild-caught adult *D. novemcinctus* specimens (Table 1) that were packed and frozen as soon as possible after collection. Armadillo carcasses were collected by W.J.L. under Georgia Department of Natural Resources Scientific Collecting Permit CN91349 and by Frank M. Knight under Arkansas Game and Fish Scientific Collecting Permit 112020121, and donated to the Museum of Comparative Zoology and Department of Organismic and Evolutionary Biology, Harvard University, for experimentation and future curation.

Specimens were thawed over two nights at temperatures just above freezing before dissection. Vertebral columns were excised and the thoracolumbar region was divided into seven 'motion segments' that each included two vertebrae connected by an intervertebral joint (Fig. 1B). The thoracic (T) region was divided into five motion segments (T1–2, T3–4, T5–6, T7–8 and T9–10; Fig. 1B), while the lumbar (L) region was divided into two motion segments (L1–2 and L3–4; Fig. 1B). Following division into motion segments, remaining musculature was removed from each motion segment while leaving the intervertebral ligaments and joint capsule intact. Motion segments displaying any damage to the vertebrae or intervertebral joint were not analyzed.

The first three thoracic motion segments articulate via pre-diaphragmatic zygapophyseal articulations, and are also defined here as pre-xenarthrous, as they do not participate in xenarthrous articulations. In *D. novemcinctus*, the diaphragmatic vertebra is T7, which is also the most cranial vertebra to participate in a xenarthrous articulation (grey vertebra, Fig. 1B). It is not uncommon, however, to find small, non-articulating anapophyses and metapophyses on T5 or T6. All motion segments caudal to T5–6 are post-diaphragmatic and xenarthrous, indicating that the constituent vertebrae are joined by xenarthrous articulations in addition to post-diaphragmatic zygapophyseal articulations. In *D. novemcinctus*, the component bones of the sacrum are fully fused, making it difficult to isolate the motion segment formed by L5 and the first sacral vertebra. Moreover, visualization of movement within the joint was hindered by the large ilia. We therefore did not include the lumbosacral motion segment in our quantitative analyses, and will instead describe lumbosacral mobility qualitatively.

Experimental setup and measuring joint deflection

Prior to experimentation, stainless steel screws were fastened into holes drilled into the cranial aspect of the anterior vertebral centra of all but the first motion segment (T1–2), and into the caudal aspect of

Table 1. *Dasypus novemcinctus* specimens included in the study

Specimen	Nose–rump length (mm)	Mass (kg)	Sex (M/F)	Vertebrae included
MCZ 67401	411	3.60	M	T2–9, L1–4
MCZ 67402	418	3.30	M	T1–L4
MCZ 67403	391	3.40	F	T3–L2
MCZ 67405	321	4.60	F	T1–L4
MCZ 67406	310	4.00	M	T1–L4
MCZ 67407	361	4.65	F	T1–L4
MCZ 67408	414	4.55	F	T1–L2
MCZ 67411	450	5.67	M	T1–6

All females were pregnant. The vertebrae included in experimentation from each specimen are noted.

Journal of Experimental Biology (2016) 219, 2991-3002 doi:10.1242/jeb.142331

the posterior vertebral centra of all motion segments following the protocol detailed by Molnar et al. (2014). Drill bits and screws were marked so as to prevent penetration of the joint capsule. Digital X-ray images were taken of the joints following experimentation to ensure that all screws were positioned appropriately. The centrum of T1 in *D. novemcinctus* is too dorsoventrally compressed to support screws, so locking surgical forceps were used instead to clamp the vertebra and secure its immobility during experimentation. In all motion segments, the cranial screw (or forceps) was fastened by a clamp while leaving the caudal vertebra free to move about the intervertebral joint during the application of load. Physiological saline was applied to the motion segments throughout the preparation and experimentation processes.

To record angular deflection of the caudal vertebra under load, pins were secured in the neural spines of both vertebrae forming the motion segment during ventroflexion, in the ventral aspect of the centra during dorsiflexion, and in the right diapophyses or transverse processes during lateroflexion (Fig. 2A,B). Intervertebral deflection was recorded with a camera positioned in plane with the vertebrae, mounted on a tripod to ensure height equality between the motion segment and the camera.

The caudal vertebra of each motion segment was loaded incrementally with increasing metric masses (g) in ventroflexion, dorsiflexion and lateroflexion (see Table S1 for applied masses). Prior to loading, a calibration image was taken of the prepared unloaded motion segment in neutral position with a scale bar oriented relative to gravity using an inbuilt level (Fig. 2A). The caudal vertebra was loaded until no further substantial deflection was detected, as judged by the experimenter. Immediately upon loading, a photograph was taken (Fig. 2B), the mass was quickly removed and the vertebra was prodded gently back into neutral position in preparation for the next load.

Determining bending properties

Following the procedure of Molnar et al. (Fig. 2A,B; fig. 4 in Molnar et al., 2014), eight points on each of the images were

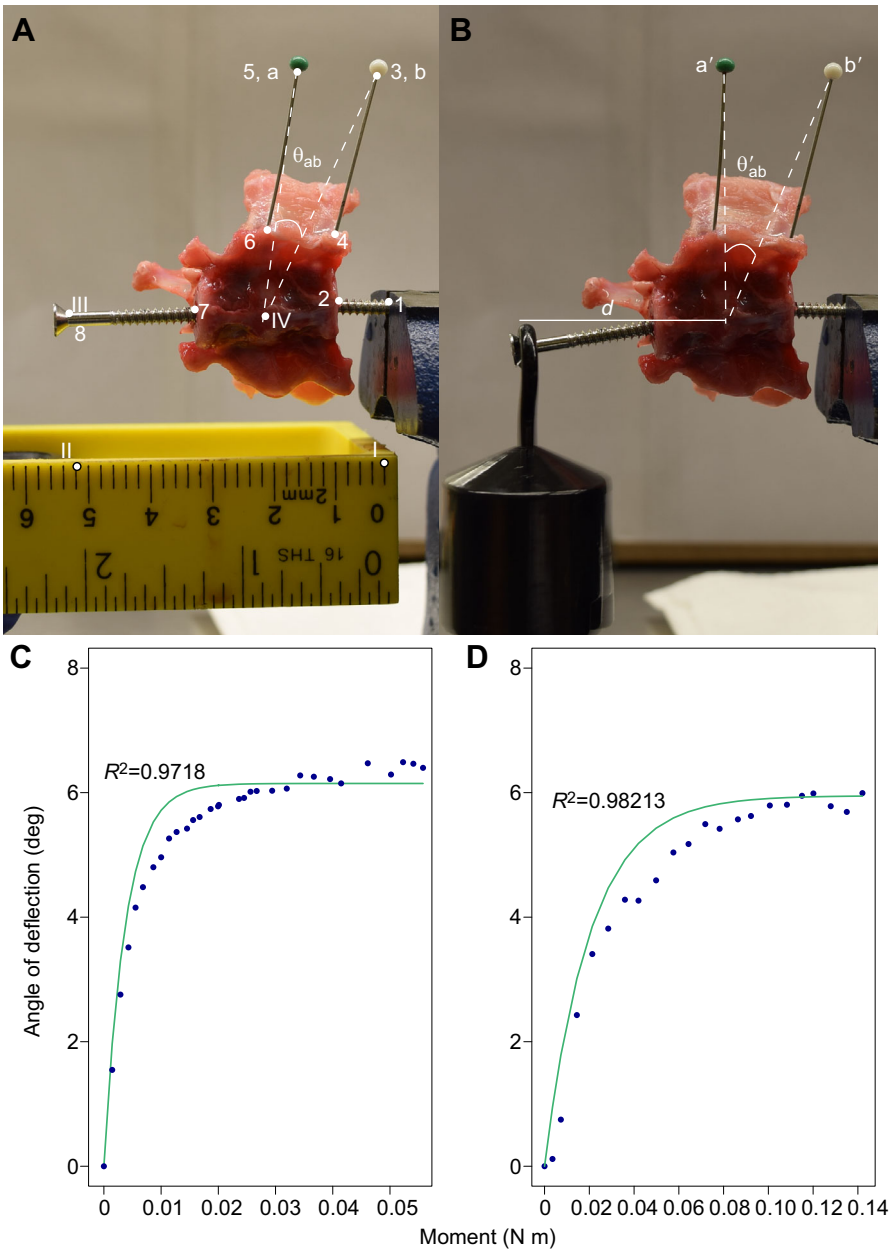

Fig. 2. Digitized points and angles of deflection on calibration and loading photos, with sample data. (A) Points I and II set the scale and orient the motion segment relative to gravity. Point III defines the location upon which a weight is placed, and Point IV defines the center of rotation. Points I–IV are digitized in calibration images only. Points 1–8 are digitized in calibration and loaded images. Points a and b are used with Point IV to define two vectors, the angle between which is the unloaded angle of deflection (θ_{ab}). (B) Points a′ and b′ are used with Point IV to define two vectors, the angle between which is the loaded angle of deflection (θ'_{ab}). The distance between Point IV and Point 8 is the moment arm, *d*. Angle of deflection according to moment in (C) ventroflexion of T3–4 and (D) lateroflexion of L1–2 in MCZ 67405 is plotted (e.g. strain-moment plot). Ventroflexion in T3–4 is characterized by high compliance, and lateroflexion in L1–2 by low compliance. Both are characterized by high range of motion. Negative exponential curves of the formula $\Delta\theta=R_m(1-e^{-CM})$ are fitted to the data. The R^2 values of the fit are provided.

Journal of Experimental Biology (2016) 219, 2991-3002 doi:10.1242/jeb.142331

digitized to measure angular deflection of and applied moment on the caudal vertebra. An additional four points were digitized on each calibration image to orient the joint relative to gravity, and to approximate the center of rotation. Center of rotation was approximated as the midpoint of the intervertebral disc. The same individual digitized all images. Digitization error was calculated as the standard deviation of deflection angles in 10 repeated digitization trials of a single randomly selected image (s.d. error=0.040 deg).

Moment and angular deflection for each applied mass in a trial were calculated using MATLAB version R2015a (MathWorks, Natick, MA, USA). The applied moment was calculated from points digitized on the images, and from the known mass applied in each image, with:

$$M = m \times \boldsymbol{g} \times d, \quad (1)$$

where m is the applied mass in kilograms, $\boldsymbol{g}$ is the acceleration due to gravity (9.81 m s^{-2}) and d is the horizontal distance in meters between the center of rotation of the joint and the point of attachment of the mass to the caudal screw, defined as the moment arm. Angle of deflection was likewise calculated from digitized points, with:

$$\Delta\theta = \theta'_{ab} - \theta_{ab}, \quad (2)$$

where the angle of deflection ($\Delta\theta$) is the angle between the two vectors created between the tips of each pin to the center of rotation in each loaded photograph (θ'_{ab}) minus the angle between the two vectors in the unloaded photograph (θ_{ab}) (as shown in Fig. 2A,B).

According to geometric similarity theory, moments were normalized by dividing by the product of body mass and nose–rump length (Hof, 1996). Nose–rump length was used in place of thoracolumbar length, which could not be consistently calculated as a result of broken vertebrae in some specimens. Angle of deflection was plotted against normalized moment to produce a strain-moment graph (e.g. Fig. 2C,D, Table S1). Deflection of the motion segment during load application was modeled as a negative exponential curve, as in Gál (1993a), with:

$$\Delta\theta = R_m(1 - e^{-CM}), \quad (3)$$

where $\Delta\theta$ is the angle of deflection in degrees, and M is the bending moment in newton meters (N m). Range of motion (R_m) is the asymptote at which the curve plateaus and is used as a measure of maximum range of motion. Compliance constant (C) is the rate constant that scales the curve, and is a measure of the rate at which the curve reaches its asymptote, R_m. C is thus proportional to compliance of the motion segment, or the inverse of stiffness. R_m and C were used to quantitatively describe bending mechanics across motion segments. For calculated R_m and C data, see Table S2.

Morphological measurements

Following experimentation, all motion segments were µCT-scanned on a SkyScan 1173 in the Museum of Comparative Zoology, Harvard University, reconstructed using NRecon version 1.6.6.0, and segmented and 3D volume rendered in Mimics Materialise software version 17.0. Thirteen linear measurements and seven angular measurements were recorded on each vertebra in Mimics by the same individual (Fig. 3). Measures were selected according to established determinants of stiffness and range of motion in other animals, and additional xenarthry-specific measures (metapophyseal and anapophyseal measures) were included in order to address the implications of xenarthry in compliance and range of motion.

Centrum height, neural spine height and pre-zygapophyseal angle have been suggested to be positively correlated with dorsoventral stiffness, centrum width and diapophysis/transverse process width positively correlated with lateral stiffness, and lamina width, pre-zygapophyseal width and transverse process/diapophysis angle positively correlated with stiffness in both planes. Centrum length has been suggested to be negatively correlated with dorsoventral stiffness, pre-zygapophyseal angle negatively correlated with lateral stiffness, and neural spine angle negatively correlated with stiffness in both planes. Dorsoventral transverse

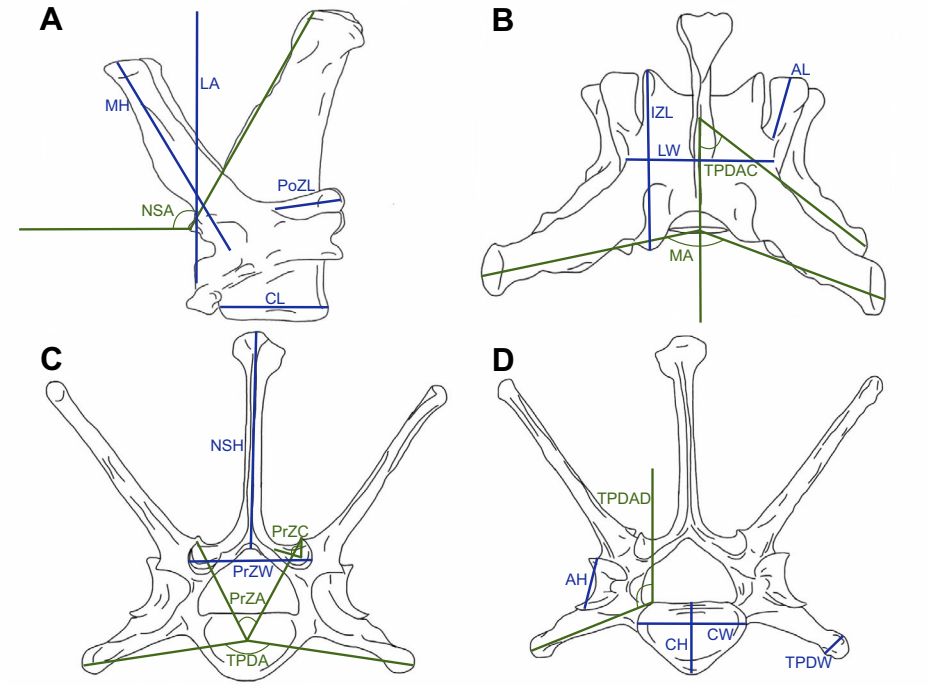

Fig. 3. Vertebral measurements. Thirteen linear measures and seven angular measures were taken on 3D models of each *D. novemcinctus* vertebra. For the purposes of this study, we are assuming homology between the thoracic diapophysis and the lumbar transverse process. (A) Lateral view. CL, centrum length; LA, lever arm; MH, metapophysis height; NSA, neural spine angle; PoZL, post-zygapophyseal length. (B) Dorsal view. AL, anapophysis length; IZL, inter-zygapophyseal length; LW, lamina width; MA, metapophysis angle; TPDAC, craniocaudal angle of transverse process/diapophysis. (C) Cranial view. NSH, neural spine height; PrZA, pre-zygapophyseal angle across vertebra; PrZC, curvature of pre-zygapophyseal facet; PrZW, pre-zygapophyseal width; TPDA, transverse process/diapophysis angle across vertebra. (D) Caudal view. AH, anapophysis height; CH, centrum height; CW, centrum width; TPDAD, dorsoventral angle of transverse process/diapophysis; TPDW, transverse process/diapophysis width. Linear measures are denoted in blue, and angular measures are denoted in green.

Journal of Experimental Biology

Journal of Experimental Biology (2016) 219, 2991-3002 doi:10.1242/jeb.142331

process/diapophysis angle and inter-zygapophyseal length have both been positively correlated with dorsoventral range of motion, and pre-zygapophyseal angle positively correlated with range of motion in lateroflexion. Centrum length, neural spine length, craniocaudal transverse process/diapophysis angle and neural spine angle have also been shown to be negatively correlated with range of motion in the sagittal plane (Buchholtz and Schur, 2004; Granatosky et al., 2014; Long et al., 1997; Molnar et al., 2014, 2015; Pierce et al., 2011).

Metapophyses and anapophyses and their corresponding linear and angular measures are, with some exception, specific to the xenarthrous region, and their influence on intervertebral mechanics is the focus of the present study. To address the almost total lack of metapophyses and anapophyses in pre-xenarthrous thoracic vertebrae, we followed the precedent set by Head and Polly (2015) and by Klingenberg (2008) in measuring the evolution of morphological novelty using homologous landmarks. Klingenberg (2008) suggested assigning landmarks to the fully formed structure of interest, and in its absence, to the position on the surface from which it would emerge. This method was coopted specifically for vertebrae by Head and Polly (2015), who were able to assign landmarks to vertebral morphologies not present in all measured vertebrae. This protocol was adapted here in pre-xenarthrous vertebrae, where measures concerning the metapophysis and anapophysis are set to zero.

Linear measures were normalized with Past version 3.07 according to nose–rump length to remove the effect of size, using the equation:

$$M_{\mathrm{adj}} = M\left(\frac{L_{\mathrm{S}}}{L_0}\right)^{b}, \tag{4}$$

where M_{adj} is the size-adjusted measurement, M is the original measurement, L_{S} is the mean nose–rump length in all specimens, L_0 is the nose–rump length of an individual and b is the slope of the regression of $\log(M)$ on $\log(L_0)$ for each measurement in all specimens (Elliott et al., 1995). Normalized, size-removed measures were used in all subsequent analyses. For raw measurement data, see Tables S3 and S4.

Statistical analyses

Two separate two-way ANOVAs were carried out on the bending data: one on the log-transformed compliance constant data, and one on the range of motion data. ANOVA models of the following design were used:

$$[C \text{ or } R_{\mathrm{m}}] = \text{Motion segment} + \text{Direction} + \text{Motion segment} \times \text{Direction} + \varepsilon, \tag{5}$$

where a significant interaction term indicates that craniocaudal patterns vary between bending directions. Compliance constant data were log transformed so as to increase the normality of their distribution. After an initial exploration of the data, a combined 64 out of 306 compliance constant and range of motion data points were removed because of low R^2 values of a motion segment (R^2<0.75), or errors in data collection. The ANOVAs were used to identify significant differences in compliance constant and range of motion between motion segments along the column, and between bending directions (independent variables). To locate differences, *post hoc* pairwise comparisons were performed with Bonferroni corrections for multiple comparisons.

A principal component analysis was performed on all normalized anatomical measures in order to identify which changes in morphology were most heavily implicated in shape variation and also to recover a series of independent and uncorrelated variables for comparison with the bending data. Following this, the first three principal components were regressed onto the compliance constant and range of motion data in each bending direction in a series of stepwise linear regressions. The first three principal components were chosen as independent variables because they each explained a minimum of 5% of the morphological variation across the thoracolumbar region and each represents a major transition across the vertebral column (see Results). Principal components were included in regression models if they contributed significantly to the R^2 value of said models. Further, each measure was regressed independently onto compliance constant and range of motion data to assess which individual measurements were most predictive of mechanical properties. All statistical analyses were carried out with SPSS version 22.0.

RESULTS

Compliance across thoracolumbar vertebrae

Changes in compliance constant (C) across the column followed a similar pattern in all three bending directions: the first motion segment exhibited low compliance, and was followed caudally by an increase, and then a decrease in compliance until T7–8, at which point the compliance constant steadied to a low plateau (Fig. 4A, see Table S2). This plateau of low compliance in all three directions

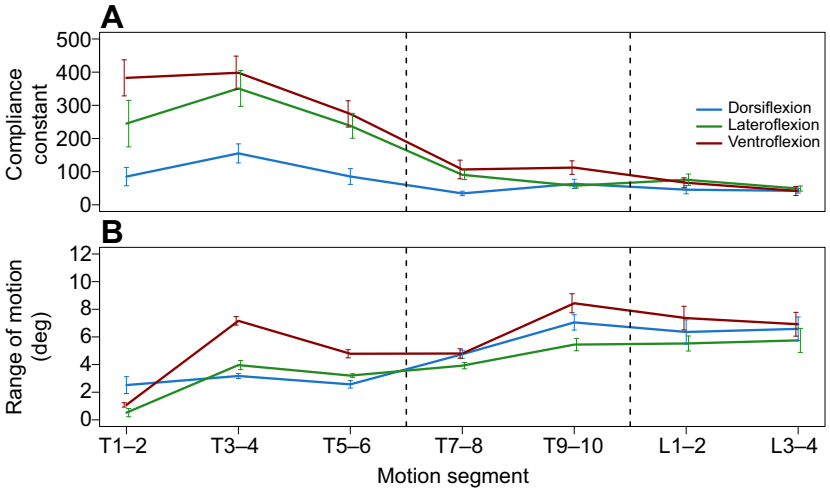

Fig. 4. Compliance and range of motion across thoracolumbar motion segments in *D. novemcinctus*. Mean normalized untransformed (A) compliance constant and (B) range of motion are plotted across thoracolumbar motion segments in all three bending directions. Error bars represent ±s.e.m. Dashed lines denote the transition from pre-diaphragmatic, pre-xenarthrous motion segments to post-diaphragmatic, xenarthrous motion segments, and the transition from thoracic to lumbar motion segments. Standard deviation of digitization error was 0.040 deg.

Journal of Experimental Biology (2016) 219, 2991-3002 doi:10.1242/jeb.142331

Table 2. Bonferroni-corrected pairwise *post hoc* comparisons of normalized, log-transformed compliance constant and range of motion between bending directions within each joint for *D. novemcinctus*

	T1–2 (10)	T3–4 (21)	T5–6 (22)	T7–8 (20)	T9–10 (21)	L1–2 (21)
Compliance constant						
Dorsiflexion–lateroflexion	0.563, 0.218, 0.033		0.514, 0.135, 0.001	0.444, 0.145, 0.008		
Dorsiflexion–ventroflexion	0.766, 0.190, <0.001	0.430, 0.140, 0.008	0.579, 0.139, <0.001	0.474, 0.145, 0.004		
Range of motion						
Dorsiflexion–ventroflexion		3.989, 0.681, <0.001	2.214, 0.674, 0.004			1.787, 0.701, 0.037
Lateroflexion–ventroflexion		3.201, 0.652, <0.001			2.989, 0.674, <0.001	1.836, 0.674, 0.022

Absolute mean difference, standard error and *P*-values are provided only for significant pairwise comparisons ($P \leq 0.05$) after correcting for multiple comparisons. Sample sizes of each motion segment are provided in parentheses. No significant pairwise differences were found between directions in either compliance or range of motion of L3–4.

spanned the entire measured post-diaphragmatic, xenarthrous portion of the thoracolumbar region. Although not quantified, visual inspection revealed that the lumbosacral joint formed by the fifth lumbar vertebra and the sacrum departed from this trend, and was very compliant in dorsiflexion and ventroflexion. In contrast, its mobility was totally restricted in lateroflexion by the ilia.

Spanning the measured motion segments, a significant difference in compliance constant was found between bending directions (Table 2, see Table S5). T3–4 was significantly less compliant in dorsiflexion than in ventroflexion (P=0.008), and T1–2, T5–6 and T7–8 were significantly less compliant in dorsiflexion than in both lateroflexion (P=0.033, 0.001, 0.008) and ventroflexion (P<0.001, <0.001, =0.004; Table 2). Compliance in all three directions was statistically indistinguishable in the region spanning T9–L4 (Table 2).

Compliance constants were significantly different across motion segments in each direction (Table 3, see Table S5). In dorsiflexion, T3–4 was significantly more compliant than T7–8 (P<0.001), L1–2 (P=0.001) and L3–4 (P=0.015; Table 3). In lateroflexion, T1–2 was significantly more compliant than L3–4 (P=0.036; Table 3). Caudally, T3–4 and T5–6 were significantly more compliant than the region spanning T7–L4 (Table 3). In ventroflexion, with the exception of significantly indistinguishable compliance constants in T5–6 and T9–10 (P=0.083), the region spanning T1–T6 was significantly more compliant than the region spanning T7–L4 (Table 3). Additionally, compliance in ventroflexion was significantly higher in T9–10 than in L3–4 (P=0.037; Table 3).

Range of motion across thoracolumbar vertebrae

As with compliance, range of motion (R_m) followed a similar pattern in all three bending directions (Fig. 4B, see Table S2). R_m was consistently lowest in T1–2, and increased caudally to reach a plateau at T9–10. A local peak in R_m was found at T3–4 in all three

Table 3. Bonferroni-corrected pairwise *post hoc* comparisons of normalized, log-transformed compliance constant and range of motion between joints, within bending directions, for *D. novemcinctus*

Compliance constant	Dorsiflexion (43)	Lateroflexion (43)	Ventroflexion (44)
T1–2 to T7–8			0.625, 0.179, 0.015
T1–2 to T9–10			0.569, 0.179, 0.041
T1–2 to L1–2			0.811, 0.179, <0.001
T1–2 to L3–4		0.700, 0.218, 0.036	1.058, 0.190, <0.001
T3–4 to T7–8	0.673, 0.150, <0.001	0.564, 0.139, 0.002	0.629, 0.135, <0.001
T3–4 to T9–10		0.740, 0.139, <0.001	0.573, 0.135, 0.001
T3–4 to L1–2	0.634, 0.145, 0.001	0.663, 0.139, <0.001	0.814, 0.135, <0.001
T3–4 to L3–4	0.548, 0.157, 0.15	0.811, 0.152, <0.001	1.061, 0.148, <0.001
T5–6 to T7–8		0.430, 0.135, 0.039	0.465, 0.139, 0.024
T5–6 to T9–10		0.606, 0.135, <0.001	
T5–6 to L1–2		0.529, 0.135, 0.003	0.651, 0.139, <0.001
T5–6 to L3–4		0.677, 0.148, <0.001	0.898, 0.152, <0.001
T9–10 to L3–4			0.488, 0.152, 0.037
Range of motion	**Dorsiflexion (42)**	**Lateroflexion (43)**	**Ventroflexion (44)**
T1–2 to T3–4		3.441, 1.010, 0.019	6.082, 0.853, <0.001
T1–2 to T5–6			3.701, 0.870, 0.001
T1–2 to T7–8		3.400, 1.010, 0.022	3.718, 0.870, 0.001
T1–2 to T9–10	4.535, 0.738, <0.001	4.923, 1.010, <0.001	7.353, 0.870, <0.001
T1–2 to L1–2	3.058, 0.763, 0.002	5.004, 1.010, <0.001	6.281, 0.870, <0.001
T1–2 to L3–4	4.068, 0.797, <0.001	5.228, 1.054, <0.001	5.836, 0.920, <0.001
T3–4 to T5–6			2.381, 0.652, 0.009
T3–4 to T7–8			2.364, 0.652, 0.009
T3–4 to T9–10	3.877, 0.701, <0.001		
T3–4 to L1–2	2.400, 0.728, 0.028		
T3–4 to L3–4	3.410, 0.763, <0.001		
T5–6 to T9–10	4.483, 0.674, <0.001	2.242, 0.652, 0.018	3.652, 0.674, <0.001
T5–6 to L1–2	3.006, 0.701, 0.001	2.323, 0.652, 0.012	2.580, 0.674, 0.005
T5–6 to L3–4	4.015, 0.738, <0.001	2.546, 0.718, 0.012	
T7–8 to T9–10	2.304, 0.701, 0.029		3.634, 0.674, <0.001
T7–8 to L1–2			2.562, 0.674, 0.005

Absolute mean difference, standard error and *P*-value are provided only for significant pairwise comparisons ($P \leq 0.05$) after correcting for multiple comparisons. Sample sizes of each direction are provided in parentheses.

Journal of Experimental Biology

Journal of Experimental Biology (2016) 219, 2991-3002 doi:10.1242/jeb.142331

directions, and was especially pronounced in ventroflexion (Fig. 4B).

Caudal to T1–2, range of motion was almost consistently higher in ventroflexion than in dorsiflexion and lateroflexion (Fig. 4B). R_m was higher in dorsiflexion than lateroflexion in all motion segments except for T3–4 and T5–6 (Fig. 4B). R_m in ventroflexion was significantly higher than in dorsiflexion and lateroflexion in T3–4 and L1–2 (Table 2). In T5–6, R_m in ventroflexion was significantly higher than in dorsiflexion (P=0.004), and in T9–10, R_m in ventroflexion was significantly higher than in lateroflexion (P<0.001; Table 2).

Range of motion differed significantly across the column in all three bending directions (Table 3, see Table S5). In dorsiflexion, the region spanning T1–T6 was characterized by a significantly lower R_m than that of T9–L4, and R_m in T7–8 was significantly lower than in T9–10 (Table 3). In lateroflexion, R_m in T1–2 was significantly lower than all motion segments except T5–6 (Table 3). R_m was significantly lower in T5–6 than in the motion segments spanning T9–L4 (Table 3). In ventroflexion, R_m in T1–2 was significantly lower than in all caudad motion segments, and R_m in T3–4 was significantly higher than in the two motion segments caudad (Table 3). R_m in T5–8 was significantly lower than in T9–L2 (Table 3). A significant interaction was found between motion segment and direction (see Table S5).

Changes in thoracolumbar morphology

A principal component analysis conducted on the morphological measures found that the first three components explained 82.7% of the variance in the thoracolumbar vertebral morphology of *D. novemcinctus* (Table 4, Fig. 5). The first three components were the only components with corresponding eigenvalues greater than 1, and that explained more than 5% of the variance (Table 4, see Table S6 for scores).

Table 4. Rotated principal component matrix, using the Varimax method with Kaiser normalization

	PC1	PC2	PC3
	10.598 (52.991)	4.342 (21.710)	1.603 (8.017)
MA	**0.943**	0.169	−0.019
AL	**0.907**	0.316	0.048
AH	**0.880**	0.344	−0.015
IZL	**0.841**	0.402	−0.048
PoZL	**−0.796**	−0.061	0.210
MH	**0.762**	0.559	0.015
NSH	−0.714	0.003	0.249
PrZA	−0.713	−0.228	0.098
PrZC	−0.690	−0.327	−0.183
CH	0.669	0.318	−0.537
TPDAC	−0.278	**−0.890**	−0.167
TPDAD	0.472	**0.839**	0.015
CL	0.551	0.601	−0.042
TPDA	0.531	0.532	0.348
CW	0.026	0.053	**0.968**
PrZW	−0.149	0.254	**0.789**
LA	−0.010	0.381	0.201
TPDW	−0.311	0.010	0.099
LW	−0.059	0.189	0.273
NSA	−0.590	−0.121	0.226

All morphological measures are presented, along with the extent to which each is weighted in the first three principal components. See Fig. 2 for measurement abbreviations. Eigenvalue scores of each principal component are included, as well as percent variance explained in parentheses. The first three principal components (PC1, PC2, PC3) each explained more than 5% of the variance and had an eigenvalue greater than 1, and were thus included in further analysis. Measures and corresponding weights are bolded when highly weighted (≥±0.75).

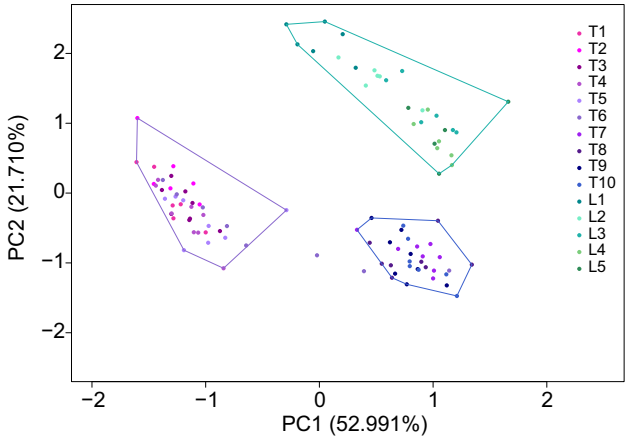

Fig. 5. Vertebrae of *D. novemcinctus* plotted according to scores of principal component 2 (PC2) against principal component 1 (PC1). Along PC1, pre-xenarthrous, pre-diaphragmatic vertebrae (T1–6) are identified by more strongly negative principal component scores, while xenarthrous, post-diaphragmatic vertebrae (T7–L5) have more strongly positive scores. Spanning the transition between pre-xenarthrous and xenarthrous vertebrae is T6, on which metapophyses and anapophyses are found only in some individuals. Along PC2, more strongly negative scores typify thoracic vertebrae, and more strongly positive scores identify lumbar vertebrae. Percent variance explained by PC1 and PC2 are provided.

The first component (PC1), which explained 53.0% of the variance, effectively distinguished between pre-diaphragmatic pre-xenarthrous, and post-diaphragmatic xenarthrous vertebrae (Table 4, Fig. 5). PC1 was most heavily weighted (≥±0.75) in six anapophyseal, metapophyseal and zygapophyseal measurements, with all measures showing substantial changes in value between T6 and T7, or between T7 and T8 (Table 4, Fig. 6A–C). As the cranialmost anapophysis and metapophysis are typically found in T7, with exceptional presence in T5 and T6, anapophysis length (AL) and height (AH), and metapophysis angle (MA) increased starkly from values close to zero prior to T7 (Fig. 6A,B). Metapophysis height (MH) followed a similar trend, although it increased steadily rather than sharply from T6 caudad, decreasing slightly in L5 (Fig. 6C). Inter-zygapophyseal length (IZL) increased and post-zygapophyseal length (PozL) decreased at T7, reflecting the post-diaphragmatic, post-zygapophyseal morphology of the diaphragmatic vertebra, T7 (Fig. 6C).

The second component, which explained 21.7% of the variance, was most heavily weighted in diapophysis and transverse process measures (Table 4, Fig. 5), with transverse process/diapophysis craniocaudal angle (TPDAC) decreasing and transverse process/diapophysis dorsoventral angle (TPDAD) increasing between T10 and L1 (Fig. 6D). These changes mark the transition from diapophysis to transverse process, which signifies a morphological switch from thoracic to lumbar vertebrae.

The third component (PC3), which accounted for 8.0% of the variance, was most heavily weighted in centrum width (CW) and pre-zygapophyseal width (PrZW), with both measures being highest in T1 and decreasing to reach a somewhat steady level by T3 (Table 4, Figs 5, 6E). PC3 therefore appears to distinguish the most anterior thoracic vertebrae from the remaining thoracolumbar region.

Predictors of compliance constant and range of motion

A series of stepwise linear regressions using the first three principal components derived above as independent variables were performed on compliance constant and range of motion data in all

Journal of Experimental Biology (2016) 219, 2991-3002 doi:10.1242/jeb.142331

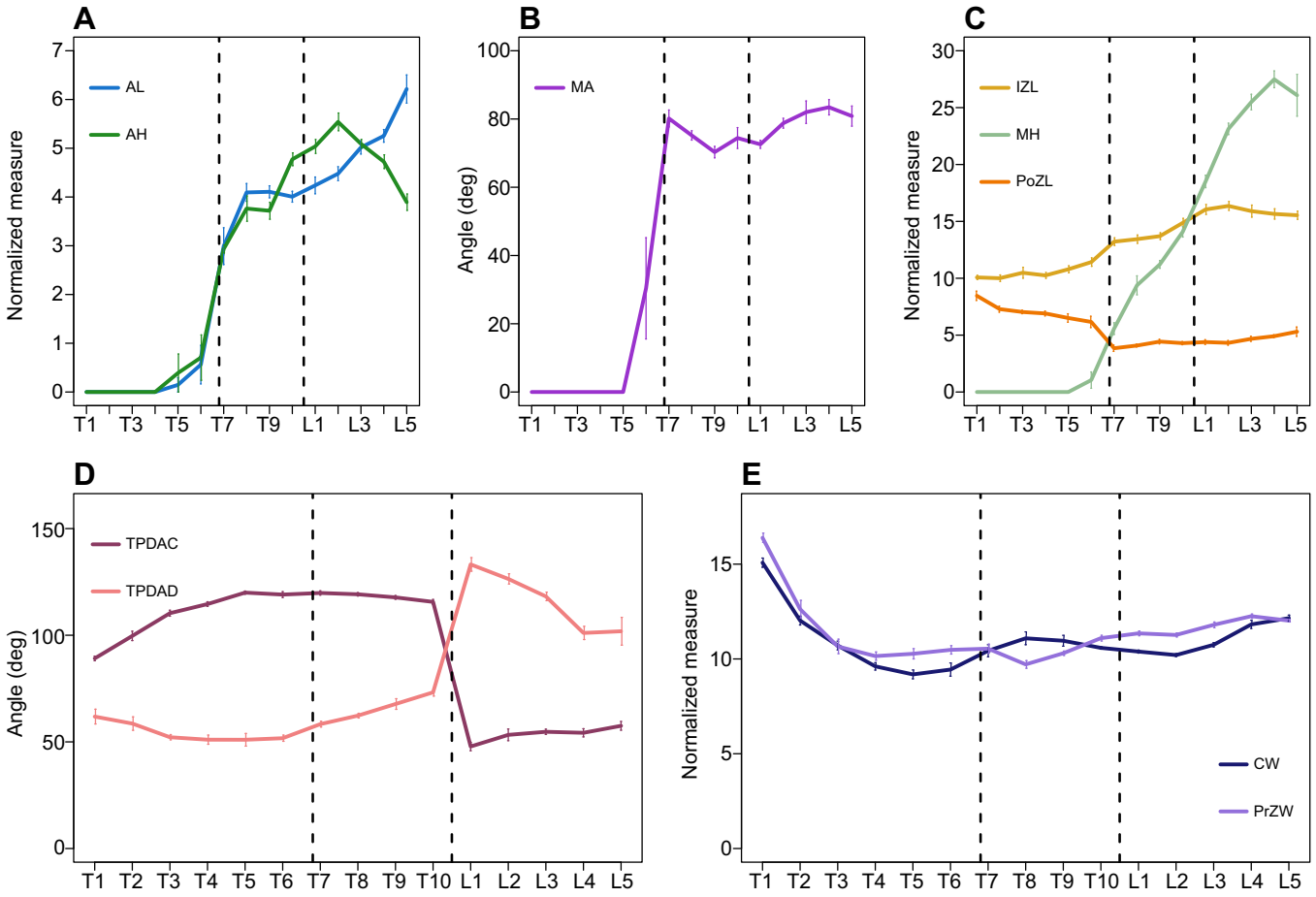

Fig. 6. Mean size-adjusted measurements in which PC1–3 are most heavily weighted (≥±0.75). PC1 is heavily weighted in (A) AL and AH, (B) MA and (C) IZL, MH and PoZL. PC2 is heavily weighted in (D) TPDAC and TPDAD. PC3 is heavily weighted in (E) CW and PrZW. Error bars represent ±s.e.m. See Fig. 2 for measurement abbreviations. Dashed lines denote the location of the diaphragmatic vertebra (T7), and the transition from thoracic to lumbar vertebrae.

three bending directions. Models composed of PC1 and PC2 were found to be predictive of compliance in all three directions, and of range of motion in dorsiflexion and lateroflexion (Table 5). A model composed of PC1 and PC3 was found to be predictive of range of motion in ventroflexion (Table 5). Several correlated measures were found to be predictive of compliance and range of motion in all three directions (see Tables S7, S8).

DISCUSSION

To illustrate the relationship between morphological regionalization and bending mechanics in the vertebral column of the nine-banded armadillo, we examined morphology, compliance and maximum range of motion during multi-axis bending in thoracolumbar vertebral joints. Although there are significant differences in mechanical properties between bending directions, compliance and range of motion follow similar patterns in all three directions: compliance decreases and range of motion increases caudally along the column in both dorsoventral (sagittal) and lateral flexion. These patterns in joint mechanics correspond to morphological regionalization prescribed by both the transition from pre-diaphragmatic, pre-xenarthrous vertebrae to post-diaphragmatic, xenarthrous vertebrae, and the transition from thoracic to lumbar vertebrae.

Of note is the first thoracic joint (T1–2), which is characterized by a very low range of motion and high compliance (Fig. 4). These traits define the intervertebral joint formed by T1 and T2 as one that will readily bend, but is restricted to a very small degree of bending, especially in lateroflexion and ventroflexion. Centrum and pre-zygapophyseal width are both substantially higher in the first two thoracic vertebrae than in all other thoracic vertebrae (Fig. 6E). Additionally, although not measured, visual observation revealed that the intervertebral disc formed between T1 and T2 is substantially thinner than in all caudad intervertebral joints. Such a wide and thin area of contact between centra has been suggested to restrict mobility of vertebral motion segments (Buchholtz and Schur, 2004; Long et al., 1997). This morphology and lack of mobility are also characteristic of the cervical region of *D. novemcinctus*. Although we did not measure compliance or range of motion in cervical vertebrae, qualitative manipulation revealed that it contains only two centers of flexion: between the atlas and axis, and between the sixth and seventh cervical vertebrae. Excluding the third and fourth cervical vertebrae, which are fused to the axis in the mesocervical bone characteristic of armadillos (Galliari et al., 2010), there is remarkable rigidity from the fourth to sixth cervical vertebrae, and between the seventh cervical and first thoracic vertebrae. With the exception of the long neural spines of the first two thoracic vertebrae, the morphology of the joint formed between them is remarkably similar to those in the cervical region. The cervical-like morphology and rigidity of T1–2 is a reflection of the transitional nature of this intervertebral joint, and especially of the first thoracic vertebra itself. In *Mus musculus*, the first thoracic vertebra is morphologically more similar to the cervical vertebrae than to the other thoracic vertebrae, and is also located in a position

Journal of Experimental Biology (2016) 219, 2991-3002 doi:10.1242/jeb.142331

Table 5. Principal component predictors of compliance constant and range of motion in three bending directions

Direction	Model	Coefficient	s.e.m.	s.c.	T (P)	R^2 (P)
Compliance constant						
Dorsiflexion (80)	Whole	1.709	0.038		45.248 (<0.001)	0.211 (<0.001)
	PC1	−0.159	0.040	−0.409	−4.029 (<0.001)	
	PC2	−0.083	0.035	−0.239	−2.356 (0.021)	
Lateroflexion (82)	Whole	2.038	0.026		77.134 (<0.001)	0.584 (<0.001)
	PC1	−0.284	0.028	−0.727	−10.006 (<0.001)	
	PC2	−0.090	0.025	−0.264	−3.638 (<0.001)	
Ventroflexion (84)	Whole	2.105	0.027		78.107 (<0.001)	0.678 (<0.001)
	PC1	−0.335	0.028	−0.750	−11.870 (<0.001)	
	PC2	−0.158	0.026	−0.391	−6.186 (<0.001)	
Range of motion						
Dorsiflexion (80)	Whole	4.853	0.176		27.538 (<0.001)	0.508 (<0.001)
	PC1	1.574	0.184	0.685	8.543 (<0.001)	
	PC2	0.514	0.165	0.249	3.110 (0.003)	
Lateroflexion (82)	Whole	4.382	0.139		31.456 (<0.001)	0.322 (<0.001)
	PC1	0.747	0.149	0.463	4.994 (<0.001)	
	PC2	0.489	0.131	0.346	3.737 (0.001)	
Ventroflexion (84)	Whole	6.101	0.241		25.352 (<0.001)	0.101 (0.014)
	PC1	0.629	0.245	0.275	2.568 (0.012)	
	PC3	−0.618	0.307	−0.216	−2.012 (0.048)	

A stepwise linear regression was performed on compliance constant and range of motion data in each direction, using PC1–3 as independent variables. Models are listed with their R^2, along with model coefficient, standard error (s.e.m.) and T-values. Components of each model are listed with their coefficient, s.e.m., standardized coefficient (s.c.) and T-values. P-values associated with T and R^2 are listed in parentheses with their corresponding values. See Table S8 for individual measure predictors. Sample sizes of each model are provided in parentheses.

of overlap of *Hox* genes prescribing cervical and thoracic patterning (Head and Polly, 2015; reviewed in Wellik, 2007). The morphological and mechanical similarities between most of the cervical vertebrae and the first two thoracic vertebrae suggests a shared function for these vertebrae.

Within each bending direction, thoracic joint T3–4 is the most compliant of all motion segments, and has the highest range of motion of all pre-diaphragmatic motion segments (Fig. 4). Additionally, visual examination during experimentation revealed that T3–4 undergoes rotational motion quite readily, particularly during lateroflexion. Together, these traits define a highly flexible and mobile joint. The high compliance found in T3–4 fits in with the other pre-xenarthrous thoracic motion segments. Barring T1–2, which has a cervical nature, T3–4 is part of a series of compliant motion segments that decreases in compliance until reaching a post-diaphragmatic plateau. Its range of motion, however, deviates from the low values of the pre-xenarthrous thoracics in ventroflexion (Fig. 4B). While range of motion in ventroflexion is predicted by a model composed of PC1 and PC3, neither principal component can account for such a spike at T3–4. Indeed, while the regression model composed of PC1 and PC3 is significantly predictive of range of motion in ventroflexion, it had the least support of all directions (Table 5). Therefore, although our methods appear successful in developing predictive models of compliance in all three bending directions, and of range of motion in lateroflexion and dorsiflexion, they are not as successful at predicting range of motion in ventroflexion. This shortcoming agrees with findings from domestic horses that bony morphology is not as powerful at predicting range of motion in ventroflexion as in dorsiflexion (Jones, 2016). Instead, architecture and elasticity of the supraspinous ligament and ligamenta flava are likely more predictive of range of motion in ventroflexion (Gál, 1993b; Jones, 2016). Gál (1993b) found that the ligamenta flava, the ligament extending from axis to sacrum that connects successive vertebral laminae, was a primary component of resistance to flexion in several small mammals, whose size range includes *D. novemcinctus*. To identify the soft tissue drivers behind range of motion in ventroflexion in *D. novemcinctus*, it may be worthwhile to perform successive lesion experiments.

Upon xenarthry, compliance and range of motion reach a relative plateau in all three bending directions (Fig. 4), with post-diaphragmatic, xenarthrous motion segments being characterized by a similarly low compliance (from T7–8 caudad) and high range of motion (from T9–10 caudad). The decrease in compliance clearly aligns with the initial appearance of xenarthry and the diaphragmatic transition at the T7–8 motion segment, and is supported by the prominence of PC1 in regression models predicting compliance (Table 5, Figs 4, 6). These results support the theory that the xenarthrous region confers a lower compliance, or a higher stiffness, to the xenarthran vertebral column (Frechkop, 1949; Gaudin, 1999; Gaudin and Biewener, 1992; Jenkins, 1970). Xenarthrous articulations thus appear to function as a stiffening mechanism in concert with the post-diaphragmatic zygapophyseal articulations found on the same vertebrae.

In their investigation into vertebral bending mechanics in *D. novemcinctus* and the Virginia opossum, *Didelphis virginiana*, Gaudin and Biewener (1992) found that the xenarthrous region of *D. novemcinctus* is stiffer in lateroflexion and dorsiflexion than is the corresponding region of *D. virginiana*. In contrast, they found that bending in ventroflexion was significantly less stiff than in lateroflexion and dorsiflexion, and was comparable to that in *D. virginiana*. Additionally, they found no difference in the degree of axial rotation between *D. novemcinctus* and *D. virginiana*. Our results appear to both support and contradict those of Gaudin and Biewener, as we found that the higher stiffness in lateral and dorsal bending is statistically indistinguishable from the similarly high stiffness in ventral bending in the region spanning T9–L4 (Table 2). This difference may be accounted for by the methods employed in our studies. In their protocol, Gaudin and Biewener measured stiffness in vertebrae including and caudal to T6 as a single unit connected by ligaments, while we measured compliance across the thoracolumbar region in units of two vertebrae. As our results demonstrate, T6, and to some extent T7, are more similar morphologically to craniad pre-xenarthrous vertebrae than to caudad xenarthrous vertebrae (Fig. 6A–

Journal of Experimental Biology (2016) 219, 2991-3002 doi:10.1242/jeb.142331

C), and the joint formed between T5 and T6 is also mechanically more similar to more cranial vertebrae (Table 3, Fig. 4). Although we did not measure compliance in the joint formed between T6 and T7, based on morphology, we assume that its compliance is likely intermediate between that of T5–6 and T7–8 (Fig. 6). In Gaudin and Biewener's results, the stiffness imparted to the column by the intervertebral joint connecting T6 and T7 cannot be distinguished from the resultant stiffness of all caudad intervertebral joints. It is therefore possible that the relative compliance of the cranialmost intervertebral joint measured by Gaudin and Biewener masks the stiffness of the remainder of the column, resulting in a low stiffness in ventroflexion that is comparable to that of *D. virginiana*.

In contrast to compliance, the link between high range of motion and post-diaphragmatic, xenarthrous morphology is less striking, because of the apparent misalignment between the diaphragmatic vertebra, T7, and the increase in range of motion at T9–10 (Figs 4B, 6A–C). Nonetheless, our data do implicate xenarthrous articulations and post-diaphragmatic zygapophyses with an increase in range of motion, as PC1, which was heavily weighted in xenarthrous and zygapophyseal measures, was found to be predictive of range of motion in all three bending directions (Tables 4, 5). It appears that, rather than acting as bony stops, xenarthrous articulations may help to amplify the observed effects of the curved, protruding post-diaphragmatic zygapophyses in mammals, which permit and secure flexion by increasing the surface area upon which vertebrae can slide without disarticulating, thereby enhancing range of motion (Filler, 2007; Jenkins, 1974; Pierce et al., 2011; Russo, 2010; Shapiro, 1995). In functioning in this way, xenarthrous articulations may extend beyond a purely stabilizing role and increase range of motion by providing greater surface area for movement. Hebrank et al. (1990) found a similar result in blue marlins. In a manner analogous to xenarthrans, marlin vertebrae have a unique interlocking morphology that allows for bending in lateroflexion, while restricting sagittal flexion and extension. Hebrank et al. (1990) suggest that these interlocking facets increase lateral bending while preventing disarticulation of the involved vertebrae. Further analysis into regional variation in bending mechanics in mammals without xenarthrous articulations would help clarify the contributions of xenarthrous articulations to range of motion, thereby elucidating whether xenarthrae enhance the suggested effects of post-diaphragmatic zygapophyses on mobility.

In addition to intervertebral articulations, we propose that enlarged metapophyses influence the high range of motion seen in the motion segments caudal to T7–8. Though metapophyses are present on T7 and T8, they are quite short (Fig. 1B, Fig. 6C, MH). Caudal to T8, metapophyses increase in height to become massive processes with the capacity for increased ligament and muscle insertion, thus enabling a higher range of motion (Buchholtz and Schur, 2004; Granatosky et al., 2014; Pierce et al., 2011; Shapiro, 1995). As evidenced by the involvement of PC2 in models predicting both compliance and range of motion, lumbar morphology is also correlated with higher range of motion (Table 5). Our results agree with those of Gaudin and Biewener (1992), who found that in *D. novemcinctus*, lumbar vertebrae reach higher levels of angular displacement than do thoracic vertebrae. Interestingly, Gaudin and Biewener found that thoracic and lumbar vertebrae in *D. virginiana* do not differ markedly in angular displacement, thus substantiating our claim that the xenarthrous and metapophyseal morphology of *D. novemcinctus* confer an increase in range of motion relative to a purported ancestral mammal.

Investigations into stiffness and compliance of the vertebral column, either as a whole unit or separated into distinct motion segments, are common (e.g. Gaudin and Biewener, 1992; Hebrank et al., 1990; Granatosky et al., 2014; Long et al., 1997; Molnar et al., 2014). Also common are data on maximum range of motion achievable by manual flexion or by simulation (e.g. Jones, 2016; Jeffcott and Dalin, 1980; Molnar et al., 2015; Townsend et al., 1983). However, the interplay between compliance or stiffness and range of motion is one that is often overlooked (Gál, 1993a; Molnar et al., 2015). Our study has shown that xenarthrous articulations do indeed appear to stiffen the armadillo vertebral column, but they may also confer an increase in range of motion. Consequently, the xenarthrous region of *D. novemcinctus* is very stiff, but also highly mobile under a substantial enough load. Gál (1993a) also found that stiff vertebral columns do not necessarily preclude mobility. Much like in post-diaphragmatic bending in *D. novemcinctus*, lumbosacral bending in monkeys and wallabies is characterized by relatively low compliance and high range of motion (Gál, 1993a). As stressed by these results, it is imperative that further investigations into vertebral bending address both compliance/stiffness and range of motion to arrive at comprehensive conclusions on bending mechanics.

The stiffness and range of motion conferred by xenarthrous articulations have significant implications for movement. Although Gaudin and Biewener (1992) concluded that the increase in lateral and dorsal stiffness they found in *D. novemcinctus* would aid in resisting the laterally and dorsally directed forces generated by digging (Gasc et al., 1986), they argued that the low stiffness they found in ventroflexion does not support Frechkop's claim that stiffness in ventroflexion would be necessary to support the weight of the forelimbs and trunk during digging (Frechkop, 1949). In contrast, our results suggest that stiffness in all three directions is fostered by xenarthrous vertebrae, allowing for the resistance of forces generated ventrally by the weight of the forelimbs and trunk, dorsally by the digging stroke against the substrate, and laterally by the alternating digging stroke (Frechkop, 1949; Gasc et al., 1986; Gaudin and Biewener, 1992). Passive stiffness of the xenarthrous region of the *D. novemcinctus* vertebral column thus precludes the need for substantial trunk muscle exertion when digging. An analogous role for passive vertebral stiffness in maintaining posture has been described by Smeathers and Gál in large mammals (Gál, 1993a; J. E. Smeathers, A mechanical analysis of the mammalian lumbar spine, PhD thesis, University of Reading, 1981).

Upon active muscle exertion, the xenarthrous region has the potential to become highly mobile because of an increase in joint range of motion. Such mobility is advantageous to an animal whose default vertebral condition is rigidity, as it facilitates the non-digging behaviours typical of mammals generally and of armadillos specifically, such as running, jumping, kicking and the rolling behaviour found in select species. Furthermore, the xenarthrous region roughly overlaps with the flexible banded portion of the nine-banded armadillo's carapace, suggesting that this potential for mobility is not limited by the carapace in *D. novemcinctus*. The extent to which xenarthry-associated range of motion can be realized in armadillos, however, likely varies according to species, reflecting the variation in carapace shape (Superina and Loughry, 2012). Also expected to be varied among armadillos is the prominence of the xenarthrous morphology itself. Armadillos demonstrate a wide range of digging behaviours, from fully subterranean to almost entirely cursorial (Vizcaíno and Milne, 2002). Although xenarthrous morphology has been described extensively in both orders of Xenarthra (Gaudin, 1999), a quantitative examination of relative size of xenarthrous articulations between species is lacking, as is a functional investigation into the relationship between extent of xenarthry and

degree of fossoriality across armadillo species. Following the proposed relationship between xenarthry and fossoriality, we expect there to be a positive correlation between the relative prominence of xenarthrous articulations and the degree of fossoriality across armadillos. As such, we also expect the most fossorial armadillos (e.g. pink fairy armadillo, giant armadillo) to be characterized by xenarthrous regions of the highest stiffness and range of motion.

Conclusions

The dual role of the post-diaphragmatic region in *D. novemcinctus* is conferred by the unique shape of the xenarthrous articulation, and by the associated enlarged metapophyses. The xenarthrous articulation itself stiffens and imparts mobility to the region through increased articular surface area. Adding to this, the metapophysis provides more room for ligament and muscle attachment and increases mechanical advantage, thereby facilitating the powered movement necessary for flexion under xenarthry (Buchholtz and Schur, 2004; Granatosky et al., 2014; Pierce et al., 2011; Shapiro, 1995). Our results demonstrate that the post-diaphragmatic region of *D. novemcinctus* is characterized by decreased compliance and increased range of motion, two traits that appear to be especially conducive to a semi-fossorial lifestyle.

Acknowledgements

We thank Judy Chupasko, Mark Omura and Mark Renczkowski [Museum of Comparative Zoology, Harvard Univeristy (MCZ)] for all of their help during the course of this project, Frank M. Knight (University of the Ozarks) for donating armadillo carcasses, and several colleagues in the MCZ for helping with experimental setup and data collection (Robert Kambic, Brianna McHorse, Blake Dickson and Hanna Barnes). A version of this paper was submitted by J.D.O. in partial fulfillment of the Erasmus Mundus Master Programme in Evolutionary Biology.

Competing interests

The authors declare no competing or financial interests.

Author contributions

Concepts and approach were developed by J.D.O., L.H. and S.E.P. Specimens were collected by W.J.L. Experiments and data analysis was performed by J.D.O., K.E.J. and S.E.P. The manuscript was prepared by J.D.O. and S.E.P., and edited by K.E.J., L.H. and W.J.L. prior to submission.

Funding

This study was partially funded by National Science Foundation grant number EAR-1524523 to S.E.P., and through a Category A Erasmus Mundus scholarship (European Commission) to J.D.O.

Supplementary information

Supplementary information available online at
http://jeb.biologists.org/lookup/doi/10.1242/jeb.142331.supplemental

References

Boszczyk, B. M., Boszczyk, A. A. and Putz, R. (2001). Comparative and functional anatomy of the mammalian lumbar spine. *Anat. Rec.* **264**, 157-168.
Buchholtz, E. A. (2001). Vertebral osteology and swimming style in living and fossil whales (Order: Cetacea). *J. Zool.* **253**, 175-190.
Buchholtz, E. A. and Schur, S. A. (2004). Vertebral osteology in Delphinidae (Cetacea). *Zool. J. Linn. Soc.* **140**, 383-401.
Cullinane, D. M. and Bertram, J. E. A. (2000). The mechanical behaviour of a novel mammalian intervertebral joint. *J. Anat.* **197**, 627-634.
Elliott, N. G., Haskard, K. and Koslow, J. A. (1995). Morphometric analysis of the orange roughy (*Hoplostethus atlanticus*) off the continental slope of southern Australia. *J. Fish Biol.* **46**, 202-220.
Emerling, C. A. and Springer, M. S. (2015). Genomic evidence for rod monochromacy in sloths and armadillos suggests early subterranean history for Xenarthra. *Proc. R. Soc. B. Biol. Sci.* **282**, 20142192.
Filler, A. G. (2007). *Axial Character Seriation in Mammals*. Boca Raton, USA: BrownWalker Press.
Frechkop, S. (1949). Explication biologique, fournie par les Tatous, d'un des caractères distinctifs des Xénarthres et d'un caractère adaptif analogue chez les Pangolins. *Inst. R. Sci. Natl. Belg.* **25**, 1-12.
Gál, J. M. (1993a). Mammalian spinal biomechanics. I. Static and dynamic mechanical properties of intact intervertebral joints. *J. Exp. Biol.* **174**, 247-280.
Gál, J. M. (1993b). Mammalian spinal biomechanics. II. Intervertebral lesion experiments and mechanisms of bending resistance. *J. Exp. Biol.* **174**, 281-297.
Galliari, F. C., Carlini, A. A. and Sánchez-Villagra, M. R. (2010). Evolution of the axial skeleton in armadillos (Mammalia, Dasypodidae). *Mamm. Biol.* **75**, 326-333.
Gasc, J. P., Jouffroy, F. K., Renous, S. and von Blottnitz, F. (1986). Morphofunctional study of the digging system of the Namib Desert golden mole (*Eremitalpa granti namibensis*): cinefluorographical and anatomical analysis. *J. Zool.* **208**, 9-35.
Gaudin, T. J. (1999). The morphology of xenarthrous vertebrae (Mammalia: Xenarthra). *Fieldiana* **41**, 1-38.
Gaudin, T. J. and Biewener, A. A. (1992). The functional morphology of xenarthrous vertebrae in the armadillo *Dasypus novemcinctus* (Mammalia, Xenarthra). *J. Morphol.* **214**, 63-81.
Granatosky, M. C., Lemelin, P., Chester, S. G. B., Pampush, J. D. and Schmitt, D. (2014). Functional and evolutionary aspects of axial stability in euarchontans and other mammals. *J. Morphol.* **275**, 313-327.
Head, J. J. and Polly, P. D. (2015). Evolution of the snake body form reveals homoplasy in amniote *Hox* gene function. *Nature* **520**, 86-89.
Hebrank, J. H., Hebrank, M. R., Long, J. H., Jr., Block, B. A. and Wright, S. A. (1990). Backbone mechanics of the blue marlin *Makaira nigricans* (Pisces, Istiophoridae). *J. Exp. Biol.* **148**, 449-459.
Hildebrand, M. (1959). Motions of the running cheetah and horse. *J. Mammal.* **40**, 481-495.
Hof, A. L. (1996). Scaling gait data to body size. *Gait Posture* **4**, 222-223.
Jeffcott, L. B. and Dalin, G. (1980). Natural rigidity of the horse's backbone. *Equine Vet. J.* **12**, 101-108.
Jenkins, F. A., Jr. (1970). Anatomy and function of expanded ribs in certain edentates and primates. *J. Mammal.* **51**, 288-301.
Jenkins, F. A., Jr. (1974). *Primate Locomotion*. New York, USA: Academic Press.
Jones, K. E. (2016). Preliminary data on the effect of osseous anatomy on *ex vivo* joint mobility in the equine thoracolumbar region. *Equine Vet. J.* **48**, 502-508.
Jones, K. E. and German, R. Z. (2014). Ontogenetic allometry in the thoracolumbar spine of mammal species with differing gait use. *Evol. Dev.* **16**, 110-120.
Jones, K. E. and Pierce, S. E. (2016). Axial allometry in a neutrally buoyant environment: effects of the terrestrial-aquatic transition on vertebral scaling. *J. Evol. Biol.* **29**, 594-601.
Klingenberg, C. P. (2008). Novelty and 'homology-free' morphometrics: what's in a name? *Evol. Biol.* **35**, 186-190.
Long, J. H., Jr., Pabst, D. A., Shepherd, W. R. and McLellan, W. A. (1997). Locomotor design of dolphin vertebral columns: bending mechanics and morphology of *Delphinus delphis*. *J. Exp. Biol.* **200**, 65-81.
Loughry, W. J. and McDonough, C. M. (2013). *The Nine-Banded Armadillo: A Natural History*. Norman, USA: University of Oklahoma Press.
Luo, Z.-X. and Wible, J. R. (2005). A late Jurassic digging mammal and early mammalian diversification. *Science* **308**, 103-107.
Martin, T., Marugán-Lobón, J., Vullo, R., Martín-Abad, H., Luo, Z.-X. and Buscalioni, A. D. (2015). A cretaceous eutriconodont and integument evolution in early mammals. *Nature* **526**, 380-384.
Molnar, J. L., Pierce, S. E. and Hutchinson, J. R. (2014). An experimental and morphometric test of the relationship between vertebral morphology and joint stiffness in Nile crocodiles (*Crocodylus niloticus*). *J. Exp. Biol.* **217**, 758-768.
Molnar, J. L., Pierce, S. E., Bhullar, B.-A. S., Turner, A. H. and Hutchinson, J. R. (2015). Morphological and functional changes in the vertebral column with increasing aquatic adaptation in crocodylomorphs. *R. Soc. Open Sci.* **2**, 150439.
Nyakatura, J. A. and Fischer, M. S. (2010). Functional morphology and three-dimensional kinematics of the thoraco-lumbar region of the spine of the two-toed sloth. *J. Exp. Biol.* **213**, 4278-4290.
Nyakatura, J. A. and Fischer, M. S. (2011). Functional morphology of the muscular sling at the pectoral girdle in tree sloths: convergent morphological solutions to new functional demands? *J. Anat.* **219**, 360-374.
Olson, R. A., Womble, M. D., Thomas, D. R., Glenn, Z. D. and Butcher, M. T. (2016). Functional morphology of the forelimb of the nine-banded armadillo (*Dasypus novemcinctus*): comparative perspectives on the myology of Dasypodidae. *J. Mamm. Evol.* **23**, 49-69.
Pierce, S. E., Clack, J. A. and Hutchinson, J. R. (2011). Comparative axial morphology in pinnipeds and its correlation with aquatic locomotory behaviour. *J. Anat.* **219**, 502-514.
Rockwell, H., Evans, F. G. and Pheasant, H. C. (1938). The comparative morphology of the vertebrate spinal column. Its form as related to function. *J. Morphol.* **63**, 87-117.
Russo, G. A. (2010). Prezygapophyseal articular facet shape in the catarrhine thoracolumbar vertebral column. *Am. J. Phys. Anthropol.* **142**, 600-612.
Schilling, N. (2011). Evolution of the axial system in craniates: morphology and function of the perivertebral musculature. *Front. Zool.* **8**, 4.
Shapiro, L. J. (1995). Functional morphology of indrid lumbar vertebrae. *Am. J. Phys. Anthropol.* **98**, 323-342.
Shapiro, L. J. (2007). Morphological and functional differentiation in the lumbar spine of lorisids and galagids. *Am. J. Primatol.* **69**, 86-102.

Simpson, G. G. (1931). Metacheiromys and the relationships of the Edentata. *Bull. Am. Mus. Nat. Hist.* **59**, 295-381.
Slijper, E. J. (1946). Comparative biologic-anatomical investigations on the vertebral column and spinal musculature of mammals. *Verh. K. Ned. Akad. Wet.* **42**, 1-128.
Superina, M. and Loughry, W. J. (2012). Life on the half-shell: consequences of a carapace in the evolution of armadillos (Xenarthra: Cingulata). *J. Mammal. Evol.* **19**, 217-224.
Townsend, H. G. G., Leach, D. H. and Fretz, P. B. (1983). Kinematics of the equine thoracolumbar spine. *Equine Vet. J.* **15**, 117-122.
Vizcaíno, S. F. and Milne, N. (2002). Structure and function in armadillo limbs (Mammalia: Xenarthra: Dasypodidae). *J. Zool.* **257**, 117-127.
Ward, A. B. and Mehta, R. S. (2014). Differential occupation of axial morphospace. *Zoology* **117**, 70-76.
Wellik, D. M. (2007). Hox patterning of the vertebrate axial skeleton. *Dev. Dyn.* **236**, 2454-2463.

Table S1. Applied masses, moments, and resultant angles of deflection in all three bending directions.

	MCZ 67401						
		Dorsiflexion		Lateroflexion		Ventroflexion	
	Mass (g)	Moment (Nm)	Angle of deflection (deg)	Moment (Nm)	Angle of deflection (deg)	Moment (Nm)	Angle of deflection (deg)
T2-3	0	0	0	0	0	0	0
	10	0.001	0.55	0.001	0.48	0.001	1.57
	20	0.003	1.47	0.003	0.47	0.003	2.88
	40	0.006	1.60	0.005	0.76	0.005	4.05
	60	0.009	1.75	0.008	0.82	0.008	4.74
	80	0.011	1.69	0.011	1.58	0.011	5.16
	100	0.014	1.79	0.013	1.55	0.013	5.53
	120	0.017	1.75	0.016	2.01	0.016	5.82
	140	0.02	2.00	0.019	1.44	0.019	5.92
	160	0.023	1.96	0.021	2.12	0.022	5.94
	180	0.025	3.03	0.024	2.37	0.024	6.07
	200	0.028	2.15	0.027	2.06	0.027	6.09
	220	0.03	2.25	0.028	2.26	0.03	6.20
	240	0.034	2.31	0.032	2.23	0.03	6.17
	260	0.036	2.30	0.034	2.61	0.032	6.28
	280	0.04	2.37	0.038	2.54	0.034	6.19
	300	0.043	2.55	0.039	2.81	0.036	6.15
	320	0.045	2.23	0.041	2.82	0.043	6.28
	340	0.049	2.62	0.045	2.96	0.045	6.37
	360	0.051	2.44	0.047	3.08	0.049	6.29
	380	0.054	2.09	0.051	2.97	0.051	6.31
	400	0.057	2.27	0.053	3.15	0.054	6.25
T4-5	0	0	0	0	0	0	0
	10	0.002	0.09	0.002	0.84	0.002	1.74
	20	0.003	0.15	0.003	1.62	0.003	2.44

	40	0.006	0.57	0.006	2.00	0.006	3.59
	60	0.01	0.53	0.009	2.05	0.009	3.90
	80	0.013	0.46	0.012	2.44	0.012	4.22
	100	0.016	0.83	0.015	2.73	0.015	4.62
	120	0.019	0.83	0.018	2.58	0.018	4.80
	140	0.022	1.21	0.021	2.96	0.021	4.80
	160	0.025	1.30	0.024	2.98	0.024	4.89
	180	0.029	1.01	0.027	3.15	0.027	5.09
	200	0.032	0.91	0.03	3.12	0.03	5.23
	220	0.035	1.11	0.034	3.29	0.033	5.30
	240	0.038	1.43	0.036	3.17	0.036	5.40
	260	0.042	1.42	0.039	3.07	0.039	5.29
	280	0.044	1.56	0.043	3.56	0.041	5.45
	300	0.048	1.86	0.045	3.37	0.045	5.42
	320	0.051	1.56	0.048	3.23	0.048	5.40
	340	0.055	1.69	0.051	3.22	0.05	5.71
	360	0.058	2.03	0.055	3.43	0.051	5.45
	380	0.062	1.57	0.058	3.56	0.052	5.48
	400	0.064	1.87	0.06	3.79	0.059	5.71
T6-7	0	0	0	0	0	0	0
	10	0.003	0.72	0.002	1.13	0.003	3.40
	20	0.006	0.88	0.005	1.46	0.006	4.31
	40	0.011	1.11	0.01	1.70	0.013	5.03
	60	0.017	1.32	0.014	1.84	0.018	5.37
	80	0.023	1.71	0.019	2.04	0.025	5.86
	100	0.029	1.74	0.024	2.29	0.031	5.85
	120	0.035	1.89	0.028	2.28	0.037	6.06
	140	0.041	2.04	0.034	2.52	0.043	6.35
	160	0.047	2.25	0.038	2.57	0.05	6.19
	180	0.053	2.37	0.044	2.53	0.055	6.37
	200	0.058	2.34	0.047	2.68	0.061	6.46

	220	0.064	2.71	0.054	2.75	0.068	6.35
	240	0.07	2.97	0.058	2.91	0.074	6.41
	260	0.076	2.75	0.064	3.10	0.079	6.61
	280	0.082	3.10	0.067	3.02	0.087	6.40
	300	0.088	3.02	0.072	2.96	0.092	6.49
	320	0.094	3.16	0.076	3.13	0.098	6.71
	340	0.097	3.36	0.082	3.14	0.104	6.55
	360	0.107	3.56	0.085	3.30	0.11	6.66
	380	0.112	3.26	0.091	3.06	0.117	6.58
	400	0.117	3.45	0.094	2.85	0.123	6.67
T8-9	0	0	0	0	0	0	0
	10	0.003	1.58	0.003	0.86	0.003	3.23
	20	0.006	2.03	0.006	1.45	0.006	4.57
	40	0.012	2.55	0.012	2.42	0.012	5.54
	60	0.017	3.49	0.017	2.69	0.018	6.04
	80	0.023	3.54	0.023	2.92	0.025	6.22
	100	0.029	3.83	0.028	3.10	0.031	6.59
	120	0.035	3.93	0.034	3.18	0.037	6.72
	140	0.041	4.36	0.04	3.50	0.043	6.85
	160	0.048	4.77	0.046	3.90	0.049	7.06
	180	0.054	4.63	0.051	3.82	0.054	7.26
	200	0.058	4.83	0.057	3.89	0.061	7.44
	220	0.065	5.40	0.062	3.94	0.068	7.38
	240	0.071	5.03	0.068	4.05	0.073	7.46
	260	0.076	4.95	0.073	4.30	0.079	7.56
	280	0.082	5.53	0.079	4.13	0.084	7.57
	300	0.089	5.82	0.086	4.19	0.092	7.63
	320	0.092	6.17	0.091	4.51	0.099	7.72
	340	0.097	5.78	0.097	4.32	0.103	7.57
	360	0.103	6.32	0.103	4.49	0.111	7.66
	380	0.11	6.18	0.108	4.55	0.116	7.75

Journal of Experimental Biology • Supplementary information

	400	0.117	6.26	0.114	4.66	0.122	8.02
L1-2	0	0	0	0	0	0	0
	10	0.003	0.55	0.003	1.72	0.003	0.93
	20	0.007	1.23	0.007	3.20	0.007	4.95
	40	0.014	3.34	0.014	5.27	0.014	7.56
	60	0.021	4.59	0.02	6.57	0.02	8.17
	80	0.028	5.02	0.027	6.95	0.026	8.90
	100	0.034	5.56	0.034	7.04	0.033	8.93
	120	0.041	5.89	0.041	7.16	0.04	9.32
	140	0.049	6.15	0.048	7.33	0.046	9.42
	160	0.055	6.26	0.055	7.19	0.053	9.58
	180	0.063	6.47	0.062	7.51	0.06	9.83
	200	0.069	6.89	0.069	7.27	0.067	9.97
	220	0.076	6.55	0.076	7.31	0.073	10.07
	240	0.083	6.96	0.082	7.31	0.079	10.27
	260	0.09	7.06	0.088	7.58	0.087	10.02
	280	0.097	7.16	0.096	7.43	0.093	10.17
	300	0.104	7.13	0.102	7.43	0.099	10.24
	320	0.111	7.46	0.108	7.47	0.106	10.26
	340	0.118	7.42	0.117	7.76	0.113	10.35
	360	0.125	7.54	0.123	7.55	0.119	10.40
	380	0.131	7.36	0.13	7.78	0.127	10.23
	400	0.138	7.57	0.137	7.55	0.133	10.53
L3-4	0	0	0	0	0	0	0
	10	0.003	1.03	0.003	0.14	0.003	0.79
	20	0.006	1.86	0.006	0.76	0.006	2.01
	40	0.013	3.85	0.012	1.94	0.013	3.21
	60	0.019	4.99	0.017	2.65	0.019	4.40
	80	0.026	5.01	0.024	2.94	0.025	4.89
	100	0.032	5.52	0.027	3.16	0.031	5.27

	120	0.039	6.00	0.035	3.42	0.037	5.67
	140	0.046	6.17	0.042	3.43	0.044	5.97
	160	0.052	6.73	0.047	3.63	0.05	6.26
	180	0.058	6.81	0.053	3.90	0.056	6.39
	200	0.065	7.01	0.056	3.87	0.063	6.52
	220	0.071	6.82	0.065	4.11	0.069	6.74
	240	0.078	7.10	0.072	4.49	0.075	6.88
	260	0.085	7.25	0.077	4.39	0.081	6.94
	280	0.092	7.13	0.082	4.38	0.088	7.13
	300	0.098	7.43	0.089	4.53	0.094	7.01
	320	0.104	7.60	0.095	4.50	0.097	6.91
	340	0.111	7.91	0.099	4.65	0.103	7.03
	360	0.118	8.04	0.107	4.70	0.109	7.06
	380	0.124	7.96	0.113	4.73	0.114	7.00
	400	0.131	8.33	0.118	4.72	0.119	7.23

MCZ 67402

		Dorsiflexion		Lateroflexion		Ventroflexion	
	Mass (g)	Moment (Nm)	Angle of deflection (deg)	Moment (Nm)	Angle of deflection (deg)	Moment (Nm)	Angle of deflection (deg)
T1-2	0	0	0	0	0	0	0
	10	0.0013	0.21	0.0012	0.24	0.0014	0.55
	20	0.0027	0.65	0.0025	0.01	0.0029	0.98
	30	0.004	0.86	0.0038	0.19	0.0043	0.97
	40	0.0054	0.93	0.005	0.11	0.0057	1.02
	50	0.0067	1.33	0.006	0.02	0.0069	0.97
	60	0.0079	1.12	0.0071	0.20	0.0083	1.17
	70	0.0095	1.33	0.0087	0.05	0.0096	1.21
	80	0.0109	1.59	0.0096	0.05	0.011	1.09
	90	0.0125	1.56	0.0108	0.20	0.0124	1.16

	100	0.0135	1.48	0.0119	0.11	0.0138	1.30
	110	0.0149	1.61	0.0136	0.13	0.0154	1.29
	120	0.0164	1.66	0.0149	0.09	0.0164	1.33
	130	0.0176	1.73	0.0162	0.05	0.0181	1.39
	140	0.0189	1.74	0.0167	0.02	0.0196	1.30
	150	0.02	1.91	0.0171	0.11	0.0211	1.34
	160	0.0219	1.81	0.019	0.01	0.0224	1.41
	170	0.0233	2.00	0.0212	0.02	0.0237	1.23
	180	0.0241	2.12	0.0216	0.01	0.0252	1.33
	190	0.0257	1.74	0.0223	0.31	0.0261	1.32
	200	0.0258	1.91	0.0244	0.09	0.0266	1.51
	220	0.0297	1.88	0.0268	0.34	0.0304	1.44
	240	0.032	2.02	0.0293	0.17	0.0335	1.35
	260	0.0355	2.18	0.0303	0.13	0.0362	1.39
	280	0.0384	1.98	0.035	0.22	0.0381	1.26
	300	0.0406	2.22	0.0357	0.07	0.0415	1.37
	320	0.0416	2.09			0.0437	1.36
	340	0.0436	2.21			0.0462	1.49
	360	0.0491	2.42			0.0498	1.37
	380	0.0527	2.39			0.0523	1.43
	400	0.0535	2.45			0.0557	1.47
T3-4	0	0	0	0	0	0	0
	10	0.001	0.79	0.001	2.32	0.001	3.52
	20	0.002	1.26	0.003	3.28	0.003	5.46
	30	0.004	1.65	0.004	4.24	0.004	6.55
	40	0.005	1.48	0.005	4.03	0.005	6.80
	50	0.006	1.73	0.006	4.48	0.006	7.13
	60	0.007	1.79	0.007	4.60	0.007	7.43
	70	0.008	2.33	0.009	4.63	0.009	7.63
	80	0.009	1.99	0.01	4.68	0.01	7.81
	90	0.011	2.08	0.011	4.73	0.011	7.94

	100	0.012	2.34	0.013	4.92	0.012	8.02
	110	0.013	2.15	0.014	4.78	0.014	8.15
	120	0.014	2.30	0.015	4.76	0.015	8.09
	130	0.015	2.56	0.016	4.87	0.016	8.26
	140	0.017	2.70	0.017	4.85	0.018	8.43
	150	0.018	2.52	0.019	5.07	0.019	8.41
	160	0.019	2.89	0.02	5.12	0.02	8.32
	170	0.02	3.05	0.021	5.24	0.021	8.55
	180	0.021	2.62	0.022	5.22	0.023	8.34
	190	0.022	2.88	0.023	4.99	0.024	8.36
	200	0.024	2.66	0.025	5.24	0.025	8.66
	220	0.026	2.81	0.028	5.15	0.026	8.61
	240	0.028	3.19	0.029	5.31	0.03	8.62
	260	0.031	3.17	0.032	5.14	0.037	8.79
	280	0.033	3.07	0.035	5.34	0.034	8.74
	300	0.036	3.47	0.038	5.38	0.039	8.70
	320	0.038	3.41	0.039	5.48	0.04	8.69
	340	0.039	3.42	0.042	5.53	0.042	8.84
	360	0.042	3.49	0.045	5.29	0.046	8.81
	380	0.045	3.59	0.047	5.53	0.047	8.90
	400	0.048	3.59	0.049	5.26	0.05	8.92
T5-6	0	0	0	0	0	0	0
	10	0.001	0.34	0.001	0.93	0.001	1.24
	20	0.003	0.17	0.003	1.40	0.003	2.35
	30	0.004	0.21	0.004	1.64	0.004	2.89
	40	0.006	0.37	0.006	1.87	0.006	2.87
	50	0.007	0.34	0.007	1.94	0.007	3.17
	60	0.009	0.56	0.008	1.89	0.009	3.58
	70	0.009	0.72	0.009	2.24	0.01	3.55
	80	0.012	0.73	0.011	2.05	0.012	3.78
	90	0.013	1.03	0.012	2.40	0.013	3.92

	100	0.014	0.72	0.014	2.41	0.014	3.96
	110	0.016	1.19	0.014	2.51	0.016	3.92
	120	0.017	1.02	0.016	2.60	0.017	4.24
	130	0.019	1.29	0.017	2.55	0.018	4.09
	140	0.02	0.99	0.019	2.71	0.02	4.15
	150	0.021	1.34	0.02	2.69	0.021	4.32
	160	0.023	1.66	0.022	2.68	0.023	4.50
	170	0.023	1.46	0.023	2.77	0.025	4.37
	180	0.026	1.55	0.024	2.89	0.026	4.52
	190	0.027	1.60	0.026	3.07	0.027	4.33
	200	0.029	1.65	0.027	3.16	0.029	4.58
	220	0.032	1.79	0.03	2.91	0.031	4.52
	240	0.035	1.71	0.032	2.94	0.034	4.60
	260	0.038	1.93	0.035	3.13	0.037	4.65
	280	0.04	1.94	0.038	2.95	0.04	4.63
	300	0.041	2.23	0.04	3.17	0.043	4.73
	320			0.044	3.17	0.046	4.70
	340			0.046	3.21	0.049	4.61
	360			0.05	3.31	0.051	4.73
	380			0.05	3.33	0.054	4.74
	400			0.054	3.40	0.057	4.80
T7-8	0	0	0	0	0	0	0
	10	0.003	0.88	0.003	1.43	0.003	0.03
	20	0.006	1.59	0.006	2.39	0.006	0.92
	30	0.01	1.69	0.009	2.72	0.01	1.32
	40	0.013	2.13	0.012	3.17	0.013	1.56
	50	0.015	2.15	0.015	3.32	0.015	1.88
	60	0.019	2.52	0.019	3.46	0.019	2.09
	70	0.022	3.01	0.022	3.68	0.022	2.25
	80	0.025	3.17	0.025	3.77	0.025	2.46
	90	0.028	3.30	0.028	3.98	0.028	2.53

	100	0.031	3.40	0.032	3.98	0.031	2.64
	110	0.035	3.42	0.035	4.22	0.034	2.77
	120	0.038	3.67	0.038	4.16	0.038	3.06
	130	0.04	3.66	0.041	4.01	0.041	3.07
	140	0.044	3.67	0.044	4.19	0.044	3.03
	150	0.047	3.42	0.047	4.11	0.047	2.99
	160	0.05	3.72	0.05	4.31	0.05	3.25
	170	0.053	4.14	0.052	4.25	0.053	3.20
	180	0.056	4.09	0.057	4.30	0.056	3.37
	190	0.06	4.25	0.06	4.46	0.06	3.28
	200	0.063	4.09	0.06	4.37	0.063	3.42
	220	0.069	4.24	0.069	4.49	0.068	3.50
	240	0.075	4.29	0.072	4.74	0.075	3.52
	260	0.081	4.24	0.08	4.50	0.083	3.59
	280	0.088	4.66	0.088	4.75	0.088	3.74
	300	0.094	5.27	0.093	4.85	0.094	3.88
	320	0.101	5.18	0.098	4.84	0.101	3.81
	340	0.105	5.15	0.106	4.82	0.106	3.83
	360	0.112	5.20	0.112	5.02	0.112	3.79
	380	0.119	5.28	0.119	5.03	0.119	3.87
	400	0.127	5.38	0.126	4.98	0.125	4.01
T9-10	0	0	0	0	0	0	0
	10	0.002	1.26	0.003	1.49	0.003	4.14
	20	0.005	2.38	0.006	2.64	0.006	6.24
	40	0.009	3.08	0.012	3.81	0.013	7.13
	60	0.014	3.48	0.017	4.43	0.019	7.63
	80	0.019	4.23	0.023	4.64	0.025	7.96
	100	0.025	4.35	0.028	5.18	0.031	8.24
	120	0.029	4.70	0.035	5.28	0.037	8.57
	140	0.035	4.74	0.041	5.54	0.043	8.85
	160	0.041	4.87	0.047	5.74	0.049	9.05

	180	0.047	5.24	0.052	5.95	0.055	9.08
	200	0.047	5.38	0.059	6.04	0.062	9.37
	220	0.051	4.98	0.063	6.12	0.068	9.58
	240	0.058	5.23	0.07	6.29	0.074	9.61
	260	0.062	5.15	0.075	6.61	0.08	9.72
	280	0.08	5.24	0.083	6.42	0.086	9.76
	300	0.086	5.43	0.088	6.47	0.092	10.00
	320	0.075	5.59	0.094	6.55	0.098	10.20
	340	0.079	5.80	0.099	6.55	0.105	10.04
	360	0.081	5.74	0.104	6.67	0.111	10.13
	380	0.103	6.01	0.111	6.81	0.117	10.19
	400	0.091	5.93	0.118	6.80	0.123	10.24
L1-2	0	0	0	0	0	0	0
	10	0.003	1.70	0.004	1.83	0.004	3.84
	20	0.007	3.13	0.007	3.56	0.007	5.72
	40	0.014	4.21	0.014	5.57	0.014	6.64
	60	0.02	4.75	0.021	5.81	0.021	7.21
	80	0.028	5.15	0.028	5.99	0.028	7.56
	100	0.035	5.36	0.035	5.96	0.035	7.94
	120	0.041	5.59	0.041	6.04	0.042	8.32
	140	0.048	5.62	0.049	6.14	0.049	8.49
	160	0.055	5.90	0.056	6.27	0.056	8.73
	180	0.063	5.87	0.062	6.38	0.063	9.04
	200	0.069	5.90	0.068	6.42	0.069	9.05
	220	0.076	5.97	0.076	6.49	0.077	9.32
	240	0.083	6.37	0.083	6.53	0.083	9.48
	260	0.09	6.26	0.09	6.52	0.091	9.62
	280	0.097	6.11	0.098	6.59	0.097	9.71
	300	0.104	6.39	0.101	6.40	0.105	9.69
	320	0.111	6.25	0.112	6.75	0.111	9.74
	340	0.118	6.91	0.119	6.62	0.118	9.86

	360	0.124	6.35	0.124	6.67	0.125	10.02
	380	0.133	6.72	0.133	6.82	0.132	10.18
	400	0.139	6.57	0.139	6.76	0.14	10.19
L3-4	0	0	0	0	0	0	0
	10	0.003	0.73	0.003	0.07	0.003	0.05
	20	0.006	1.21	0.007	1.81	0.006	4.87
	40	0.013	2.25	0.014	4.35	0.013	6.05
	60	0.019	2.80	0.02	6.64	0.019	6.69
	80	0.025	4.01	0.027	7.53	0.025	7.08
	100	0.032	5.08	0.033	7.76	0.032	7.63
	120	0.038	5.56	0.041	8.13	0.038	8.01
	140	0.044	6.13	0.047	8.42	0.044	8.29
	160	0.051	6.48	0.054	8.52	0.051	8.60
	180	0.057	6.63	0.06	8.65	0.058	8.75
	200	0.063	6.73	0.067	8.63	0.063	9.27
	220	0.069	6.88	0.073	8.62	0.07	9.22
	240	0.076	6.93	0.08	8.78	0.075	9.54
	260	0.082	7.18	0.088	8.74	0.082	9.62
	280	0.088	7.34	0.094	8.94	0.088	9.62
	300	0.095	7.32	0.1	8.93	0.095	9.70
	320	0.101	7.25	0.107	8.95	0.102	9.92
	340	0.107	7.52	0.114	9.10	0.107	9.93
	360	0.113	7.51	0.121	8.97	0.113	10.00
	380	0.12	7.42	0.127	9.22	0.12	10.14
	400	0.126	7.41	0.133	8.98	0.126	10.13

MCZ 67403						
	Dorsiflexion		Lateroflexion		Ventroflexion	
Mass (g)	Moment (Nm)	Angle of deflection (deg)	Moment (Nm)	Angle of deflection (deg)	Moment (Nm)	Angle of deflection (deg)

T3-4	0	0	0	0	0	0	0
	10	0.002	0.74	0.002	1.97	0.002	3.07
	20	0.003	1.19	0.003	2.37	0.003	4.27
	40	0.006	1.29	0.006	2.95	0.006	5.44
	60	0.009	1.54	0.009	3.37	0.009	5.89
	80	0.013	1.74	0.012	3.38	0.012	6.24
	100	0.016	1.69	0.015	3.66	0.015	6.44
	120	0.019	1.94	0.018	3.69	0.018	6.86
	140	0.022	1.63	0.021	3.70	0.02	6.78
	160	0.025	1.92	0.024	3.68	0.023	6.83
	180	0.028	1.92	0.027	3.76	0.027	6.95
	200	0.031	2.19	0.03	3.86	0.029	6.86
	220	0.033	1.95	0.033	3.74	0.032	6.99
	240	0.037	2.27	0.036	3.86	0.036	7.07
	260	0.041	2.43	0.039	4.03	0.038	7.15
	280	0.044	2.17	0.042	4.11	0.042	7.17
	300	0.046	2.61	0.042	4.22	0.045	7.07
	320	0.049	2.69	0.046	3.81	0.041	7.08
	340	0.052	2.12	0.052	4.02	0.052	7.16
	360	0.055	2.60	0.054	4.04	0.055	7.12
	380	0.06	2.56	0.058	4.07	0.055	7.18
	400	0.063	2.27	0.06	4.18	0.059	7.31
T5-6	0	0	0	0	0		
	10	0.001	0.13	0.001	1.01		
	20	0.003	0.35	0.003	1.54		
	40	0.006	0.38	0.006	2.14		
	60	0.008	0.64	0.009	2.40		
	80	0.011	0.78	0.012	2.39		
	100	0.014	0.92	0.014	2.71		
	120	0.017	1.00	0.018	2.83		

	140	0.02	1.10	0.02	2.92		
	160	0.022	1.41	0.022	2.86		
	180	0.024	1.15	0.025	2.74		
	200	0.028	1.40	0.03	2.87		
	220	0.03	1.66	0.033	3.01		
	240	0.032	1.57	0.036	3.12		
	260	0.036	1.71	0.038	3.21		
	280	0.037	1.91	0.04	3.32		
	300	0.042	1.70	0.038	3.18		
	320	0.043	1.89	0.048	3.34		
	340	0.04	1.61	0.051	3.33		
	360	0.052	1.96	0.052	3.45		
	380	0.054	1.92	0.057	3.39		
	400	0.057	1.71	0.057	3.32		
T7-8	0	0	0	0	0	0	0
	10	0.003	0.35	0.003	1.17	0.003	1.14
	20	0.006	0.60	0.006	1.25	0.006	1.22
	40	0.013	0.87	0.013	1.84	0.013	1.70
	60	0.019	1.58	0.019	2.13	0.019	2.22
	80	0.025	1.71	0.025	2.45	0.025	2.40
	100	0.031	1.85	0.031	2.58	0.032	2.76
	120	0.038	1.97	0.038	2.89	0.038	2.86
	140	0.044	2.15	0.044	2.97	0.044	3.29
	160	0.05	2.28	0.05	3.28	0.05	3.49
	180	0.057	2.57	0.057	3.40	0.055	3.59
	200	0.062	2.50	0.062	3.42	0.064	3.80
	220	0.07	3.03	0.07	3.61	0.069	3.88
	240	0.076	2.97	0.076	3.64	0.076	3.81
	260	0.082	3.05	0.082	3.78	0.082	4.20
	280	0.089	3.06	0.088	3.68	0.088	4.31
	300	0.094	2.91	0.094	3.92	0.094	4.40

	320	0.101	3.78	0.101	3.99	0.101	4.33
	340	0.108	3.78	0.107	3.94	0.107	4.34
	360	0.116	3.50	0.113	4.10	0.114	4.49
	380	0.121	3.69	0.119	4.03	0.119	4.50
	400	0.126	3.84	0.126	3.87	0.126	4.49
T9-10	0	0	0	0	0	0	0
	10	0.003	0.18	0.003	0.89	0.003	1.20
	20	0.007	0.22	0.007	1.27	0.007	1.77
	40	0.014	0.26	0.013	1.76	0.013	2.88
	60	0.02	1.23	0.019	2.27	0.019	3.60
	80	0.026	2.62	0.026	2.66	0.025	3.90
	100	0.033	1.64	0.032	2.90	0.032	4.24
	120	0.04	2.17	0.038	2.99	0.038	4.80
	140	0.046	2.79	0.045	3.15	0.045	4.96
	160	0.054	2.80	0.051	3.12	0.049	5.27
	180	0.059	3.41	0.058	3.60	0.057	5.43
	200	0.066	3.33	0.064	3.50	0.064	5.55
	220	0.073	3.46	0.071	3.68	0.07	5.87
	240	0.08	4.29	0.078	3.81	0.076	5.79
	260	0.087	4.60	0.084	3.68	0.084	5.91
	280	0.094	4.63	0.091	3.60	0.09	6.14
	300	0.099	4.76	0.095	3.78	0.097	6.09
	320	0.107	3.95	0.103	3.86	0.103	5.98
	340	0.114	4.15	0.11	4.04	0.11	5.97
	360	0.121	4.78	0.117	4.04	0.116	6.60
	380	0.127	4.96	0.123	4.05	0.121	6.23
	400	0.133	5.00	0.128	4.18	0.128	6.22
	420	0.142	4.83			0.134	6.31
	440	0.148	4.64			0.14	6.36
	460	0.155	5.61			0.146	6.25
	480	0.162	5.73			0.153	6.64

	500	0.163	5.87			0.157	6.34
L1-2	0	0	0	0	0	0	0
	10	0.003	0.13	0.004	0.06	0.003	0.45
	20	0.007	0.76	0.007	0.63	0.007	0.85
	40	0.014	0.94	0.014	1.27	0.014	1.46
	60	0.02	1.22	0.021	1.38	0.021	2.03
	80	0.026	1.54	0.028	1.60	0.028	2.26
	100	0.033	1.96	0.036	1.94	0.035	2.62
	120	0.039	2.06	0.043	1.98	0.042	3.13
	140	0.046	2.63	0.049	2.16	0.049	3.26
	160	0.053	2.08	0.056	2.20	0.056	3.52
	180	0.06	2.96	0.064	2.26	0.063	3.79
	200	0.067	3.29	0.071	2.39	0.07	3.90
	220	0.072	2.91	0.077	2.69	0.078	4.02
	240	0.079	3.57	0.085	2.61	0.085	4.23
	260	0.086	3.44	0.09	2.88	0.091	4.58
	280	0.092	3.80	0.095	2.59	0.099	4.54
	300	0.099	3.78	0.106	2.79	0.105	4.65
	320	0.106	3.99	0.11	2.76	0.111	4.65
	340	0.112	4.20	0.122	2.87	0.118	4.72
	360	0.118	4.28	0.129	3.09	0.125	4.86
	380	0.125	4.20	0.135	3.11	0.131	4.95
	400	0.133	4.48	0.141	2.85	0.137	4.89

MCZ 67405							
		Dorsiflexion		Lateroflexion		Ventroflexion	
	Mass (g)	Moment (Nm)	Angle of deflection (deg)	Moment (Nm)	Angle of deflection (deg)	Moment (Nm)	Angle of deflection (deg)
T1-2	0	0	0	0	0	0	0
	10	0.001	0.11	0.001	0.02	0.001	0.01

	20	0.003	0.16	0.003	0.13	0.003	0.00
	30	0.004	0.28	0.004	0.03	0.004	0.16
	40	0.005	0.17	0.005	0.21	0.005	0.20
	50	0.007	0.10	0.006	0.32	0.006	0.05
	60	0.008	0.31	0.008	0.04	0.008	0.18
	70	0.009	0.30	0.009	0.34	0.009	0.31
	80	0.01	0.17	0.01	0.13	0.01	0.15
	90	0.012	0.09	0.012	0.06	0.012	0.09
	100	0.013	0.20	0.013	0.36	0.013	0.19
	110	0.014	0.31	0.014	0.16	0.014	0.23
	120	0.015	0.14	0.015	0.18	0.015	0.04
	130	0.017	0.38	0.017	0.06	0.017	0.11
	140	0.018	0.17	0.018	0.33	0.018	0.18
	150	0.019	0.40	0.019	0.34	0.019	0.31
	160	0.021	0.44	0.02	0.01	0.02	0.22
	170	0.022	0.09	0.022	0.48	0.022	0.01
	180	0.023	0.45	0.023	0.01	0.023	0.34
	190	0.025	0.79	0.024	0.15	0.024	0.27
	200	0.026	0.13	0.026	0.35	0.025	0.19
	220	0.028	0.43	0.029	0.33	0.028	0.19
	240	0.031	0.34	0.031	0.18	0.031	0.23
	260	0.033	0.49	0.033	0.17	0.033	0.34
	280	0.036	0.47	0.035	0.19	0.036	0.29
	300	0.038	0.26	0.038	0.02	0.038	0.32
	320	0.041	0.37	0.041	0.34	0.041	0.41
	340	0.043	0.21	0.044	0.37	0.044	0.38
	360	0.046	0.33	0.046	0.18	0.045	0.30
	380	0.048	0.37	0.049	0.18	0.048	0.17
	400	0.051	0.32	0.052	0.35	0.051	0.35
T3-4	0	0	0	0	0	0	0
	10	0.001	0.68	0.001	2.32	0.001	1.55

	20	0.003	1.31	0.003	2.94	0.003	2.76
	30	0.004	1.84	0.004	3.46	0.004	3.52
	40	0.006	1.53	0.006	3.47	0.006	4.15
	50	0.007	1.54	0.007	3.77	0.007	4.48
	60	0.008	2.05	0.009	3.83	0.009	4.80
	70	0.01	1.99	0.01	4.11	0.01	4.96
	80	0.012	2.31	0.012	4.24	0.011	5.26
	90	0.012	2.05	0.013	4.24	0.013	5.37
	100	0.014	2.10	0.015	4.42	0.015	5.42
	110	0.015	2.31	0.016	4.57	0.016	5.56
	120	0.017	2.36	0.017	4.64	0.017	5.61
	130	0.018	2.27	0.019	4.58	0.019	5.74
	140	0.019	2.51	0.02	4.54	0.02	5.80
	150	0.02	2.35	0.021	4.75	0.02	5.78
	160	0.022	2.41	0.022	4.55	0.024	5.90
	170	0.024	2.51	0.025	4.92	0.025	5.92
	180	0.026	2.42	0.026	4.90	0.026	6.02
	190	0.026	2.59	0.026	4.89	0.027	6.03
	200	0.028	2.61	0.028	4.90	0.029	6.03
	220	0.03	2.71	0.03	5.12	0.032	6.07
	240	0.035	2.83	0.034	5.06	0.034	6.28
	260	0.036	2.51	0.038	5.07	0.037	6.26
	280	0.039	2.46	0.04	5.10	0.04	6.22
	300	0.042	3.01	0.043	5.25	0.041	6.15
	320	0.044	2.80	0.045	5.25	0.046	6.47
	340	0.046	2.85	0.05	5.26	0.05	6.29
	360	0.051	3.12	0.054	5.27	0.052	6.49
	380	0.052	3.05	0.057	5.62	0.054	6.46
	400	0.056	3.02	0.058	5.26	0.056	6.40
T5-6	0	0	0	0	0	0	0
	10	0.001	0.76	0.002	1.50	0.001	0.49

	20	0.003	0.96	0.003	1.70	0.003	1.01
	30	0.004	1.49	0.005	2.26	0.004	1.67
	40	0.006	1.60	0.007	2.94	0.006	2.07
	50	0.007	1.69	0.008	2.29	0.007	2.48
	60	0.009	1.70	0.01	2.70	0.009	2.80
	70	0.01	1.72	0.011	2.89	0.01	3.04
	80	0.012	2.04	0.013	3.07	0.011	3.16
	90	0.013	2.06	0.015	2.99	0.013	2.96
	100	0.015	2.35	0.016	3.16	0.014	2.92
	110	0.016	2.10	0.018	3.31	0.016	3.14
	120	0.018	2.25	0.019	3.44	0.017	2.90
	130	0.019	2.36	0.021	3.39	0.019	3.32
	140	0.02	2.35	0.022	3.43	0.019	3.34
	150	0.02	2.37	0.024	3.50	0.021	3.41
	160	0.024	2.47	0.026	3.58	0.023	3.20
	170	0.025	2.42	0.028	3.62	0.024	3.32
	180	0.027	2.73	0.03	3.67	0.026	3.18
	190	0.027	2.68	0.031	3.69	0.027	3.15
	200	0.029	2.67	0.032	3.99	0.028	3.33
	220	0.032	2.67	0.036	3.59	0.031	3.26
	240	0.032	2.73	0.033	3.69	0.034	3.06
	260	0.038	2.80	0.043	4.15	0.032	3.16
	280	0.041	2.96	0.046	4.20	0.04	3.18
	300	0.044	2.92	0.05	4.00	0.043	3.10
	320	0.047	3.01	0.052	4.08	0.045	3.32
	340	0.049	3.23	0.055	4.33	0.049	3.27
	360	0.053	3.07	0.059	4.47	0.051	3.39
	380	0.056	3.21	0.062	4.49	0.055	3.33
	400	0.059	3.21	0.066	4.47	0.057	3.29
T7-8	0	0	0	0	0	0	0
	10	0.003	0.24	0.003	0.34	0.003	0.45

	20	0.006	0.30	0.006	0.79	0.005	1.16
	40	0.012	0.56	0.012	1.57	0.011	2.00
	60	0.018	0.81	0.018	2.27	0.016	2.41
	80	0.024	0.12	0.024	2.44	0.021	2.94
	100	0.029	0.92	0.029	2.80	0.026	2.90
	120	0.035	1.12	0.036	2.80	0.032	3.04
	140	0.042	1.33	0.043	3.18	0.037	3.11
	160	0.047	1.03	0.048	3.17	0.041	3.39
	180	0.054	1.37	0.054	3.41	0.047	3.61
	200	0.059	1.59	0.06	3.51	0.053	3.58
	220	0.064	1.59	0.066	3.56	0.057	3.61
	240	0.07	1.83	0.072	3.82	0.063	3.61
	260	0.076	1.60	0.078	3.86	0.068	3.88
	280	0.082	1.98	0.084	3.76	0.074	3.79
	300	0.088	2.12	0.089	3.94	0.079	3.81
	320	0.093	2.68	0.096	4.06	0.085	3.74
	340	0.099	2.58	0.102	4.06	0.09	3.72
	360	0.107	2.01	0.108	4.30	0.095	3.89
	380	0.113	2.91	0.113	4.17	0.101	3.95
	400	0.12	2.38	0.118	4.11	0.107	3.82
T9-10	0	0	0	0	0	0	0
	10	0.003	4.63	0.003	0.07	0.003	0.34
	20	0.006	5.12	0.006	1.15	0.006	1.21
	40	0.013	5.13	0.013	2.28	0.012	7.24
	60	0.019	6.36	0.019	3.30	0.018	7.67
	80	0.025	6.90	0.025	4.00	0.024	8.22
	100	0.032	7.17	0.032	4.61	0.03	8.56
	120	0.038	6.89	0.038	4.82	0.036	8.77
	140	0.044	8.07	0.045	4.88	0.041	9.06
	160	0.051	8.45	0.051	5.51	0.047	9.35
	180	0.057	8.64	0.057	5.63	0.052	9.58

	200	0.063	9.13	0.063	6.01	0.06	9.62
	220	0.07	9.02	0.07	5.97	0.065	9.58
	240	0.077	9.01	0.076	6.11	0.071	9.90
	260	0.082	9.55	0.084	6.25	0.077	9.88
	280	0.089	9.49	0.089	6.18	0.084	9.82
	300	0.096	9.59	0.095	6.52	0.089	10.08
	320	0.102	10.14	0.102	6.55	0.095	10.13
	340	0.108	10.08	0.108	6.73	0.101	10.05
	360	0.114	10.25	0.116	6.60	0.107	10.21
	380	0.122	10.13	0.12	6.79	0.112	10.12
	400	0.129	10.45	0.127	6.69	0.119	10.28
L1-2	0	0	0	0	0	0	0
	10	0.003	0.07	0.004	0.12	0.004	0.19
	20	0.007	0.04	0.007	0.75	0.007	1.27
	40			0.014	2.43	0.014	2.39
	60	0.02	0.02	0.021	3.41	0.02	3.06
	80	0.027	0.46	0.028	3.82	0.027	3.40
	100	0.034	0.97	0.036	4.28	0.034	3.62
	120	0.04	1.07	0.042	4.27	0.041	4.01
	140	0.047	1.53	0.05	4.59	0.048	4.01
	160	0.054	1.70	0.058	5.04	0.055	4.48
	180	0.06	2.10	0.064	5.18	0.062	4.54
	200	0.066	2.31	0.072	5.50	0.069	4.71
	220	0.074	2.40	0.078	5.42	0.075	4.91
	240	0.081	2.34	0.086	5.57	0.082	5.18
	260	0.087	2.71	0.092	5.63	0.089	5.17
	280	0.094	3.02	0.101	5.79	0.096	5.23
	300	0.1	3.03	0.108	5.81	0.102	5.24
	320	0.108	2.98	0.115	5.95	0.109	5.51
	340	0.114	3.52	0.12	5.99	0.117	5.38
	360	0.121	3.26	0.128	5.78	0.123	5.59

	380	0.127	3.37	0.135	5.69	0.128	5.68
	400	0.133	3.55	0.142	5.99	0.136	5.50
L3-4	0	0	0	0	0	0	0
	10	0.003	0.41	0.003	0.07	0.003	0.44
	20	0.007	0.47	0.007	0.31	0.007	0.32
	40	0.014	1.05	0.013	1.28	0.014	0.87
	60	0.02	1.67	0.019	1.82	0.02	1.42
	80	0.027	2.04	0.026	2.16	0.027	1.71
	100	0.034	2.28	0.033	2.38	0.033	2.01
	120	0.04	2.74	0.04	2.81	0.04	2.42
	140	0.047	2.94	0.046	2.92	0.047	2.59
	160	0.054	3.44	0.053	3.01	0.054	2.80
	180	0.061	3.49	0.059	2.98	0.06	2.90
	200	0.067	3.86	0.066	3.50	0.068	3.14
	220	0.074	4.02	0.072	3.64	0.075	3.40
	240	0.081	4.02	0.079	3.72	0.08	3.30
	260	0.087	4.16	0.085	3.69	0.088	3.48
	280	0.094	4.12	0.092	3.87	0.095	3.69
	300	0.101	4.69	0.098	3.95	0.102	3.86
	320	0.108	4.65	0.106	4.05	0.108	3.97
	340	0.114	5.12	0.111	4.17	0.114	3.97
	360	0.12	5.04	0.117	4.10	0.122	4.09
	380	0.128	5.23	0.124	4.36	0.128	4.16
	400	0.133	5.23	0.132	4.30	0.133	4.28

MCZ 67406							
		Dorsiflexion		Lateroflexion		Ventroflexion	
	Mass (g)	Moment (Nm)	Angle of deflection (deg)	Moment (Nm)	Angle of deflection (deg)	Moment (Nm)	Angle of deflection (deg)
T1-2	0	0	0			0	0

	10	0.001	0.01			0.001	0.08
	20	0.002	0.22			0.002	0.27
	30	0.003	0.27			0.003	0.38
	40	0.004	0.42			0.004	0.47
	50	0.006	0.68			0.005	0.62
	60	0.007	0.62			0.006	0.65
	70	0.008	0.71			0.007	0.69
	80	0.009	0.96			0.008	0.69
	90	0.01	0.89			0.009	0.68
	100	0.011	1.01			0.01	0.76
	110	0.012	1.13			0.01	0.71
	120	0.013	1.24			0.011	0.78
	130	0.015	1.26			0.012	0.73
	140	0.016	1.32			0.013	0.77
	150	0.017	1.44			0.014	0.78
	160	0.018	1.36			0.015	0.73
	170	0.019	1.53			0.016	0.73
	180	0.02	1.51			0.016	0.79
	190	0.021	1.63			0.017	0.79
	200	0.022	1.74			0.018	0.83
	220					0.021	0.81
	240					0.022	0.83
	260					0.024	0.84
	280					0.026	0.81
	300					0.028	0.87
T3-4	0	0	0	0	0	0	0
	10	0.003	0.97	0.003	1.92	0.003	5.21
	20	0.006	1.41	0.006	2.30	0.006	6.07
	30	0.008	1.65	0.009	2.45	0.008	6.66
	40	0.011	1.84	0.012	2.54	0.01	6.84
	50	0.014	2.02	0.015	2.66	0.014	7.54

	60	0.017	2.23	0.018	2.69	0.016	7.68
	70	0.02	2.35	0.021	2.70	0.02	7.83
	80	0.023	2.40	0.023	2.65	0.025	7.79
	90	0.025	2.60	0.026	2.74	0.028	7.89
	100	0.028	2.76	0.029	2.77	0.026	8.03
	110	0.031	2.81	0.032	2.84	0.029	8.10
	120	0.033	2.98	0.035	3.02	0.033	8.18
	130	0.036	3.03	0.038	2.84	0.035	8.21
	140	0.039	3.11	0.041	2.94	0.032	8.29
	150	0.042	3.11	0.044	2.95	0.038	8.27
	160	0.045	3.22	0.047	3.07	0.039	8.37
	170	0.048	3.34	0.05	2.96	0.047	8.52
	180	0.051	3.41	0.053	3.02	0.049	8.49
	190	0.053	3.49	0.056	2.94	0.049	8.49
	200	0.056	3.61	0.058	3.00	0.059	8.61
	220	0.062	3.67	0.065	3.07	0.055	8.54
	240	0.068	3.83	0.07	3.08	0.07	8.69
	260	0.073	3.94	0.077	3.09	0.07	8.70
	280	0.079	4.03	0.082	3.13	0.071	8.74
	300	0.084	4.13	0.088	3.21	0.087	8.81
T5-6	0	0	0	0	0	0	0
	10	0.003	0.39	0.003	1.42	0.003	3.05
	20	0.006	0.50	0.007	1.93	0.007	3.80
	30	0.009	0.71	0.01	1.98	0.01	4.23
	40	0.012	0.97	0.013	2.22	0.013	4.40
	50	0.015	1.09	0.016	2.25	0.016	4.63
	60	0.019	1.04	0.019	2.27	0.019	4.80
	70	0.022	1.10	0.022	2.35	0.023	4.91
	80	0.025	0.93	0.026	2.41	0.026	5.06
	90	0.028	1.08	0.028	2.59	0.029	5.26
	100	0.03	1.43	0.032	2.71	0.033	5.30

	110	0.034	1.45	0.035	2.70	0.035	5.31
	120	0.037	1.41	0.038	2.76	0.039	5.56
	130	0.04	1.45	0.041	2.78	0.042	5.61
	140	0.043	1.43	0.044	2.81	0.046	5.56
	150	0.045	1.52	0.048	2.75	0.049	5.66
	160	0.049	1.62	0.051	2.92	0.052	5.72
	170	0.053	1.71	0.054	2.91	0.056	5.75
	180	0.056	1.79	0.058	2.78	0.059	5.76
	190	0.059	1.72	0.06	2.83	0.062	5.77
	200	0.062	1.84	0.063	2.90	0.065	5.95
	220	0.068	1.82	0.07	2.90	0.071	5.72
	240	0.074	1.88	0.076	3.01	0.078	5.95
	260	0.08	2.04	0.082	2.86	0.085	5.96
	280	0.087	1.85	0.089	3.04	0.091	5.94
	300	0.093	2.06	0.095	3.10	0.099	5.88
T7-8	0			0	0	0	0
	10			0.003	1.66	0.003	2.15
	20			0.006	2.16	0.006	2.79
	30			0.009	2.45	0.009	3.26
	40			0.012	2.68	0.013	3.60
	50			0.015	2.79	0.015	3.71
	60			0.018	2.92	0.019	3.94
	70			0.021	3.01	0.022	4.00
	80			0.024	3.16	0.025	4.19
	90			0.028	3.09	0.028	4.25
	100			0.03	3.40	0.031	4.37
	120			0.036	3.44	0.037	4.49
	140			0.043	3.37	0.043	4.56
	160			0.048	3.53	0.049	4.68
	180			0.055	3.55	0.055	4.88
	200			0.061	3.69	0.062	4.81

	220			0.067	3.76	0.068	4.80
	240			0.073	3.87	0.074	4.83
	260			0.079	3.77	0.08	5.02
	280			0.085	3.77	0.086	5.15
	300			0.09	3.96	0.092	5.05
T9-10	0	0	0	0	0	0	0
	10	0.003	1.31	0.003	0.42	0.003	0.85
	20	0.007	2.82	0.007	0.94	0.006	3.68
	30	0.01	3.77	0.01	1.34	0.01	7.34
	40	0.013	4.00	0.013	1.75	0.013	8.25
	50	0.016	4.57	0.015	2.04	0.016	8.59
	60	0.02	4.70	0.019	2.42	0.019	8.80
	70	0.023	4.96	0.022	2.74	0.022	9.05
	80	0.026	4.97	0.025	3.12	0.025	9.10
	90	0.029	5.24	0.028	3.50	0.028	9.18
	100	0.032	5.28	0.032	3.66	0.031	9.43
	120	0.039	5.56	0.037	3.92	0.038	9.62
	140	0.046	5.62	0.044	4.24	0.044	9.74
	160	0.052	5.83	0.051	4.47	0.05	9.78
	180	0.058	6.14	0.057	4.54	0.056	9.79
	200	0.066	6.18	0.064	4.91	0.061	9.94
	220	0.071	6.18	0.07	4.92	0.068	10.05
	240	0.077	6.29	0.077	5.23	0.075	9.99
	260	0.085	6.54	0.082	5.28	0.082	10.16
	280	0.09	6.51	0.089	5.27	0.088	10.25
	300	0.096	6.69	0.096	5.41	0.093	10.30
L1-2	0	0	0	0	0	0	0
	10	0.003	0.58	0.003	0.66	0.003	0.45
	20	0.007	1.10	0.007	1.59	0.007	1.22
	30	0.01	1.53	0.01	2.10	0.01	3.12

	40	0.013	1.69	0.014	2.63	0.014	3.26
	50	0.015	1.96	0.016	2.97	0.017	4.06
	60	0.021	2.03	0.02	3.55	0.02	5.06
	70	0.024	2.29	0.024	4.16	0.023	5.99
	80	0.027	2.43	0.027	4.47	0.027	6.49
	90	0.029	2.69	0.03	4.74	0.03	6.88
	100	0.031	2.73	0.034	4.64	0.033	7.15
	120	0.041	2.84	0.04	5.02	0.04	7.56
	140	0.048	3.12	0.047	5.36	0.046	7.89
	160	0.055	3.16	0.053	5.36	0.053	8.27
	180	0.06	3.36	0.06	5.59	0.059	8.44
	200	0.067	3.59	0.068	5.68	0.067	8.85
	220	0.074	3.66	0.073	5.70	0.073	8.97
	240	0.083	3.81	0.079	5.72	0.08	9.05
	260	0.088	4.15	0.087	5.77	0.086	9.31
	280	0.095	4.22	0.094	5.86	0.093	9.49
	300	0.102	4.26	0.101	5.86	0.1	9.57
L3-4	0	0	0	0	0	0	0
	10	0.003	0.30	0.003	0.23	0.003	0.13
	20	0.006	0.81	0.006	1.06	0.007	0.56
	30	0.01	1.17	0.01	1.55	0.01	0.85
	40	0.013	1.24	0.013	1.98	0.013	1.20
	50	0.016	1.38	0.016	2.18	0.016	1.64
	60	0.019	1.53	0.019	2.52	0.02	1.68
	70	0.022	1.46	0.023	2.52	0.023	2.07
	80	0.025	1.75	0.025	2.87	0.026	2.23
	90	0.029	2.07	0.029	3.05	0.029	2.35
	100	0.032	2.10	0.032	3.23	0.033	2.59
	120	0.038	2.26	0.038	3.37	0.039	2.83
	140	0.045	2.45	0.045	3.55	0.045	3.20
	160	0.051	2.74	0.051	3.68	0.052	3.44

	180	0.057	2.73	0.058	3.90	0.059	3.60
	200	0.064	2.86	0.064	4.12	0.066	3.87
	220	0.07	3.12	0.071	4.29	0.072	4.12
	240	0.076	3.21	0.077	4.25	0.078	4.32
	260	0.083	3.19	0.083	4.36	0.085	4.41
	280	0.089	3.23	0.09	4.61	0.091	4.55
	300	0.096	3.23	0.096	4.64	0.098	4.67

MCZ 67407

		Dorsiflexion		Lateroflexion		Ventroflexion	
	Mass (g)	Moment (Nm)	Angle of deflection (deg)	Moment (Nm)	Angle of deflection (deg)	Moment (Nm)	Angle of deflection (deg)
T1-2	0	0	0	0	0	0	0
	10	0.001	0.21	0.002	0.11	0.002	0.18
	20	0.003	0.09	0.003	0.16	0.003	0.18
	30	0.004	0.02	0.004	0.07	0.005	0.43
	40	0.005	0.06	0.006	0.08	0.006	0.24
	50	0.007	0.14	0.007	0.00	0.008	0.49
	60	0.008	0.01	0.009	0.17	0.009	0.42
	70	0.01	0.17	0.01	0.10	0.011	0.39
	80	0.011	0.36	0.012	0.18	0.012	0.63
	90	0.013	0.36	0.013	0.07	0.014	0.54
	100	0.014	0.34	0.014	0.09	0.015	0.53
	110	0.015	0.30	0.016	0.05	0.017	0.43
	120	0.017	0.43	0.017	0.03	0.018	0.65
	130	0.017	0.42	0.019	0.19	0.02	0.59
	140	0.02	0.42	0.02	0.13	0.021	0.57
	150	0.021	0.70	0.022	0.20	0.023	0.49
	160	0.021	0.57	0.023	0.20	0.024	0.54
	170	0.024	0.68	0.025	0.13	0.025	0.36

	180	0.025	0.72	0.026	0.05	0.027	0.52
	190	0.026	0.79	0.028	0.26	0.028	0.68
	200	0.027	0.76	0.029	0.18	0.031	0.58
	220	0.03	0.94	0.032	0.18	0.033	0.50
	240	0.033	0.83	0.036	0.12	0.036	0.47
	260	0.035	0.82	0.038	0.12	0.039	0.46
	280	0.038	0.87	0.041	0.19	0.042	0.63
	300	0.041	0.93	0.043	0.21	0.044	0.56
	320	0.044	1.38	0.046	0.04	0.048	0.63
	340	0.045	0.89	0.052	0.18	0.05	0.50
	360	0.047	1.03	0.053	0.26	0.054	0.48
	380	0.048	1.25	0.055	0.27	0.058	0.47
	400	0.05	1.00	0.056	0.18	0.061	0.50
T3-4	0	0	0	0	0	0	0
	10	0.002	0.56	0.002	1.45	0.002	2.30
	20	0.003	0.85	0.003	2.36	0.003	3.95
	30	0.005	1.15	0.005	2.95	0.005	4.67
	40	0.006	1.33	0.006	3.15	0.006	5.15
	50	0.007	1.60	0.007	3.36	0.007	5.53
	60	0.009	1.77	0.009	3.73	0.009	5.71
	70	0.011	2.04	0.01	3.81	0.011	5.89
	80	0.012	1.91	0.012	3.99	0.012	6.14
	90	0.014	1.92	0.014	4.03	0.014	6.20
	100	0.015	2.21	0.015	4.09	0.015	6.48
	110	0.017	2.16	0.016	4.04	0.017	6.57
	120	0.018	2.14	0.018	3.90	0.018	6.49
	130	0.02	2.09	0.02	4.17	0.02	6.62
	140	0.021	2.39	0.021	4.22	0.021	6.78
	150	0.023	2.39	0.023	4.37	0.023	6.92
	160	0.024	2.66	0.024	4.30	0.024	6.96
	170	0.026	2.46	0.025	4.21	0.026	7.16

	180	0.028	2.58	0.027	4.29	0.027	7.13
	190	0.029	2.74	0.029	4.11	0.029	7.16
	200	0.03	2.89	0.03	4.27	0.03	7.11
	220	0.034	3.06	0.033	4.48	0.033	7.24
	240	0.037	3.09	0.037	4.43	0.036	7.40
	260	0.041	2.99	0.038	4.38	0.039	7.68
	280	0.044	3.03	0.041	4.59	0.043	7.61
	300	0.047	3.08	0.044	4.44	0.046	7.68
	320	0.051	3.18	0.047	4.62	0.049	7.71
	340	0.053	3.33	0.05	4.53	0.051	7.87
	360	0.056	3.34	0.053	4.65	0.055	7.92
	380	0.059	3.47	0.057	4.62	0.057	7.83
	400	0.062	3.61	0.059	4.67	0.061	8.05
T5-6	0	0	0	0	0	0	0
	10	0.001	0.55	0.001	0.59	0.001	1.47
	20	0.003	0.76	0.003	1.56	0.003	2.65
	30	0.005	0.77	0.004	1.60	0.005	3.24
	40	0.006	1.01	0.005	1.66	0.006	3.25
	50	0.008	1.22	0.007	1.78	0.007	3.46
	60	0.009	0.94	0.008	1.93	0.009	3.57
	70	0.01	1.23	0.009	1.95	0.01	3.74
	80	0.012	1.21	0.01	2.54	0.011	3.94
	90	0.014	1.43	0.012	2.61	0.013	3.93
	100	0.015	1.31	0.013	2.09	0.014	4.01
	110	0.016	1.44	0.015	2.40	0.016	4.09
	120	0.018	1.50	0.015	2.77	0.017	3.99
	130	0.02	1.38	0.018	2.87	0.018	4.28
	140	0.021	1.33	0.018	2.46	0.02	4.38
	150	0.023	1.46	0.019	2.85	0.022	4.37
	160	0.024	1.54	0.02	2.39	0.023	4.35
	170	0.025	1.50	0.021	2.70	0.024	4.34

	180	0.027	1.60	0.022	2.81	0.026	4.47
	190	0.028	1.65	0.025	2.98	0.027	4.67
	200	0.03	1.62	0.025	2.15	0.028	4.50
	220	0.034	1.49	0.028	2.68	0.031	4.66
	240	0.037	1.83	0.031	2.95	0.033	4.69
	260	0.04	1.97	0.032	3.07	0.036	4.81
	280	0.043	1.74	0.036	3.11	0.039	4.93
	300	0.046	2.06	0.038	2.97	0.042	4.97
	320					0.043	4.88
	340					0.049	4.89
	360					0.051	4.94
	380					0.054	4.94
	400					0.057	5.22
T7-8	0	0	0	0	0	0	0
	10	0.003	0.77	0.003	0.74	0.003	1.36
	20	0.006	1.33	0.007	1.81	0.007	2.58
	40	0.012	2.11	0.013	3.10	0.013	3.38
	60	0.018	2.76	0.02	3.65	0.019	3.71
	80	0.025	3.27	0.026	3.86	0.025	4.19
	100	0.031	3.65	0.033	4.05	0.032	4.22
	120	0.036	3.56	0.04	4.30	0.039	4.51
	140	0.043	4.16	0.046	4.28	0.045	4.69
	160	0.049	4.03	0.053	4.23	0.052	4.77
	180	0.054	4.28	0.059	4.23	0.058	4.98
	200	0.061	4.55	0.066	4.46	0.065	5.10
	220	0.067	4.89	0.072	4.44	0.07	5.34
	240	0.073	4.93	0.079	4.59	0.078	5.30
	260	0.079	4.74	0.085	4.66	0.084	5.39
	280	0.085	4.93	0.092	4.74	0.089	5.56
	300	0.092	5.11	0.099	4.78	0.096	5.51
	320	0.099	5.34	0.106	4.89	0.103	5.55

	340	0.104	5.50	0.112	4.73	0.11	5.68
	360	0.109	5.73	0.118	4.87	0.117	5.61
	380	0.117	5.77	0.124	4.77	0.123	5.77
	400	0.122	5.61	0.131	4.96	0.129	5.68
T9-10	0	0	0	0	0	0	0
	10	0.003	1.01	0.003	0.50	0.003	0.21
	20	0.006	2.12	0.007	1.41	0.006	1.87
	40	0.013	3.51	0.014	2.75	0.013	5.77
	60	0.019	4.67	0.02	3.44	0.018	7.11
	80	0.025	5.14	0.026	3.97	0.024	7.38
	100	0.031	5.09	0.033	4.64	0.031	7.91
	120	0.038	5.91	0.04	4.95	0.037	8.11
	140	0.044	5.82	0.046	5.14	0.043	8.42
	160	0.051	6.32	0.053	5.33	0.049	8.71
	180	0.056	6.75	0.06	5.72	0.055	8.97
	200	0.063	6.92	0.066	5.85	0.062	9.15
	220	0.068	6.91	0.072	6.10	0.068	9.34
	240	0.076	7.01	0.08	6.22	0.074	9.44
	260	0.082	7.09	0.085	6.11	0.08	9.56
	280	0.09	7.41	0.093	6.43	0.087	9.70
	300	0.093	7.50	0.099	6.31	0.092	9.96
	320	0.1	7.31	0.106	6.29	0.098	9.95
	340	0.108	7.72	0.112	6.20	0.105	10.09
	360	0.115	7.83	0.118	6.27	0.11	10.02
	380	0.12	8.14	0.125	6.52	0.116	10.23
	400	0.127	8.31	0.131	6.49	0.123	10.23
L1-2	0	0	0	0	0	0	0
	10	0.003	0.44	0.003	0.38	0.004	0.36
	20	0.006	1.12	0.006	1.09	0.007	1.22
	40	0.013	2.41	0.013	2.06	0.014	2.65

	60	0.019	3.20	0.019	2.52	0.021	3.27
	80	0.026	3.60	0.026	2.97	0.028	3.76
	100	0.032	3.93	0.032	3.26	0.035	4.12
	120	0.038	4.31	0.038	3.65	0.042	4.47
	140	0.045	4.57	0.045	4.07	0.049	4.72
	160	0.051	4.74	0.051	4.18	0.056	4.93
	180	0.058	4.97	0.058	4.46	0.063	4.99
	200	0.064	5.00	0.064	4.44	0.07	5.29
	220	0.07	5.00	0.071	4.55	0.077	5.49
	240	0.077	5.22	0.077	4.62	0.084	5.66
	260	0.083	5.30	0.083	4.60	0.092	5.61
	280	0.09	5.62	0.09	4.89	0.098	5.78
	300	0.096	5.64	0.096	4.98	0.105	6.00
	320	0.102	5.50	0.102	4.84	0.112	6.01
	340	0.11	5.78	0.109	4.91	0.12	6.09
	360	0.115	5.73	0.115	4.94	0.127	6.21
	380	0.122	5.76	0.122	5.03	0.134	6.53
	400	0.128	5.80	0.128	4.93	0.142	6.43
L3-4	0	0	0	0	0	0	0
	10	0.003	0.47	0.003	0.28	0.003	0.12
	20	0.007	1.11	0.006	0.41	0.007	0.00
	40	0.013	2.16	0.013	0.37	0.013	0.27
	60	0.02	3.36	0.02	1.81	0.02	0.55
	80	0.026	4.44	0.026	2.78	0.026	0.88
	100	0.033	4.99	0.033	3.11	0.033	1.48
	120	0.039	5.51	0.04	3.59	0.04	1.87
	140	0.046	5.76	0.046	3.85	0.046	2.29
	160	0.052	5.98	0.053	4.09	0.053	2.38
	180	0.059	6.32	0.059	4.22	0.06	2.85
	200	0.065	6.73	0.065	4.51	0.066	3.16
	220	0.072	6.62	0.072	4.44	0.073	3.43

	240	0.078	6.71	0.079	4.81	0.079	3.42
	260	0.084	7.09	0.086	5.15	0.085	3.66
	280	0.091	7.13	0.092	5.21	0.093	3.88
	300	0.098	7.51	0.099	5.08	0.099	4.03
	320	0.104	7.58	0.106	5.39	0.106	4.24
	340	0.11	7.55	0.111	5.42	0.113	4.25
	360	0.118	7.94	0.118	5.36	0.119	4.16
	380	0.123	8.12	0.125	5.50	0.125	4.40
	400	0.13	7.78	0.131	5.58	0.132	4.53

MCZ 67408

		Dorsiflexion		Lateroflexion		Ventroflexion	
	Mass (g)	Moment (Nm)	Angle of deflection (deg)	Moment (Nm)	Angle of deflection (deg)	Moment (Nm)	Angle of deflection (deg)
T1-2	0	0	0	0	0	0	0
	10	0.001	0.08	0.001	0.01	0.001	0.08
	20	0.003	0.05	0.003	0.11	0.003	0.15
	30	0.004	0.29	0.004	0.02	0.004	0.31
	40	0.006	0.42	0.006	0.12	0.006	0.32
	50	0.007	0.30	0.007	0.03	0.007	0.16
	60	0.009	0.42	0.009	0.12	0.009	0.18
	70	0.01	0.38	0.01	0.01	0.01	0.17
	80	0.012	0.52	0.012	0.10	0.012	0.22
	90	0.013	0.52	0.013	0.14	0.013	0.25
	100	0.015	0.39	0.015	0.14	0.015	0.24
	110	0.016	0.48	0.016	0.24	0.016	0.23
	120	0.018	0.57	0.018	0.01	0.017	0.21
	130	0.019	0.47	0.019	0.22	0.019	0.15
	140	0.021	0.48	0.021	0.27	0.021	0.21
	150	0.022	0.47	0.022	0.14	0.022	0.12

	160	0.024	0.66	0.024	0.27	0.024	0.21
	170	0.025	0.76	0.025	0.25	0.025	0.21
	180	0.026	0.65	0.027	0.29	0.027	0.20
	190	0.028	0.55	0.028	0.12	0.028	0.21
	200	0.029	0.43	0.03	0.24	0.03	0.27
	220	0.032	0.60	0.032	0.27	0.033	0.07
	240	0.035	0.60	0.035	0.31	0.036	0.32
	260	0.037	0.75	0.038	0.27	0.038	0.27
	280	0.04	0.80	0.041	0.25	0.042	0.19
	300	0.043	1.12	0.044	0.14	0.045	0.17
	320	0.046	0.79	0.047	0.42	0.048	0.26
	340	0.049	0.75	0.049	0.44	0.051	0.17
	360	0.052	0.93	0.053	0.14	0.054	0.29
	380	0.055	1.11	0.056	0.28	0.057	0.25
	400	0.057	1.07	0.058	0.29	0.059	0.23
T3-4	0	0	0			0	0
	10	0.001	0.71			0.002	3.28
	20	0.003	0.84			0.003	4.34
	30	0.004	1.03			0.005	5.33
	40	0.006	1.23			0.006	5.83
	50	0.007	1.40			0.008	6.08
	60	0.009	1.44			0.009	6.23
	70	0.01	1.59			0.011	6.49
	80	0.012	1.59			0.012	6.59
	90	0.013	1.55			0.014	6.83
	100	0.014	1.75			0.016	6.85
	110	0.016	1.99			0.017	6.94
	120	0.018	1.83			0.019	6.48
	130	0.019	1.75			0.02	6.79
	140	0.02	2.02			0.022	6.48
	150	0.022	2.00			0.023	6.74

	160	0.023	2.10			0.025	6.41
	170	0.025	2.12			0.027	6.66
	180	0.026	2.12			0.028	6.58
	190	0.028	2.31			0.029	6.71
	200	0.029	2.24			0.031	6.69
	220	0.032	2.49			0.034	6.76
	240	0.034	2.53			0.037	6.81
	260	0.037	2.30			0.04	6.81
	280	0.039	2.41			0.043	6.94
	300	0.042	2.67			0.046	7.18
	320	0.046	2.61			0.049	7.12
	340	0.048	2.67			0.052	7.06
	360	0.051	2.68			0.055	7.16
	380	0.053	2.82			0.058	6.94
	400	0.056	3.02			0.061	7.04
T5-6	0	0	0	0	0	0	0
	10	0.001	0.11	0.001	0.88	0.001	0.85
	20	0.003	0.48	0.003	1.40	0.003	1.76
	30	0.004	0.84	0.004	1.58	0.004	2.23
	40	0.005	0.77	0.006	1.86	0.006	2.40
	50	0.006	2.32	0.007	2.04	0.007	2.67
	60	0.009	1.00	0.008	2.13	0.009	2.87
	70	0.01	1.25	0.01	2.24	0.01	3.16
	80	0.012	1.27	0.011	2.45	0.012	3.11
	90	0.013	1.23	0.013	2.56	0.013	3.21
	100	0.014	1.38	0.014	2.82	0.014	3.49
	110	0.014	0.85	0.015	2.71	0.016	3.45
	120	0.017	1.13	0.017	2.82	0.017	3.57
	130	0.019	0.82	0.018	2.59	0.019	3.64
	140	0.02	1.19	0.02	2.71	0.02	3.71
	150	0.019	1.22	0.021	2.82	0.022	3.88

	160	0.023	1.22	0.022	2.82	0.023	4.00
	170	0.024	0.94	0.024	2.96	0.025	3.98
	180	0.026	1.13	0.025	2.93	0.026	3.96
	190	0.027	1.13	0.027	3.17	0.028	4.11
	200	0.028	1.25	0.028	3.11	0.029	4.36
	220	0.032	1.50	0.031	3.07	0.032	4.32
	240	0.035	1.37	0.035	3.17	0.035	4.54
	260	0.038	1.50	0.037	3.19	0.038	4.56
	280	0.04	1.60	0.04	3.28	0.04	4.78
	300	0.043	1.74	0.042	3.39	0.044	4.71
	320	0.046	1.90	0.045	3.57	0.046	4.73
	340	0.049	1.90	0.048	3.22	0.049	5.06
	360	0.051	1.86	0.051	3.64	0.052	4.94
	380	0.054	2.04	0.054	3.65	0.055	5.15
	400	0.057	1.80	0.056	3.83	0.058	5.02
T7-8	0	0	0	0	0	0	0
	10	0.003	0.53	0.003	0.58	0.003	0.40
	20	0.006	1.23	0.007	0.82	0.006	1.14
	40	0.013	1.49	0.014	1.28	0.013	1.95
	60	0.019	1.69	0.02	1.68	0.018	2.31
	80	0.025	2.17	0.027	1.95	0.025	2.72
	100	0.032	2.55	0.034	2.12	0.031	3.09
	120	0.038	2.89	0.04	2.34	0.037	3.34
	140	0.043	2.83	0.045	2.49	0.043	3.50
	160	0.051	3.15	0.053	2.55	0.049	3.71
	180	0.057	3.38	0.061	2.63	0.055	3.91
	200	0.063	3.33	0.066	2.81	0.062	3.93
	220	0.071	3.90	0.073	2.88	0.068	4.28
	240	0.077	4.05	0.08	3.06	0.074	4.38
	260	0.083	4.23	0.086	3.19	0.08	4.51
	280	0.089	4.19	0.092	3.35	0.086	4.64

	300	0.096	4.20	0.1	3.37	0.092	4.74
	320	0.102	4.40	0.108	3.50	0.099	4.74
	340	0.109	4.56	0.113	3.48	0.105	5.00
	360	0.114	4.77	0.122	3.46	0.111	4.95
	380	0.121	4.69	0.127	3.58	0.117	4.97
	400	0.126	4.94	0.135	3.77	0.123	4.90
T9-10	0	0	0	0	0	0	0
	10	0.003	0.25	0.003	0.35	0.003	0.07
	20	0.007	0.62	0.007	0.71	0.006	1.12
	40	0.013	0.93	0.014	1.56	0.012	2.49
	60	0.019	1.14	0.02	1.81	0.018	2.84
	80	0.026	1.48	0.027	2.05	0.024	3.40
	100	0.032	1.96	0.034	2.19	0.03	3.63
	120	0.039	2.12	0.04	2.50	0.036	3.87
	140	0.045	2.90	0.047	2.65	0.042	4.15
	160	0.051	2.98	0.053	2.83	0.049	4.51
	180	0.058	3.52	0.06	3.04	0.054	4.46
	200	0.065	3.60	0.066	3.24	0.06	4.97
	220	0.071	3.91	0.073	3.47	0.066	5.09
	240	0.077	4.30	0.08	3.40	0.072	5.25
	260	0.083	4.17	0.087	3.66	0.078	5.42
	280	0.09	4.52	0.094	3.85	0.084	5.43
	300	0.096	4.75	0.101	4.16	0.09	5.61
	320	0.103	4.86	0.106	4.01	0.096	5.96
	340	0.109	4.80	0.113	4.19	0.103	5.73
	360	0.115	5.47	0.12	4.02	0.108	5.94
	380	0.122	5.52	0.127	4.32	0.113	5.91
	400	0.129	5.50	0.133	4.28	0.121	6.11
L1-2	0	0	0	0	0	0	0
	10	0.003	0.51	0.004	0.79	0.004	0.82

20	0.007	0.78	0.007	1.12	0.007	1.10
40	0.013	0.86	0.015	1.68	0.015	2.10
60	0.02	1.42	0.022	2.14	0.022	2.60
80	0.026	1.75	0.029	2.53	0.029	2.93
100	0.033	1.93	0.037	2.82	0.036	3.21
120	0.039	2.43	0.044	3.08	0.044	3.42
140	0.047	2.49	0.051	3.33	0.051	3.71
160	0.053	2.61	0.058	3.77	0.059	3.89
180	0.06	3.25	0.066	3.70	0.066	4.07
200	0.067	3.04	0.073	3.82	0.073	4.39
220	0.073	3.44	0.08	4.18	0.079	4.55
240	0.079	3.53	0.087	4.07	0.087	4.75
260	0.086	3.73	0.095	4.19	0.095	4.93
280	0.093	3.68	0.102	4.39	0.103	5.02
300	0.1	3.76	0.111	4.76	0.11	5.07
320	0.106	3.80	0.117	4.64	0.116	5.13
340	0.113	3.78	0.124	4.77	0.125	5.09
360	0.12	4.00	0.131	4.64	0.132	5.29
380	0.125	4.36	0.138	4.57	0.139	5.31
400	0.134	4.27	0.145	4.88	0.145	5.40

MCZ 67411

		Dorsiflexion		Lateroflexion		Ventroflexion	
	Mass (g)	Moment (Nm)	Angle of deflection (deg)	Moment (Nm)	Angle of deflection (deg)	Moment (Nm)	Angle of deflection (deg)
T1-2	0	0	0	0	0	0	0
	10	0.002	0.10	0.002	0.26	0.002	0.42
	20	0.003	0.12	0.005	0.40	0.003	0.55
	30	0.005	0.71	0.007	0.39	0.005	0.66
	40	0.007	0.56	0.009	0.48	0.006	0.74

	50	0.008	0.63	0.011	0.33	0.007	0.78
	60	0.01	0.94	0.013	0.59	0.009	0.84
	70	0.011	1.18	0.016	0.47	0.01	0.98
	80	0.013	0.94	0.018	0.56	0.012	0.89
	90	0.015	1.25	0.02	0.60	0.013	1.00
	100	0.016	1.36	0.023	0.61	0.015	0.94
	110	0.018	1.37	0.025	0.59	0.016	0.84
	120	0.02	1.70	0.027	0.70	0.018	1.10
	130	0.021	1.86	0.029	0.84	0.019	0.88
	140	0.023	1.84	0.031	0.81	0.021	0.93
	150	0.025	1.88	0.034	0.59	0.022	0.96
	160	0.026	1.90	0.036	0.58	0.023	0.97
	170	0.028	1.87	0.038	0.71	0.025	0.97
	180	0.03	2.13	0.039	0.68	0.026	0.97
	190	0.031	2.34	0.043	0.71	0.028	1.05
	200	0.033	2.51	0.045	0.69	0.029	1.11
	220	0.036	2.46	0.05	0.81	0.031	0.99
	240	0.039	2.56	0.053	0.81	0.036	1.19
	260	0.043	2.62	0.058	0.80	0.039	1.15
	280	0.046	2.76	0.064	0.86	0.041	1.16
	300	0.049	2.95	0.069	0.94	0.044	1.03
	320	0.053	3.08	0.073	0.82	0.048	1.16
	340	0.056	3.22	0.077	0.81	0.051	1.21
	360	0.06	3.05	0.082	0.91	0.053	1.28
	380	0.063	3.12	0.087	0.96	0.057	1.23
	400	0.066	3.24	0.09	0.75	0.059	1.10
T3-4	0	0	0	0	0	0	0
	10	0.002	0.75	0.002	1.10	0.002	2.72
	20	0.003	1.28	0.003	1.51	0.003	4.15
	30	0.004	1.38	0.005	1.86	0.005	4.81
	40	0.006	1.63	0.007	2.19	0.006	5.00

	50	0.007	1.84	0.008	2.41	0.008	5.52
	60	0.008	1.98	0.009	2.66	0.009	5.90
	70	0.01	1.78	0.011	2.56	0.011	6.02
	80	0.012	2.12	0.013	2.51	0.012	6.27
	90	0.013	2.13	0.014	2.96	0.014	6.69
	100	0.015	2.37	0.015	2.88	0.015	6.66
	110	0.016	2.46	0.017	2.83	0.017	6.72
	120	0.018	2.51	0.018	2.85	0.018	7.08
	130	0.019	2.56	0.02	2.92	0.02	7.00
	140	0.021	2.72	0.022	2.85	0.021	7.12
	150	0.021	2.60	0.023	2.94	0.022	7.09
	160	0.024	2.70	0.025	3.10	0.024	7.23
	170	0.025	2.76	0.026	3.08	0.026	7.21
	180	0.027	2.83	0.028	3.24	0.027	7.24
	190	0.028	2.96	0.029	3.19	0.029	7.36
	200	0.03	2.97	0.03	3.19	0.03	7.32
	220	0.033	3.17	0.034	3.35		
	240	0.036	3.20	0.036	3.10		
	260	0.038	3.24	0.041	3.27		
	280	0.042	3.39	0.042	3.43		
	300	0.045	3.35	0.045	3.43		
T5-6	0	0	0	0	0	0	0
	10	0.001	0.32	0.002	1.37	0.001	1.92
	20	0.003	0.66	0.003	1.75	0.003	2.94
	30	0.004	0.57	0.005	2.02	0.004	3.35
	40	0.006	0.94	0.006	2.19	0.006	3.79
	50	0.007	0.77	0.008	2.44	0.007	3.95
	60	0.009	0.89	0.009	2.47	0.008	4.02
	70	0.011	1.31	0.011	2.37	0.009	4.21
	80	0.012	1.05	0.012	2.64	0.011	4.12
	90	0.014	1.25	0.014	2.60	0.013	4.51

100	0.016	1.76	0.015	2.64	0.014	4.58
110	0.017	1.58	0.017	2.66	0.016	4.62
120	0.019	1.57	0.018	2.90	0.018	4.73
130	0.02	1.62	0.02	2.86	0.019	4.96
140	0.02	1.61	0.02	2.80	0.02	4.92
150	0.023	1.95	0.022	3.05	0.022	5.20
160	0.025	1.86	0.024	3.06	0.023	5.01
170	0.026	1.99	0.026	3.07	0.024	5.30
180	0.028	2.02	0.027	3.16	0.024	5.06
190	0.03	2.20	0.029	3.14	0.028	5.47
200	0.031	2.33	0.031	3.30	0.028	5.53
220	0.035	2.22	0.034	3.31	0.033	5.56
240	0.037	2.45	0.036	3.28	0.034	5.70
260	0.039	2.44	0.04	3.39	0.036	5.93
280	0.043	2.59	0.043	3.32	0.041	5.70
300	0.046	2.72	0.045	3.59	0.043	5.75
320	0.05	2.63			0.045	5.69
340	0.053	2.90				
360	0.056	3.03				
380	0.06	3.03				
400	0.062	3.07				

Cases in which motion segments are missing all data in one direction signify errors in data collection in that direction, not physical issues with the motion segment itself. Cases in which all directions are missing for a motion segment signify physical issues in the motion segment, such as breakage or cut ligaments. In several cases, when no further bending was detected during loading, the same number of masses was not applied to the motion segment in all three directions

Table S2. Range of motion and compliance constant for all motion segments in all three bending directions.

			R_m	C	R_m SE	C SE	SS_{resid}	SS_{total}	R^2
MCZ 67401	T2-3	Dorsiflexion	2.2888	262.89	0.082581	54.674	1.7059	5.2273	0.67365
		Lateroflexion	3.3521	64.621	0.214	9.1489	0.83871	14.831	**0.94345**
		Ventroflexion	6.1838	285.94	0.041463	11.171	0.43488	31.886	**0.98636**
	T4-5	Dorsiflexion	2.3104	36.176	0.34238	9.4844	0.60792	6.3693	**0.90455**
		Lateroflexion	3.3262	177.32	0.075541	19.177	1.1155	10.471	**0.89347**
		Ventroflexion	5.3344	236.78	0.076542	19.017	1.4225	22.328	**0.93629**
	T6-7	Dorsiflexion	3.6076	33.432	0.1817	4.0933	0.9144	15.422	**0.94071**
		Lateroflexion	2.9534	105.51	0.086947	14.356	1.403	7.3272	**0.80852**
		Ventroflexion	6.3482	254.88	0.086741	27.154	2.447	14.562	**0.83197**
	T8-9	Dorsiflexion	5.8963	56.147	0.21159	7.0723	4.3847	38.794	**0.88698**
		Lateroflexion	4.3249	75.063	0.087396	6.3082	1.1535	21.013	**0.94511**
		Ventroflexion	7.3463	188.86	0.11838	21.271	4.2211	28.079	**0.84967**
	L1-2	Dorsiflexion	7.3631	57.593	0.098217	3.0583	1.3229	79.455	**0.98335**
		Lateroflexion	7.4906	128.07	0.046894	4.9693	0.59814	47.914	**0.98752**
		Ventroflexion	10.103	121.72	0.1253	9.0476	4.1074	102.39	**0.95989**
	L3-4	Dorsiflexion	7.6615	62.613	0.13289	4.3962	2.5066	76.347	**0.96717**
		Lateroflexion	4.6578	56.268	0.086663	3.6691	0.75972	33.31	**0.97719**
		Ventroflexion	7.0637	68.465	0.050833	2.0546	0.38462	64.713	**0.99406**
MCZ 67402	T1-2	Dorsiflexion	2.2146	130.07	0.052556	9.9844	0.56352	8.3808	**0.93276**
		Lateroflexion	0.11767	2.94E+06	0.01913	0	0.21957	0.21957	0
		Ventroflexion	1.3519	378.81	0.022146	39.392	0.28352	1.1922	**0.76218**
	T3-4	Dorsiflexion	3.3378	141.92	0.10241	13.68	1.9974	15.871	**0.87415**
		Lateroflexion	5.1231	512.68	0.053883	38.538	1.8166	13.39	**0.86433**
		Ventroflexion	8.488	469.01	0.066174	24.841	2.653	38.745	**0.93153**
	T5-6	Dorsiflexion	3.544	29.852	0.68339	7.8968	0.44582	8.8724	**0.94975**
		Lateroflexion	3.091	181.69	0.061914	14.479	1.2426	11.101	**0.88807**
		Ventroflexion	4.5406	241.76	0.051532	13.596	1.1946	19.812	**0.93971**
	T7-8	Dorsiflexion	5.0412	46.74	0.13939	3.7347	2.9188	40.865	**0.92857**

		Lateroflexion	4.5654	114.72	0.068888	8.7878	2.1892	19.716	**0.88896**
		Ventroflexion	3.8371	52.845	0.050721	2.1794	0.48364	27.451	**0.98238**
	T9-10	Dorsiflexion	5.4497	109.15	0.10279	10.338	2.2231	30.164	**0.9263**
		Lateroflexion	6.4306	87.085	0.099365	6.4744	1.9642	40.649	**0.95168**
		Ventroflexion	9.4781	174.24	0.17854	22.934	9.6006	47.704	**0.79875**
	L1-2	Dorsiflexion	6.2193	102.29	0.092851	8.8028	2.1777	31.396	**0.93064**
		Lateroflexion	6.4819	152.72	0.060301	9.8528	1.0886	27.881	**0.96095**
		Ventroflexion	9.3502	124.92	0.19132	16.3	10.22	53.448	**0.80878**
	L3-4	Dorsiflexion	7.7469	43.165	0.11434	2.0534	1.0141	96.322	**0.98947**
		Lateroflexion	9.0312	74.344	0.14902	5.8548	4.3381	123.53	**0.96488**
		Ventroflexion	9.6475	79.716	0.219	8.7363	9.4585	113.36	**0.91656**
MCZ 67403	T3-4	Dorsiflexion	2.3072	143.91	0.088976	25.564	1.4289	5.1968	0.72504
		Lateroflexion	3.8671	406.04	0.060702	47.157	1.161	6.6597	**0.82567**
		Ventroflexion	6.9654	376	0.071829	27.688	1.5819	22.956	**0.93109**
	T5-6	Dorsiflexion	2.128	55.178	0.11922	6.7701	0.25762	6.4639	**0.96014**
		Lateroflexion	3.1525	217.16	0.06195	23.768	0.92124	7.9428	**0.88401**
		Ventroflexion							
	T7-8	Dorsiflexion	4.12	23.483	0.22639	2.8048	0.85664	21.994	**0.96105**
		Lateroflexion	3.9177	52.269	0.093292	4.6909	1.0438	16.601	**0.93712**
		Ventroflexion	4.4994	41.626	0.11374	3.385	1.003	24.242	**0.95863**
	T9-10	Dorsiflexion	6.4024	15.485	0.49766	2.3977	4.0789	73.989	**0.94487**
		Lateroflexion	3.9102	55.816	0.07179	4.0978	0.71166	17.523	**0.95939**
		Ventroflexion	6.2629	52.478	0.069958	2.5823	1.2919	53.976	**0.97607**
	L1-2	Dorsiflexion	5.4416	16.602	0.35081	1.9455	0.74815	34.217	**0.97814**
		Lateroflexion	2.9835	35.837	0.075291	2.8294	0.40148	13.277	**0.96976**
		Ventroflexion	5.1928	27.781	0.070948	0.98764	0.18053	38.442	**0.9953**
MCZ 67405	T1-2	Dorsiflexion	0.36201	166.91	0.047091	76.412	0.55338	0.68935	0.19724
		Lateroflexion	0.2237	314.89	0.031677	233.68	0.47973	0.53681	0.10633
		Ventroflexion	0.33248	80.176	0.063175	34.054	0.22484	0.38582	0.41724
	T3-4	Dorsiflexion	2.7201	211.95	0.065973	22.158	1.5883	8.8029	**0.81957**

		Lateroflexion	4.9472	329.85	0.083282	32.028	3.6563	16.836	**0.78283**
		Ventroflexion	6.1474	265.63	0.048969	10.61	1.0955	38.846	**0.9718**
	T5-6	Dorsiflexion	2.9601	141.18	0.070582	11.507	1.177	11.982	**0.90177**
		Lateroflexion	3.9987	174.6	0.098653	18.06	3.3953	17.411	**0.80499**
		Ventroflexion	3.2818	273.51	0.039311	16.726	0.7159	14.377	**0.95021**
	T7-8	Dorsiflexion	5.1394	8.9517	2.1556	4.9221	1.3657	13.341	**0.89763**
		Lateroflexion	4.1336	52.024	0.06661	2.8339	0.39568	24.734	**0.984**
		Ventroflexion	3.7888	90.227	0.044329	4.6877	0.34049	17.796	**0.98087**
	T9-10	Dorsiflexion	9.5354	84.138	0.32742	13.823	21.027	67.452	**0.68826**
		Lateroflexion	6.7734	47.994	0.093092	2.1999	0.74482	73.599	**0.98988**
		Ventroflexion	10.015	97.105	0.22394	10.87	10.476	148.76	**0.92958**
	L1-2	Dorsiflexion	11.051	4.5243	5.9579	2.8539	1.1039	28.208	**0.96087**
		Lateroflexion	5.9502	48.872	0.095811	2.8752	1.0192	57.029	**0.98213**
		Ventroflexion	5.5142	47.752	0.096008	2.9059	0.90118	44.144	**0.97959**
	L3-4	Dorsiflexion	6.063	21.294	0.19918	1.3907	0.40855	47.426	**0.99139**
		Lateroflexion	4.4605	33.622	0.10784	2.1509	0.45342	31.832	**0.98576**
		Ventroflexion	4.7263	24.189	0.10132	1.1176	0.16267	30.881	**0.99473**
MCZ 67406	T1-2	Dorsiflexion	2.9842	46.487	0.40085	8.5538	0.07737	4.8544	**0.98406**
		Lateroflexion							
		Ventroflexion	0.81608	290.72	0.012768	18.58	0.034871	0.8702	**0.95993**
	T3-4	Dorsiflexion	3.8613	59.573	0.11345	5.1089	1.2145	17.322	**0.92989**
		Lateroflexion	2.9139	330.72	0.039283	38.977	0.7344	2.0916	0.64889
		Ventroflexion	8.2868	291.13	0.093139	25.002	3.9327	18.928	**0.79223**
	T5-6	Dorsiflexion	1.9937	45.584	0.078566	4.6647	0.39113	5.1954	**0.92472**
		Lateroflexion	2.8146	157.26	0.048755	16.209	0.88499	3.9754	**0.77739**
		Ventroflexion	5.615	176.92	0.083658	17	2.8002	13.469	**0.7921**
	T7-8	Dorsiflexion							
		Lateroflexion	3.5962	142.4	0.077292	14.702	1.165	7.1612	**0.83731**
		Ventroflexion	4.7297	144.84	0.087876	13.192	1.5392	12.135	**0.87316**
	T9-10	Dorsiflexion	6.1939	94.188	0.10523	6.3076	1.668	35.425	**0.95292**
		Lateroflexion	5.7222	37.344	0.075395	1.158	0.17423	47.498	**0.99633**

		Ventroflexion	10.038	128.07	0.20429	11.953	7.7311	106.34	**0.9273**
	L1-2	Dorsiflexion	4.1044	42.674	0.12852	3.5187	0.82168	21.306	**0.96144**
		Lateroflexion	5.9285	57.988	0.060458	1.8261	0.31714	48.152	**0.99341**
		Ventroflexion	9.7792	44.69	0.21733	2.6495	2.4657	149.38	**0.98349**
	L3-4	Dorsiflexion	3.4293	37.768	0.09344	2.449	0.27851	15.4	**0.98191**
		Lateroflexion	4.5526	47.234	0.087113	2.4424	0.41552	28.88	**0.98561**
		Ventroflexion	5.4885	23.798	0.12626	1.0259	0.13707	37.596	**0.99635**
MCZ 67407	T1-2	Dorsiflexion	3.0089	16.432	1.6293	10.676	0.41349	4.1016	**0.89919**
		Lateroflexion	0.18325	126.08	0.028452	57.59	0.12925	0.14821	0.12792
		Ventroflexion	0.53474	349.2	0.019372	71.527	0.19652	0.45012	0.56341
	T3-4	Dorsiflexion	3.3039	113.72	0.087078	8.5756	1.1284	17.954	**0.93715**
		Lateroflexion	4.3785	356.76	0.040881	19.077	0.88112	15.078	**0.94156**
		Ventroflexion	7.3474	298.37	0.10238	21.545	4.9624	48.223	**0.8971**
	T5-6	Dorsiflexion	1.7059	197.86	0.062885	25.727	0.63415	3.2543	**0.80513**
		Lateroflexion	2.8064	289.95	0.088269	37.485	1.7003	9.0141	**0.81138**
		Ventroflexion	4.6385	329.46	0.073505	27.571	2.6192	18.551	**0.85881**
	T7-8	Dorsiflexion	5.5233	54.525	0.12903	4.1102	1.3046	40.524	**0.96781**
		Lateroflexion	4.6564	117.74	0.055761	7.7246	0.73809	22.366	**0.967**
		Ventroflexion	5.4009	104.75	0.098843	9.7065	2.0985	26.366	**0.92041**
	T9-10	Dorsiflexion	7.671	67.294	0.14498	4.8597	2.605	75.903	**0.96568**
		Lateroflexion	6.4582	61.978	0.051869	1.8542	0.31327	60.035	**0.99478**
		Ventroflexion	9.8602	88.276	0.18188	7.2977	5.7704	141.85	**0.95932**
	L1-2	Dorsiflexion	5.6962	62.818	0.064531	2.6258	0.47209	46.994	**0.98995**
		Lateroflexion	5.0138	59.526	0.041442	1.747	0.17711	36.512	**0.99515**
		Ventroflexion	6.2263	51.075	0.10299	2.8783	0.97627	56.422	**0.9827**
	L3-4	Dorsiflexion	8.0171	45.977	0.1225	2.1062	0.92426	101.37	**0.99088**
		Lateroflexion	6.0413	34.047	0.2379	3.2783	1.6047	62.4	**0.97428**
		Ventroflexion	7.6597	12.11	1.1773	2.6619	1.1724	48.703	**0.97593**
MCZ 67408	T1-2	Dorsiflexion	1.0889	65.581	0.14592	16.532	0.46833	2.0171	**0.76783**
		Lateroflexion	0.33187	76.763	0.069127	32.924	0.1765	0.38405	0.54041

		Ventroflexion	0.21518	1170.4	0.011582	657.18	0.098929	0.11318	0.12594
	T3-4	Dorsiflexion	2.6607	146.83	0.081868	13.505	1.0894	10.355	**0.89479**
		Lateroflexion							
		Ventroflexion	6.796	636.09	0.047314	33.647	1.4601	20.314	**0.92812**
	T5-6	Dorsiflexion	1.4482	362.71	0.095292	123.58	4.35	6.5967	0.34059
		Lateroflexion	3.3076	229.32	0.070657	19.134	1.5593	14.003	**0.88864**
		Ventroflexion	4.7187	180.87	0.10379	13.618	2.547	31.68	**0.9196**
	T7-8	Dorsiflexion	5.0514	39.306	0.17923	3.4057	0.90818	33.021	**0.9725**
		Lateroflexion	3.6278	48.854	0.092101	3.6374	0.49194	17.064	**0.97117**
		Ventroflexion	4.9925	57.066	0.085851	3.0444	0.50671	34.76	**0.98542**
	T9-10	Dorsiflexion	8.2096	16.765	0.53395	1.6683	0.46858	58.59	**0.992**
		Lateroflexion	4.4924	38.985	0.13661	2.9686	0.58815	27.507	**0.97862**
		Ventroflexion	6.0363	56.71	0.13756	3.9155	1.2062	54.423	**0.97784**
	L1-2	Dorsiflexion	4.6207	33.21	0.1548	2.4932	0.45943	28.82	**0.98406**
		Lateroflexion	4.8302	46.291	0.099335	2.8654	0.61532	30.89	**0.98008**
		Ventroflexion	5.3661	47.685	0.10471	2.8582	0.73621	38.106	**0.98068**
MCZ	T1-2	Dorsiflexion	4.0103	66.052	0.17584	5.0323	0.41115	26.074	**0.98423**
67411		Lateroflexion	0.81863	174.92	0.030766	24.016	0.25888	0.9682	0.73261
		Ventroflexion	1.0753	478.69	0.024695	57.553	0.29359	1.1424	0.74301
	T3-4	Dorsiflexion	3.1605	256.7	0.091463	23.302	0.97831	11.675	**0.9162**
		Lateroflexion	3.1554	454.61	0.04858	32.803	0.66023	8.2626	**0.92009**
		Ventroflexion	7.0905	563.18	0.10111	37.646	1.7413	29.756	**0.94148**
	T5-6	Dorsiflexion	3.3359	91.887	0.13334	7.3074	0.55624	18.424	**0.96981**
		Lateroflexion	3.1254	478.8	0.071872	52.872	1.4945	7.0894	**0.7892**
		Ventroflexion	5.3459	479.05	0.10474	44.064	3.4516	23.734	**0.85457**

Ranges of motion (R_m) and compliance constants (C) generated through modeling negative exponential curves to moment and angle of deflection data. Standard error (SE) of R_m and of C are provided, as well as the residual and total sums of squares of the model (SS_{resid}, SS_{total}). R^2 values of each model are listed. Bolded values indicate $R^2 \geq 0.75$, and designate the data used in calculating average compliance and range of motion.

Table S3. Non-normalized linear measurements.

		CL	CW	CH	NSH	TPDW	PrZW	IZL	LW	MH	AL	AH	PoZL	LA
MCZ	T1	7.4674	14.8445	2.2048	32.4676	10.9787	17.5406	9.6885	14.5542	0	0	0	8.9837	29.021
67401	T2	8.4947	11.8719	3.4049	29.5302	11.8503	13.9339	10.3176	10.7699	0	0	0	7.0086	28.527
	T3	7.7856	10.7478	3.9648	28.1678	10.813	10.3099	9.4073	10.4648	0	0	0	7.3636	27.538
	T4	7.6007	9.5442	4.4139	26.7207	10.7985	11.0388	9.8464	10.5807	0	0	0	7.4559	25.557
	T5	7.3883	8.9554	4.4434	23.9386	9.3518	10.6957	10.4001	10.2985	0	0	0	7.0101	23.606
	T6	7.9176	8.9196	4.594	22.1117	10.2188	9.4009	10.8075	9.4367	0	0	0	7.3872	23.159
	T7	8.1028	9.6467	4.7393	20.0249	9.2579	10.3461	13.0806	10.0329	4.0121	3.2164	2.8196	2.9265	22.021
	T8	8.186	10.6279	4.8504	17.046	9.0115	9.2214	13.2485	9.912	8.2043	3.953	3.5094	3.7565	22.558
	T9	8.4172	10.6704	5.0409	15.4712	8.5572	10.325	13.4962	9.7722	9.6359	4.4872	4.0768	3.7739	22.533
	T10	9.1754	10.3898	5.1175	15.6998	6.9357	11.0251	14.54	9.7826	12.714	4.5794	4.7695	3.9537	23.04
	L1	9.7542	10.472	5.5402	16.7208	7.6527	11.3193	14.9018	10.0284	16.4102	4.0339	4.8826	4.0764	24.643
	L2	9.7601	10.1538	5.4314	19.6827	8.0617	11.1275	15.5739	10.543	21.6167	4.1511	5.9733	3.9397	26.244
	L3	10.2735	10.8404	5.5057	21.0814	10.1322	11.3528	15.1697	10.8683	25.6995	5.4363	4.9181	4.2788	27.826
	L4	10.0938	11.5299	5.2253	21.336	9.619	11.9765	14.9251	11.5362	26.4159	5.7318	5.1236	4.5604	27.77
	L5	9.1368	12.2605	4.8693	18.7024	8.3381	12.0591	15.1236	16.3449	28.328	6.1352	3.4986	4.829	24.335
MCZ	T1	6.7311	15.7296	1.9472	32.9373	9.461	15.9393	10.8091	13.1424	0	0	0	9.6398	26.566
67402	T2	7.9379	11.985	3.1492	30.4264	11.105	11.9456	8.994	10.5532	0	0	0	7.2541	23.51
	T3	7.5638	10.3617	3.6487	28.7185	10.8725	10.0612	10.2888	10.2027	0	0	0	6.7283	23.943
	T4	7.2436	9.2092	4.2036	25.9111	9.6336	9.51	10.1257	10.6036	0	0	0	6.7757	23.231
	T5	7.2049	8.4854	4.2674	24.1879	9.7206	9.9458	10.1456	11.2341	0	0	0	6.8363	22.185
	T6	7.4242	8.9655	4.56	21.6703	10.0353	10.2553	10.8119	11.5485	0	0	0	5.6602	21.234
	T7	7.808	9.4765	4.7363	18.747	9.1286	10.3495	12.5613	10.7332	4.8719	3.6336	3.1911	4.1929	20.85
	T8	7.7924	11.483	4.8162	16.1136	8.47	9.9869	12.7804	11.348	8.0282	4.6008	2.9371	4.4443	20.346
	T9	8.2211	10.2141	4.879	14.3827	7.9694	10.9247	13.3048	10.9284	10.8637	4.4383	3.0144	4.1481	19.991
	T10	8.5857	10.6502	5.0802	15.0264	7.2642	11.8119	13.9778	11.5005	12.9467	4.0395	4.3322	4.3841	19.84
	L3	10.3904	10.3428	5.8897	20.2233	10.0133	12.2537	15.1998	11.6351	23.2517	5.1532	5.1599	4.5588	25.404
	L4	10.7599	11.2393	6.039	21.196	11.236	12.7168	15.1813	11.7892	25.6991	5.0227	4.481	4.9465	27.494
	L5	9.4343	11.7486	4.9011	19.6575	9.81	12.3626	15.8005	11.4537	27.3385	5.3781	3.9414	5.144	24.3
MCZ	T1	7.8218	15.3544	2.6559	36.1258	11.1735	16.6754	9.6487	14.5057	0	0	0	10.1145	27.526
67403	T2	8.5856	12.3941	3.5475	31.5737	11.4675	13.5074	10.9275	10.4344	0	0	0	7.6988	26.491
	T3	8.0079	10.6635	4.3429	29.9647	11.5663	9.9789	9.9499	10.241	0	0	0	6.6675	24.325

	T4	7.701	9.3273	4.7455	28.0123	9.9457	10.1479	9.7629	10.8245	0	0	0	7.3001	23.704
	T5	7.8203	8.7189	4.882	25.1624	9.8499	10.3468	10.6111	11.6581	0	0	0	6.7533	22.428
	T6	7.9865	8.1464	4.8951	22.6746	9.1833	10.4774	11.1401	10.9257	0	0	0	6.1583	22.104
	T7	7.9356	9.8564	4.9988	20.0921	9.3166	10.2605	13.3222	10.0459	5.7418	2.8013	3.0208	3.1635	23.209
	T8	8.3075	11.0584	5.1033	18.0129	8.2977	9.6016	12.5661	9.5686	9.0201	3.2913	3.4958	3.7657	23.958
	T9	8.3122	12.5224	5.2234	18.1732	10.0568	10.5283	12.6719	11.0154	10.9759	3.5619	4.5614	3.8893	23.063
	T10	8.6888	10.5664	5.5743	17.9549	8.3174	11.0884	14.3506	12.598	14.3659	3.8043	4.7432	4.191	23.752
	L1	9.4908	10.3032	5.9363	19.0423	7.1403	11.7389	15.8024	12.0684	19.5519	3.675	4.8317	3.708	25.344
	L2	10.1133	10.1517	6.0387	21.4334	9.057	11.5407	15.8851	11.17	23.8332	4.2671	5.0935	3.6978	26.624
	L3	10.393	11.0863	6.4198	23.7929	10.575	12.1233	16.2097	12.5646	25.6635	4.4103	5.1888	4.2478	29.08
	L4	10.0251	12.7308	5.8503	23.4205	10.9551	12.6704	15.8266	11.5466	28.0953	5.4576	4.4442	5.2399	28.904
	L5	8.8278	12.2779	5.201	21.0062	10.3079	12.3506	15.6714	10.3639	20.3576	6.1881	3.5951	4.5668	25.793
MCZ	T3	8.3629	10.5946	3.9037	30.3437	9.4332	11.2354	10.9433	10.5941	0	0	0	6.8839	25.269
67405	T4	7.8861	9.7222	4.9901	28.2764	9.3942	10.6779	11.3084	11.2018	0	0	0	7.4163	25.161
	T5	8.2022	9.1153	5.68	25.2447	10.0722	10.9368	10.8488	11.3515	0	0	0	7.0098	21.637
	T6	8.4349	9.3653	5.936	22.6582	9.2143	10.5503	11.4152	11.4728	1.0609	0	0	7.222	21.599
	T7	8.0989	10.7561	5.044	19.3845	8.6737	11.0243	13.5194	9.6987	6.1741	2.7303	2.7653	3.3858	21.362
	T8	8.092	12.1528	5.3185	17.847	8.6554	9.249	13.0887	9.0169	8.8418	4.0339	3.4516	4.2096	22.299
	T9	8.4014	11.3346	5.641	16.8826	8.7134	10.2458	14.1939	10.0489	12.0862	3.7873	3.2183	4.5603	22.353
	T10	9.0168	10.6382	5.4678	16.8567	7.332	11.153	15.3441	10.2617	14.9049	3.8028	4.8984	4.1979	22.182
	L1	9.5911	10.4407	6.203	18.4137	7.6115	11.2749	16.5432	11.122	18.2472	3.9878	5.6096	4.5579	24.15
	L2	10.6504	10.3087	6.1491	19.8286	8.4557	11.4032	16.8231	10.8632	22.7623	4.5683	5.1143	4.6842	26.599
	L3	10.6802	10.7319	5.9664	21.2165	10.6555	11.7893	17.2168	12.1061	25.8499	4.9981	4.7944	5.2267	28.379
	L4	10.5404	11.9003	5.6008	21.6258	10.596	11.9845	16.6044	12.0971	28.2677	4.7249	4.8566	4.9289	29.079
MCZ	T3	8.557	12.0382	4.185	31.8252	11.0417	12.4097	10.8818	10.1102	0	0	0	6.7634	26.1454
67406	T4	7.8473	10.5606	4.644	30.9391	10.2552	9.9015	11.0691	10.6806	0	0	0	6.6831	26.7175
	T5	7.6696	9.6595	4.642	28.0166	10.261	10.4844	10.9495	11.3837	0	0	0	6.6791	21.3515
	T6	7.941	9.9997	4.6762	25.2592	10.367	10.9014	11.1068	11.9197	0	0	0	6.8176	22.2949
	T7	8.1972	10.2386	5.0392	22.2419	9.675	10.8933	13.4651	8.4797	4.5847	0.6918	2.5039	5.0567	21.4166
	T8	8.0084	10.4316	4.9947	19.9945	9.028	9.2112	13.8636	8.6994	8.1255	4.1545	3.6113	3.5936	15.9369
	T9	8.2623	10.5706	5.1358	17.1248	8.0627	9.4828	13.5912	9.8042	10.9712	3.7241	3.4702	4.3098	21.37
	T10	8.5793	10.7279	5.4332	17.3942	6.7328	10.5012	15.2599	10.6043	14.0658	4.1181	4.9887	4.759	22.3482
	L1	8.9093	10.5368	6.0175	18.573	6.987	11.2485	15.521	10.9915	18.6796	4.4356	4.9036	4.1953	22.3372

	L2	9.855	10.343	6.2037	20.4694	8.5043	11.0623	15.9081	10.8229	23.5729	4.3211	5.1878	4.1457	26.0488
	L3	9.8892	10.5319	6.1582	21.5812	10.3874	11.2423	15.3244	11.5239	25.4345	4.9811	5.0397	4.571	27.3108
	L4	9.9741	11.6991	5.9344	22.7681	9.6538	12.0794	16.011	11.607	27.5407	5.222	5.0445	4.6566	28.9773
	L5	9.0808	12.5132	5.2212	22.4063	10.1664	11.6768	16.5211	10.3212	30.0745	6.9118	4.1223	6.3112	27.7894
MCZ	T1	7.9125	15.2521	2.8224	34.0935	9.8849	16.8163	10.1122	13.4436	0	0	0	8.0402	26.652
67407	T2	8.9468	13.0229	3.8731	30.736	10.8181	12.532	10.5113	10.654	0	0	0	6.7107	25.469
	T3	7.6999	10.8501	4.3051	27.6136	9.8456	9.5896	12.7755	9.608	0	0	0	7.6779	26.814
	T4	7.6057	9.2738	4.6885	26.5315	10.0422	9.4558	10.3746	10.5183	0	0	0	7.2107	24.747
	T5	7.2488	9.3361	4.7053	24.5649	9.4095	10.3712	10.7605	11.008	0	0	0	6.7586	23.194
	T6	7.9035	10.1103	4.921	21.7544	11.0225	10.402	11.2499	12.646	0	0	0	6.1021	21.294
	T7	7.9729	11.7168	4.876	19.4351	9.5003	10.8051	13.6609	9.9283	5.176	2.8781	3.1502	4.1106	22.148
	T8	8.1632	9.3235	5.0244	16.7068	9.8036	9.9469	13.4487	8.8825	8.9789	3.8191	3.7852	4.0275	22.923
	T9	8.0902	10.574	5.3438	16.2435	9.0765	10.5687	14.3466	10.2362	11.7076	4.3922	4.0564	4.9553	23.162
	T10	8.6696	10.6006	5.775	17.5959	7.4107	11.5136	15.5612	11.0522	15.2276	3.6206	5.2567	4.2767	23.622
	L1	10.1009	10.1038	6.0569	18.2436	7.8855	11.4591	16.6732	10.5736	19.3123	4.7985	5.1944	4.9167	25.873
	L2	10.6254	10.1904	6.4923	20.721	9.6438	11.2056	16.577	11.3971	23.5841	5.0809	6.1563	4.5701	27.97
	L3	10.8868	10.9366	6.2652	22.2731	12.0241	12.0217	16.1418	11.3946	26.8571	5.1181	5.4438	5.0922	30.055
	L4	10.2917	11.8114	5.6875	22.0745	10.2836	12.0937	16.1617	10.8538	28.6743	5.3687	4.3849	5.0829	28.697
	L5	9.2144	12.0493	4.7748	18.4701	10.2514	11.8835	16.4581	11.301	24.945	6.5217	4.3392	5.7695	25.451
MCZ	T1	7.7611	15.7006	2.2649	32.2299	9.9816	16.3839	10.6934	13.5292	0	0	0	8.0009	32.8
67408	T2	9.0354	11.8014	3.6525	31.6765	10.9238	13.7722	10.0133	11.0587	0	0	0	8.8313	31.803
	T3	8.5021	10.178	4.1527	29.7648	10.8747	11.5793	9.6189	8.804	0	0	0	7.6598	30.245
	T4	8.2901	9.1973	5.0992	28.3734	10.0783	9.9006	10.4834	8.7553	0	0	0	6.02	30.891
	T5	8.0433	8.8416	4.5482	26.4151	9.8373	8.8123	10.9245	11.0588	0	0	0	7.2494	28.103
	T6	8.0398	8.8785	4.7319	24.1965	9.2676	10.8429	11.6968	12.0518	1.4319	1.4981	2.5675	6.9716	25.155
	T7	8.4096	10.1602	4.9069	21.535	7.9136	11.4394	14.9523	11.0907	5.417	3.7747	3.2154	3.7324	24.544
	T8	8.5151	12.2452	4.6893	19.4099	8.3321	9.6769	14.5535	9.698	8.9615	3.9397	3.9011	4.5043	24.772
	T9	8.8821	10.2641	4.8062	19.0085	8.9862	10.5275	14.59	9.5177	12.2397	4.1106	3.7083	4.7224	24.769
	T10	9.4283	10.5916	5.2966	19.1819	7.971	10.7717	16.2293	10.5979	14.6344	4.1379	4.4525	4.4142	25.449
	L1	10.695	10.4539	5.7625	20.4825	7.2973	11.0159	16.7528	10.8412	18.6764	4.481	4.7807	4.8365	27.548
	L2	11.2182	10.0569	6.3358	21.2546	8.5949	11.2132	17.3902	11.1326	23.2247	4.4619	5.7224	4.824	28.905
MCZ	T1	8.6531	14.2535	3.2426	29.7467	9.4478	16.4886	10.7621	11.6665	0	0	0	7.7143	26.097
67411	T2	7.8996	11.6024	3.7163	31.407	10.5009	11.2045	10.4893	10.7124	0	0	0	7.7782	27.073

T3	7.7506	10.4486	4.183	29.3173	10.6848	10.5417	11.3553	11.7558	0	0	0	7.257	25.816
T4	7.5406	10.2395	4.4578	28.5414	10.2012	11.0463	10.8044	11.705	0	0	0	7.0204	23.05
T5	7.8212	10.5749	4.6127	25.2495	9.4642	11.0258	12.918	10.5258	0	1.1966	3.1652	4.2662	21.497
T6	8.1036	11.3429	4.741	21.0249	10.0677	11.4774	13.9923	10.5398	6.1847	3.093	3.154	3.3565	22.959
T7	8.1425	11.8274	4.9693	19.1422	8.854	9.6591	12.6656	9.2294	9.1594	4.4239	2.892	4.5543	23.338
T8	8.6848	11.65	4.7252	17.8404	8.5175	11.298	15.7492	10.9086	15.8828	5.1275	5.5206	4.8662	23.634
T9	8.4043	11.7747	5.2106	17.4212	9.6891	10.306	14.6099	11.0708	12.098	4.5291	3.7348	5.5729	23.974

Non-normalized linear measurements taken in millimeters (mm). Missing vertebrae represent damaged or otherwise abnormal vertebrae, and were not used in analyses. See Fig. 2 for measurement abbreviations.

Table S4. Angular measurements.

		PrZA	NSA	TPDA	MA	PrZC	TPDAD	TPDAC
MCZ	T1	122.6691	154.0374	120.4244	0	127.9681	54.7694	92.1304
67401	T2	118.4189	133.5423	104.1602	0	167.1119	56.7	106.7749
	T3	107.248	130.5162	95.1379	0	159.6772	51.4711	114.4991
	T4	109.7396	141.1717	87.8108	0	165.7428	51.8727	114.5332
	T5	109.929	127.2307	81.1063	0	156.9029	53.1566	118.5753
	T6	99.9094	133.7393	87.019	0	151.9667	48.6362	112.9493
	T7	110.3226	121.666	88.1902	79.5457	154.4123	53.4648	116.9313
	T8	64.1325	126.8182	96.2721	83.3508	95.6723	61.3478	123.0209
	T9	62.3385	121.8306	112.773	75.0479	98.4724	76.2292	114.8956
	T10	64.2495	121.8967	118.1887	81.6168	98.2023	77.3141	116.5237
	L1	66.135	112.9016	122.9781	71.8574	95.0579	133.9428	54.485
	L2	72.9237	117.092	141.7888	73.0858	107.5627	126.8581	56.1512
	L3	74.8545	121.3439	148.1162	73.4335	100.2748	115.0943	52.9322
	L4	72.9705	131.8293	153.1251	83.3116	91.6611	92.9885	60.9897
	L5	75.7315	143.3096	158.3673	83.4828	97.8951	89.2766	58.1522
MCZ	T1	121.3401	152.0535	136.1467	0	96.4772	75.3464	88.1317
67402	T2	121.1912	146.2981	111.2035	0	160.7233	70.69	96.888
	T3	111.094	136.3752	95.6168	0	162.256	56.1224	112.378
	T4	108.8828	136.1556	91.0169	0	161.8475	53.5627	111.3112
	T5	114.153	138.588	89.9691	0	156.8764	51.1062	117.4146
	T6	117.9627	141.172	92.58	0	161.2409	52.5693	122.8304
	T7	125.6625	129.6833	111.5642	88.6967	152.955	63.5095	124.0959
	T8	66.1788	117.9147	130.5545	74.9642	90.9245	67.5503	117.252
	T9	70.5919	116.8036	113.2587	76.8409	91.3227	79.6637	118.2665
	T10	81.7135	127.1245	119.7192	83.2396	100.3029	78.2781	115.9234
	L3	81.0197	119.1576	144.8206	95.2199	98.3602	126.9103	58.9749
	L4	80.1518	132.268	154.2802	90.2809	96.6853	110.7127	59.5928
	L5	74.4348	132.9168	162.2826	90.5973	62.4831	106.2688	63.1854
MCZ	T1	122.1014	147.3953	125.9503	0	128.4012	63.8803	92.6187
67403	T2	125.2901	144.8511	109.1227	0	165.5371	58.177	104.2449
	T3	97.008	144.3027	98.3684	0	159.7346	58.0827	115.1827

	T4	103.3756	137.1567	93.9214	0	161.2091	61.6928	114.9451
	T5	111.6261	140.6544	90.4053	0	155.5566	65.5641	123.8742
	T6	109.1627	144.0704	100.8783	0	157.7173	58.151	117.6746
	T7	99.2666	130.9756	110.3418	86.8456	159.5828	58.4762	122.8071
	T8	61.6195	123.8564	100.9637	73.8134	103.3874	62.6959	120.2496
	T9	65.3739	119.4019	116.2881	66.9024	97.0876	66.6935	119.6249
	T10	70.2023	124.696	121.0052	64.1745	91.5612	77.1766	116.2989
	L1	78.9304	124.0886	133.1961	69.4989	99.986	132.0126	49.8055
	L2	77.5127	128.7089	147.3314	78.919	105.2893	116.6349	46.5524
	L3	78.1154	128.8408	158.16	78.6564	94.3712	113.3645	53.2126
	L4	72.4329	128.7061	154.0423	77.073	96.0136	91.3919	50.8028
	L5	70.5663	134.9918	159.7593	80.43	78.7154	88.0987	58.9307
MCZ	T3	123.7013	139.4847	94.8643	0	152.1364	50.751	109.6588
67405	T4	115.6956	130.3638	83.5478	0	157.3262	54.513	113.8127
	T5	120.6812	144.4006	80.2791	0	159.7611	43.1365	119.4951
	T6	119.937	140.8179	82.9427	85.8397	147.6067	48.1057	117.7944
	T7	122.8538	131.653	109.8541	77.4342	144.8726	57.5167	116.8493
	T8	56.5414	119.7768	131.9036	70.8939	85.304	60.3698	120.5039
	T9	64.0218	119.2586	113.4572	63.3168	81.8677	60.339	120.4898
	T10	69.8216	126.3449	119.7889	80.3864	89.0498	71.1657	117.5071
	L1	71.5833	122.7524	123.191	73.9857	87.3043	140.124	42.5575
	L2	67.7475	121.2321	135.8883	83.8136	60.0961	128.168	46.5196
	L3	68.9303	119.826	141.4119	87.4919	70.554	118.015	52.5504
	L4	63.0522	122.4653	158.116	88.6888	54.4491	106.5123	51.9138
MCZ	T3	122.1299	139.7491	99.4072	0	157.9721	49.9858	109.8131
67406	T4	105.8533	137.9792	91.3464	0	157.0205	45.9557	118.2332
	T5	108.6872	136.251	89.4985	0	158.4562	50.4061	118.1354
	T6	118.5872	148.961	92.9514	0	154.0339	56.6823	116.3414
	T7	119.4484	132.8202	94.7596	87.4248	150.3321	52.3867	120.7872
	T8	84.8571	124.2129	99.6307	78.0704	178.6345	56.8809	120.2641
	T9	56.0722	116.597	102.8554	68.7046	86.2646	61.7951	120.1169
	T10	63.3587	122.4876	123.5771	66.9269	80.3656	73.2348	109.1145
	L1	68.1333	127.0133	128.9547	74.0887	99.7708	141.791	42.4064

	L2	69.9676	121.0776	136.2062	79.7026	81.917	131.6298	49.7668
	L3	70.0051	126.1381	145.3481	81.007	96.0418	120.1824	52.4631
	L4	68.862	122.0845	159.7535	83.8987	78.6573	101.0392	51.2241
	L5	69.3158	152.3593	80.4612	74.2123	103.1238	123.7516	50.516
MCZ	T1	120.0319	158.8808	130.3343	0	136.9643	60.6186	87.7976
67407	T2	123.0483	142.3492	105.6101	0	158.3023	59.5627	95.6213
	T3	101.3391	133.3231	93.3968	0	152.2621	51.5068	111.4892
	T4	105.2346	140.749	83.8698	0	155.1472	42.4918	116.0896
	T5	110.0471	139.6503	82.1349	0	156.9232	41.4172	120.0875
	T6	105.6802	147.5405	83.9377	0	148.6643	46.2987	122.614
	T7	115.4748	134.9927	94.6441	75.4949	154.2934	58.5727	119.5857
	T8	56.5443	117.7218	101.8251	73.3032	85.5527	62.4272	118.5917
	T9	63.4584	122.4553	112.6645	73.858	81.441	61.5948	118.5663
	T10	69.6805	123.9743	110.8141	77.7413	81.649	65.9776	118.5499
	L1	69.3683	118.2179	132.73	76.6427	84.0748	119.9165	46.6798
	L2	70.646	113.2683	137.2606	79.8739	83.4641	122.9925	57.952
	L3	68.599	123.9554	148.2294	76.1817	79.2504	115.6514	58.2601
	L4	62.6149	122.7646	152.0233	77.4035	61.7621	103.7918	51.0615
	L5	62.0169	134.1799	157.3245	75.5545	63.8263	101.9189	56.8429
MCZ	T1	120.3869	141.1027	128.9179	0	119.3728	65.268	85.846
67408	T2	126.7218	127.9608	105.9947	0	163.0924	59.9414	92.9268
	T3	110.8199	132.7411	92.2029	0	157.7636	52.6628	103.6397
	T4	100.081	124.7657	83.108	0	170.2686	52.3097	109.5594
	T5	96.6185	130.6005	90.3389	0	155.9792	43.7861	120.4432
	T6	113.1062	133.319	95.3908	78.6583	153.008	51.6938	117.9002
	T7	113.2101	125.593	110.7344	77.3751	158.1865	60.6486	120.9817
	T8	57.7446	111.6543	102.2867	72.5478	91.5382	62.3206	118.0257
	T9	57.8449	117.7115	118.327	71.2771	86.6377	69.5357	113.7771
	T10	61.4645	117.8633	121.2707	66.8978	84.5543	69.4064	115.4819
	L1	67.1084	112.2143	127.398	69.4188	91.3652	131.4577	51.061
	L2	66.3242	112.9869	129.914	77.1714	77.3684	132.2334	62.8093
MCZ	T1	131.2062	145.8509	116.1566	0	143.3915	51.2913	88.2462
67411	T2	117.3622	144.5725	101.5597	0	157.2775	46.4786	101.6506

T3	113.9666	143.4373	98.1963	0	158.2596	46.9086	106.0332
T4	117.834	151.6889	92.1705	0	158.7684	45.8538	118.4172
T5	116.4856	151.3624	95.3415	0	154.3656	59.3893	121.7906
T6	120.6227	129.0508	106.7075	78.5224	159.8352	51.6549	124.3868
T7	77.2633	116.8925	123.6595	68.4365	118.896	62.0078	116.4834
T8	78.3849	125.8634	121.2131	74.5621	104.4021	64.848	115.6576
T9	70.7037	120.01	117.1523	66.3805	91.6208	66.1592	116.2238

Angular measurements in degrees. Missing vertebrae represent damaged or otherwise abnormal vertebrae, and were not used in analyses. See Fig. 2 for measurement abbreviations.

Table S5. Summary of *F*-values (Type III sums of squares) from ANOVAs in (A) compliance constant, and (B) range of motion.

A. ANOVA in compliance	*F*	Mean square	d.f.	*P*	Type III SS
Direction	26.143	1.768	2	<0.001	3.537
Motion segment	25.952	1.756	6	<0.001	10.534
Direction * Motion segment	1.782	0.121	12	0.060	1.447
Error		0.068	109		7.373
B. ANOVA in range of motion					
Direction	19.038	30.238	2	<0.001	60.476
Motion segment	32.249	51.221	6	<0.001	307.327
Direction * Motion segment	3.120	4.955	12	0.001	59.462
Error		1.588	108		171.538

F-values, mean squares, degrees of freedom (d.f.), *P*-values, and Type III sums of squares (SS) for direction, motion segment, and the interaction effect in both compliance and range of motion.

Table S6. Scores of the first three principal components (PC1, PC2, PC3).

		PC1	PC2	PC3
MCZ	T1	-0.99986	-0.56299	2.77636
67401	T2	-1.05313	-0.16299	1.06422
	T3	-1.30202	-0.29895	-0.2541
	T4	-1.12561	-0.19655	-0.80849
	T5	-1.35829	-0.08106	-0.94918
	T6	-1.37677	0.18741	-1.19121
	T7	0.85957	-0.76509	-0.42103
	T8	0.93534	-1.06177	-0.21494
	T9	0.72117	-0.527	0.0646
	T10	0.77997	-0.6547	0.04702
	L1	-0.29063	2.4164	0.04682
	L2	0.16782	1.94213	-0.3968
	L3	0.58695	1.61578	-0.15717
	L4	1.0363	0.64286	0.20186
	L5	1.05237	0.27708	0.02995
MCZ	T1	-1.60818	0.44332	3.19851
67402	T2	-1.60078	1.07421	0.79504
	T3	-1.30257	0.246	-0.39008
	T4	-1.41891	0.18967	-1.1849
	T5	-1.26493	-0.04991	-1.57196
	T6	-1.02539	-0.205	-1.23394
	T7	0.97659	-0.72924	-0.69807
	T8	0.44254	-0.71133	0.28776
	T9	0.45865	-0.35619	-0.09397
	T10	0.73773	-0.46677	0.19624
	L3	0.72793	1.74798	-0.25056
	L4	0.95354	1.1956	0.1149
	L5	0.78203	1.22017	0.50236
MCZ	T1	-1.29043	-0.17719	2.92906
67403	T2	-1.10815	0.13751	1.27879
	T3	-1.17879	0.02391	-0.38255
	T4	-1.43834	0.1069	-1.10539
	T5	-1.19748	-0.10317	-1.475
	T6	-1.25434	-0.01778	-1.68584
	T7	1.00763	-1.11046	-0.51239
	T8	0.54866	-1.01128	0.11892
	T9	0.86479	-1.08853	0.95548
	T10	0.87281	-1.09771	-0.36144
	L1	-0.05502	2.03228	-0.40587
	L2	0.48449	1.75785	-0.57371
	L3	0.89542	1.0148	-0.28632
	L4	1.05174	0.74138	0.9573
	L5	1.0129	0.70673	0.87711
MCZ	T3	-1.14409	-0.38598	-0.17901

67405	T4	-1.10428	-0.56099	-0.83655
	T5	-0.82795	-0.64004	-1.10847
	T6	-0.02091	-0.89102	-1.01871
	T7	0.90881	-0.90645	0.29674
	T8	0.63847	-1.21248	0.72338
	T9	0.76857	-1.30624	0.35654
	T10	1.11625	-1.16401	0.10259
	L1	0.20496	2.27562	-0.27188
	L2	0.5311	1.67101	-0.44769
	L3	1.17396	0.90275	-0.40846
	L4	1.16149	0.54093	0.23031
MCZ	T3	-0.87457	-0.5439	0.91104
67406	T4	-0.84296	-1.07683	-0.60775
	T5	-0.97401	-0.47062	-0.84968
	T6	-0.81293	-0.47256	-0.75846
	T7	0.69236	-0.79961	0.12035
	T8	1.04287	-0.3959	0.15836
	T9	0.66581	-1.15397	-0.11699
	T10	0.79389	-0.97891	-0.05558
	L1	0.04785	2.45579	-0.16206
	L2	0.51083	1.67939	-0.47143
	L3	1.03005	1.1078	-0.57582
	L4	1.16565	0.40075	0.21092
	L5	1.661	1.30814	0.85051
MCZ	T1	-1.21944	-0.16027	3.04632
67407	T2	-1.28446	0.38472	1.47319
	T3	-1.13804	-0.36603	-0.2456
	T4	-1.0658	-0.56637	-1.29045
	T5	-0.9781	-0.71155	-1.01717
	T6	-0.64401	-0.75028	-0.7879
	T7	1.05872	-0.91755	0.76439
	T8	0.89636	-0.98354	-0.68835
	T9	1.12028	-1.32202	-0.09319
	T10	1.20946	-1.47358	0.01222
	L1	0.31936	1.79438	-0.39283
	L2	0.90648	1.18497	-0.61975
	L3	1.20556	0.86956	-0.24817
	L4	0.82906	0.98887	0.43505
	L5	1.10435	0.90234	0.53508
MCZ	T1	-1.28367	-0.36148	3.13269
67408	T2	-1.45616	0.13097	0.83319
	T3	-1.38487	0.04416	-0.20809
	T4	-1.29982	-0.29202	-1.05384
	T5	-1.19135	-0.81749	-1.76759
	T6	0.39191	-1.11855	-1.34811
	T7	1.00004	-1.22213	-0.21238

	T8	0.62862	-1.03414	0.86425
	T9	0.62041	-0.70477	-0.1973
	T10	0.79481	-1.04632	-0.128
	L1	-0.19294	2.12967	-0.28414
	L2	0.40819	1.5395	-0.62005
MCZ	T1	-1.45328	0.37626	2.83697
67411	T2	-1.31004	0.0677	0.29585
	T3	-1.11603	-0.14217	-0.59545
	T4	-1.02039	-0.31331	-0.54255
	T5	-0.29011	-0.24422	-0.07474
	T6	1.14145	-1.10993	0.5942
	T7	0.33067	-0.52606	0.63986
	T8	1.34066	-1.02456	0.60133
	T9	0.80262	-0.87169	0.42145

Scores from PC1, PC2, and PC3 were used in stepwise linear regressions on compliance and range of motion data. Specimens are listed according to MCZ accession number.

Table S7. Correlation matrix of linear and angular measurements.

	CL	CW	CH	NSH	TPDW	PrZW	IZL	LW	MH	AL	AH	PoZL	LA	PrZA	NSA	TPDA	MA	PrZC	TPDAD	TPDAC
CL	1.000																			
CW	.050	1.000																		
CH	.702	-.477	1.000																	
NSH	-.196	.300	-.609	1.000																
TPDW	.019	.188	-.285	.682	1.000															
PrZW	.151	.778	-.445	.450	.247	1.000														
IZL	.818	.016	.774	-.573	-.334	-.043	1.000													
LW	.155	.402	-.138	.277	.159	.605	.046	1.000												
MH	.844	.114	.709	-.497	-.174	.077	.908	.182	1.000											
AL	.662	.095	.681	-.720	-.372	-.077	.897	-.008	.905	1.000										
AH	.717	.011	.752	-.717	-.458	-.084	.926	-.034	.877	.932	1.000									
PoZL	-.367	.248	-.682	.842	.551	.409	-.673	.323	-.564	-.754	-.798	1.000								
LA	.600	.332	.086	.477	.457	.441	.267	.291	.368	.088	.101	.308	1.000							
PrZA	-.582	.030	-.677	.698	.408	.272	-.775	.129	-.777	-.844	-.823	.646	-.100	1.000						
NSA	-.488	.250	-.653	.679	.485	.394	-.624	.383	-.527	-.650	-.716	.691	-.019	.743	1.000					
TPDA	.661	.430	.356	-.298	-.107	.404	.664	.371	.809	.714	.679	-.373	.349	-.554	-.346	1.000				
MA	.603	-.011	.702	-.751	-.431	-.135	.846	-.077	.784	.906	.904	-.806	-.022	-.726	-.682	.594	1.000			
PrZC	-.661	-.258	-.536	.563	.339	-.117	-.808	-.169	-.836	-.831	-.815	.490	-.260	.870	.590	-.761	-.722	1.000		
TPDAD	.816	.084	.610	-.344	-.220	.182	.780	.212	.857	.710	.758	-.420	.393	-.611	-.459	.730	.597	-.704	1.000	
TPDAC	-.781	-.269	-.398	.042	-.045	-.405	-.623	-.366	-.784	-.543	-.537	.141	-.600	.403	.200	-.764	-.388	.575	-.896	1.000

Table S8. Linear regressions of each measure individually onto compliance and range of motion data in each direction.

	log(*C*) in Dorsiflexion			log(*C*) in Lateroflexion			log(*C*) in Ventroflexion			R_m in Dorsiflexion			R_m in Lateroflexion			R_m in Ventroflexion		
	R^2	b_0	b_1	R^2	b_0	b_1	R^2	b_0	b_1	R^2	b_0	b_1	R^2	b_0	b_1	R^2	b_0	b_1
CL	**0.154 (<0.001)**	2.793	-0.126	**0.437 (<0.001)**	3.828	-0.210	**0.559 (<0.001)**	4.473	-0.276	**0.322 (<0.001)**	-4.399	1.076	**0.253 (<0.001)**	-1.271	0.659	**0.062 (0.022)**	2.194	0.473
CW	0.024 (0.166)	2.188	-0.045	**0.113 (0.002)**	3.293	-0.122	0.028 (0.129)	2.777	-0.064	0.015 (0.279)	2.653	0.210	0.007 (0.465)	3.130	0.123	0.026 (0.144)	9.586	-0.317
CH	**0.103 (0.004)**	2.434	-0.145	**0.451 (<0.001)**	3.882	-0.364	**0.516 (<0.001)**	4.094	-0.395	**0.306 (<0.001)**	-2.542	1.474	**0.327 (<0.001)**	-2.134	1.281	**0.133 (0.001)**	1.075	1.028
NSH	**0.065 (0.014)**	1.259	0.020	**0.31 (<0.001)**	1.066	0.044	**0.211 (<0.001)**	1.193	0.041	**0.301 (<0.001)**	10.174	-0.241	**0.168 (<0.001)**	7.312	-0.134	**0.064 (0.02)**	8.817	-1.16
TPDW	0.025 (0.164)	1.261	0.048	**0.107 (0.003)**	1.119	0.098	0.03 (0.113)	1.533	0.061	**0.115 (0.002)**	10.542	-0.614	**0.054 (0.036)**	7.060	-0.288	0.037 (0.08)	9.465	-0.347
PrZW	0.011 (0.361)	2.029	-0.029	**0.077 (0.011)**	3.086	-0.098	0.032 (0.103)	2.825	-0.067	0.004 (0.556)	3.650	0.112	0.022 (0.18)	2.049	0.218	0.02 (0.201)	9.170	-0.268
IZL	**0.203 (<0.001)**	2.649	-0.071	**0.591 (<0.001)**	3.614	-0.120	**0.686 (<0.001)**	4.045	-0.148	**0.514 (<0.001)**	-3.970	0.668	**0.3 (<0.001)**	-0.273	0.353	**0.088 (0.006)**	2.682	0.271
LW	0.003 (0.651)	1.919	-0.020	0.005 (0.519)	2.344	-0.030	**0.065 (0.019)**	3.328	-0.115	0.003 (0.624)	6.243	-0.126	0.001 (0.821	3.941	0.043	0.009 (0.388)	8.601	-0.220
MH	**0.165 (<0.001)**	1.857	-0.015	**0.59 (<0.001)**	2.303	-0.029	**0.708 (<0.001)**	2.454	-0.037	**0.472 (<0.001)**	3.369	0.155	**0.348 (<0.001)**	3.518	0.092	**0.106 (0.003)**	5.553	0.074
AL	**0.188 (<0.001)**	1.905	-0.077	**0.643 (<0.001)**	2.387	-0.140	**0.658 (<0.001)**	2.522	-0.165	**0.549 (<0.001)**	2.877	0.774	**0.335 (<0.001)**	3.322	0.416	**0.101 (0.003)**	5.409	0.332
AH	**0.208 (<0.001)**	1.914	-0.076	**0.609 (<0.001)**	2.381	-0.130	**0.638 (<0.001)**	2.520	-0.155	**0.565 (<0.001)**	2.863	0.743	**0.333 (<0.001)**	3.314	0.396	**0.111 (0.002)**	5.358	0.332
PoZL	**0.179 (<0.001)**	1.133	0.108	**0.359 (<0.001)**	1.198	0.157	**0.329 (<0.001)**	1.204	0.169	**0.306 (<0.001)**	9.300	-0.836	**0.126 (0.001)**	6.426	-0.385	**0.065 (0.019)**	8.297	-0.385
LA	0.026 (0.151)	2.176	-0.019	**0.116 (0.002)**	2.985	-0.040	**0.158 (<0.001)**	3.423	-0.055	0.029 (0.134)	1.989	0.119	0.034 (0.1)	2.266	0.089	0.009 (0.379	4.595	0.069
PrZA	**0.135 (0.001)**	1.200	0.006	**0.535 (<0.001)**	1.014	0.011	**0.467 (<0.001)**	0.992	0.012	**0.455 (<0.001)**	10.370	-0.061	**0.289 (<0.001)**	7.468	-0.034	**0.18 (<0.001)**	9.788	-0.039
NSA	**0.124 (0.001)**	0.169	0.012	**0.515 (<0.001)**	- 1.290	0.026	**0.432 (<0.001)**	-1.418	0.027	**0.382 (<0.001)**	20.803	-0.123	**0.291 (<0.001)**	14.703	-0.080	**0.133 (0.001)**	16.261	-0.077
TPDA	**0.177 (<0.001)**	2.525	-0.007	**0.492 (<0.001)**	3.337	-0.012	**0.573 (<0.001)**	3.766	-0.015	**0.347 (<0.001)**	-1.879	0.060	**0.265 (<0.001)**	0.421	0.036	0.028 (0.127)	4.362	0.017
MA	**0.189 (<0.001)**	1.913	-0.004	**0.547 (<0.001)**	2.381	-0.007	**0.554 (<0.001)**	2.513	-0.008	**0.467 (<0.001)**	2.960	0.040	**0.266 (<0.001)**	3.373	0.021	**0.046 (0.05)**	5.645	0.012
PrZC	**0.164 (<0.001)**	1.188	0.004	**0.615 (<0.001)**	1.048	0.008	**0.547 (<0.001)**	1.019	0.009	**0.529 (<0.001)**	10.375	-0.046	**0.334 (<0.001)**	7.378	-0.024	**0.095 (0.004)**	8.558	-0.019
TPDAD	**0.165 (<0.001)**	2.092	-0.005	**0.362 (<0.001)**	2.567	-0.007	**0.489 (<0.001)**	2.849	-0.010	**0.286 (<0.001)**	1.884	0.039	**0.309 (<0.001)**	2.329	0.038	**0.07 (0.015)**	4.806	0.019
TPDAC	**0.102 (0.004)**	0.319	0.102	**0.232 (<0.001)**	1.423	0.006	**0.354 (<0.001)**	1.219	0.009	**0.149 (<0.001)**	7.760	-0.029	**0.163 (<0.001)**	6.484	-0.021	0.017 (0.239)	7.239	-0.010

R^2 and corresponding *P*-value of each linear regression is provided. Significant R^2 and *P*-values are bolded according to $P \leq 0.05$. *Y*-intercepts (b_0) and slopes (b_1) are listed for each regression, and can be used along with the R^2 value in predicting mechanics from morphology.